KURENAI
Kyoto University Research Information Repository

KYOTO UNIVERSITY

Title	Orientation and Conformation of Single Polymer Chain Studied by Scanning Near-Field Optical Microscopy(Dissertation_)
Author(s)	Ube, Toru
Citation	Kyoto University ( )
Issue Date	2011-03-23
URL	http://dx.doi.org/10.14989/doctor.k16106
Right	2012-04-01
Type	Thesis or Dissertation
Textversion	author

Kyoto University

Orientation and Conformation of Single Polymer Chain

Studied by Scanning Near-Field Optical Microscopy

Toru UBE

2011

Contents

Chapter 1

General Introduction

1.1   Background and Motivation

Polymeric materials show unique mechanical and optical properties, which are applied to various fields in modern industry and human life. The macroscopic properties of polymers originate from the microscopic structure and dynamics of the polymer chain. The understanding of the polymer physics and chemistry from the basis on the single chain is essential to design and improve the performance of polymer materials. The conformation of the polymer chain has long been investigated since the beginning of the polymer science.[1–5] The rotational freedom of backbone bonds of polymer chains induces various conformations even at the equilibrium state. This equilibrium conformation can be distorted by applying the external field. The conformational change is reflected in macroscopic properties such as optical birefringence. Furthermore, the distortion from the equilibrium conformation leads to the loss in entropy. The chain motion to recover the equilibrium state generates the entropic force. The macroscopic mechanical properties of polymer materials thus originate from the behavior of the single polymer chain.

The unique viscoelasticity of polymer materials arises from the dynamics of the polymer chain, which is different from that of the low molecular weight monomers. The motion of each monomer unit in a polymer chain is restricted because it is connected to adjacent units by covalent bonds. In a dense system with sufficiently long chains, the chains become entangled. These intramolecular connectivity and intermolecular uncrossability dominate the structure and dynamics of the polymer chain. A lot of theoretical models have been developed to describe the universal feature of a polymer chain incorporating these complexities. The viscoelastic properties have been derived from the models and compared with the rheological experiments.[6,7] This interplay with

theories and experiments has enhanced our understanding of the chain behavior. Besides rheological measurements, experimental methods to probe the structure and the dynamics of polymer chains have also been employed: optical birefringence, infrared absorption dichroism, small angle neutron scattering (SANS), and dielectric measurement.[7] The complementary information by different methods enables us to investigate the properties of polymer chains on various spatial and time scales.

In addition to the polymer chain in the bulk, the polymer chain near the interface plays an important role in determining the performance of polymer materials. The surface properties of polymer materials such as wettability, friction, and liquid crystal alignment are dominated by the behavior of the polymer chain near the surface.[8,9] The structure and motion of the polymer chain near the surface differ from those in a bulk state because of the air–polymer interface.[10] Therefore, investigation of the polymer surface at the molecular level is essential to understand the property of polymer materials.

The present thesis focuses on the direct observation of the single polymer chain under the external force. Scanning near-field optical microscopy (SNOM) is applied to the direct observation of a single polymer chain in bulk and thin films. This enables us to study polymer physics on the basis of the single polymer chain. The conformations of polymer chains under the uniaxial extension and the surface rubbing are analyzed and compared with macroscopic mechanical properties, optical properties, and theoretical models.

1.1.1 Theories on Structure and Dynamics of Polymer Chain

The studies on the conformation of flexible polymer chain began in the early 1930s. Guth, Mark,[11] and Kuhn[12] introduced the concept of random walk as a model of polymer conformation. The distribution function of the end-to-end vector, $\mathbf{R}$, of the random walk with n steps at a length of l, is expressed by Gaussian distribution, which is written as

$$P(\mathbf{R}) = \left(\frac{3}{2\pi \langle R^2 \rangle} \right)^{\frac{3}{2}} \exp \left(-\frac{3\mathbf{R} \cdot \mathbf{R}}{2\langle R^2 \rangle} \right),$$

(1.1)

where $\langle R^2 \rangle = \langle \mathbf{R} \cdot \mathbf{R} \rangle = nl^2$. The root mean square radius of gyration, R_g, of the random walk is $nl^2/6$ for sufficiently large n. The experimental investigation on the chain dimension with light scattering measurements of dilute solutions began in 1940s with Debye[13] and Zimm.[14] The radius of gyration of various polymers in solutions has been widely studied.[2] The molecular weight (M) dependence of R_g is expressed by the power law: $R_g \propto M^\nu$. At the Θ condition, the excluded volume effect disappears and the molecular weight dependence of R_g for linear polymer agrees with the theoretical prediction of the random walk ($\nu = 0.5$). Under this condition, the dimension of the real linear chain is expressed as

$$\langle R^2 \rangle = C_\infty n_b l_b^2, \tag{1.2}$$

where C_∞ is the characteristic ratio, n_b is the number of the backbone bonds, and l_b is the length of the bond. The characteristic ratio reflects the rigidity of the chain determined by the chemical structure of the monomer unit. Thus the universal feature of the long flexible chain is expressed by the random walk. In the 1970s, the SANS experiment showed that the chain dimension in a bulk state also takes a Gaussian conformation.[15] The random walk model remains significant for the basic understanding of the polymer physics.

The mechanical properties of polymer chains were also derived from the random walk model in the early studies.[11] The increase in R restricts the number of the conformation and leads to the decrease in entropy. Therefore, an entropic force is generated between the ends of the chain, which is related to the distribution function of $\mathbf{R}$ and calculated as

$$\mathbf{f} = -kT \frac{\partial \ln P(\mathbf{R})}{\partial \mathbf{R}} = -\frac{3kT}{\langle R^2 \rangle} \mathbf{R}, \tag{1.3}$$

where k is the Boltzmann constant and T is the temperature. This is equivalent to the Hookean force with zero rest length and the spring constant of $3kT/\langle R^2 \rangle$. This is a basic equation for the force–conformation relationship of polymer chains.

The macroscopic stress of polymeric matters was first predicted theoretically for cross-linked rubber systems.[16–20] In the classical rubber elasticity theory, it is assumed

that the distribution of the end-to-end distance of the chain strand between cross-links in the equilibrium state is expressed by Gaussian distribution; therefore, each strand between the cross-links behaves as a spring. Furthermore, each cross-link is assumed to change its position in the same way as the macroscopic deformation (affine deformation). Then, the macroscopic stress–strain relationship is derived from the total change in the elastic potential. Although the deviations from the experiment is observed at a large deformation due to the finite extension of a chain, the mechanical property of the cross-linked polymer system is well described by the entropic elasticity and the affine deformation.

In an uncross-linked polymer system, the relaxation process plays an important role in the viscoelasticity. Rouse developed the bead–spring model to describe the dynamics of the polymer chain in a dilute solution.[21] A polymer chain is divided into n_s sub-molecules with an equilibrium length l_s. Each sub-molecule is long enough to obey the Gaussian distribution. Therefore, the force arisen from each sub-molecule is represented by the spring with the constant of $3kT/n_s l_s^2$. The conformational change of the polymer chain is calculated from the motions of their representative points (beads). Each bead is moved by three kinds of force: the spring force, the frictional force from the surrounding liquid molecules, the osmotic force. The time evolution of macroscopic stress is calculated through the average orientation of the sub-molecules. The Rouse model was found to well describe the viscoelastic behaviors of short linear chains in concentrated systems, even though it was formulated for isolated chains.[22] Thus, the connectivity of monomers has been successfully modeled.

The theoretical description of the chain dynamics in an entangled system requires modeling of the mutual uncrossability of chains. In 1971, de Gennes introduced the tube model to the entangled polymer system.[23] He considered the dynamics of a long linear flexible chain in the presence of fixed obstacles. The chain is free to move between the obstacles, but it cannot cross any of them. This is equivalent to the chain surrounded by the tube. The tube suppresses the chain motion perpendicular to the chain backbone and permits the curve-linear diffusional motion along the chain contour, which
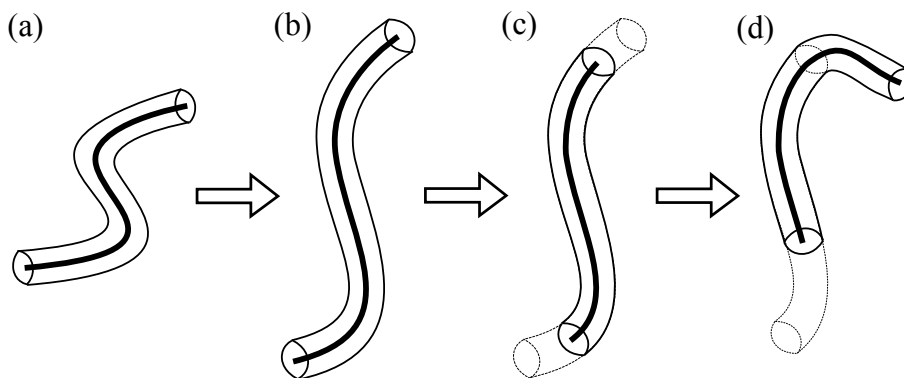
Figure 1.1: The schematic illustration of the relaxation after the step strain assumed in Doi–Edwards model: (a) before stretching, (b) immediately after the deformation, (c) contraction and (d) reptation.

is called reptation. In 1978, Doi and Edwards extended this concept and calculated various dynamic properties of entangled linear chains at equilibrium and under strains.[24–27] They considered the Rouse chain in a tube and calculated stress from the orientation of the Rouse segments. The chain motion assumed in the Doi–Edwards model is shown in Figure 1.1. When the system is deformed by a large step strain, the chains are deformed according to affine deformation (Figure 1.1b). Then, these chains relax through the motions along the tube: the contraction of the chain contour and the reptation (Figure 1.1c and d, respectively). The Doi–Edwards model showed great success in describing the slow relaxation of entangled linear polymer chains.

The development of the tube model stimulated the theoretical and experimental studies on the dynamics of entangled polymer systems including various chain architectures and polydispersity. Through this process, the original Doi–Edwards model has been improved by considering the additional relaxation modes shown in Figure 1.2.[5–7] The contour length fluctuation (Figure 1.2b and c) was incorporated to explain the experimental result for the molecular weight dependence of the longest relaxation time (the power law with a factor of 3.4), whereas the original Doi–Edwards model predicts the scaling factor of 3.[28–30] Furthermore, the assumption of the fixed network is no longer valid especially
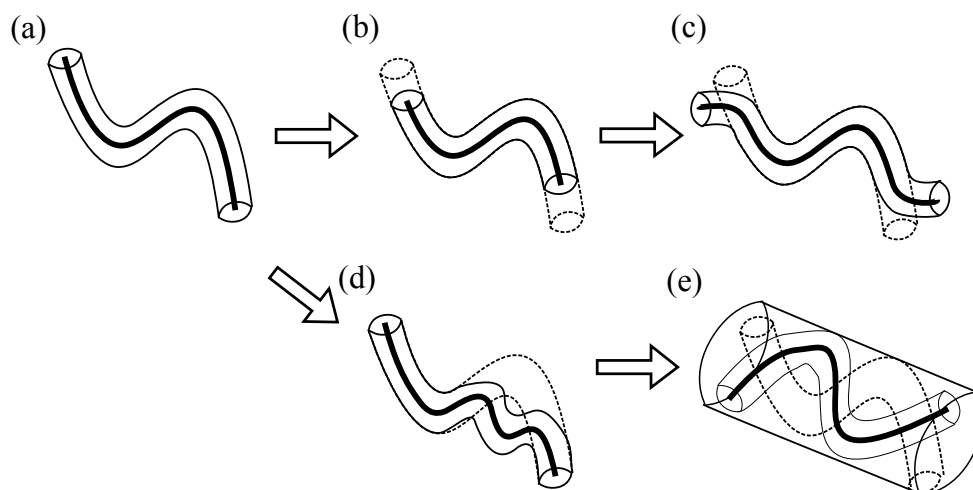
Figure 1.2: The schematic illustration of the chain motion to modify the tube model : (a) initial state, (b, c) contour length fluctuation, (d) constraint release and (e) dynamic tube dilation.

for polydisperse systems. The fast relaxation of the surrounding chains releases the constraint and allows the local motion perpendicular to the tube direction. This is known as the constraint release shown schematically in Figure 1.2d.[31–38] The accumulation of this event can be considered as the increase in tube diameter (dynamic tube dilation, Figure 1.2e),[39–41] which accelerates the reptation. Incorporation of these effects has been found to improve the prediction of the viscoelasticity both for monodisperse systems and binary blends of the same chemical species with different molecular weights. Recently, the stochastic simulation methods has been developed to predict the rheological behaviors of entangled systems.[42–44] As simulations can deal with multi body problems without using mean-field approach, they are convenient for predicting the behavior of the polydisperse system. The improvement of theoretical models and calculation methods are still in progress.

1.1.2 Experimental Techniques to Observe Chain Behavior

Experimentally, the dynamics of polymer chains has been investigated mostly through rheological measurements.[45] The stress originates from the segmental orientation of polymer chains. The proportionality between stress and birefringence (stress–optical rule) ensures the investigation of chain dynamics through the rheological measurements in terms of the segmental orientation.[27] On the other hand, the various experimental methods provide information on different length and time scales, which are essential to describe the chain behavior. The average dimension of a whole single chain under external stress has been measured by SANS in concentrated polymer systems.[46–52] The dielectric relaxation measurement can probe the dynamics of the dipole moment. The dynamics of end-to-end vector has been probed by dielectric measurements for polymers with dipoles that are aligned in the same direction along the backbone such as *cis*-polyisoprene.[6,53] The combination of various measurements is a powerful approach to clarify the chain structure and dynamics. The experimental techniques to investigate the surface properties have been limited because the weak signal from a small sample volume of the surface region has to be detected. Recent development of apparatus has made possible the quantitative analysis on the surface properties. For example, the viscoelasticity and the average orientation of the chemical bonds near the surface have been measured by scanning force microscopy[54,55] and grazing-incidence X-ray scattering,[56] respectively. The increased mobility of the chain in the surface region has been found by these techniques.

By the methods mentioned above, however, the variety of chain conformations is canceled in the observed average value. The observation of individual single polymer chains would reveal the exact behavior of real chains, which should be different from each other. Understanding of the distribution of the chain motion will help improve theoretical models, which have been based on the pre-averaged chain dynamics. Several studies on the direct observation of single polymer chains have been reported using atomic force microscopy (AFM).[57–59] Since AFM probes the surface topography, it has been applied to the isolated polymer chains adsorbed on a flat substrate in an extremely dilute condition.

7

It cannot be used to observe a single polymer chain embedded in a bulk medium. In order to detect in-situ features of polymer chains located inside a bulk medium, a single chain must be distinguished from surrounding ones. Fluorescence labeling is an established method to detect the structure and motion of the labeled chains with high sensitivity. The direct observation of a single polymer chain using the fluorescence microscopy has been demonstrated for the observation of single DNA molecules.[60–67] However, the conventional fluorescence microscopy suffers from the low spatial resolution of ∼ 250 nm due to the diffraction-limit of light. Therefore, the application of the optical microscopy to single macromolecular imaging has been limited to the observation of huge biomacromolecules such as DNA. A higher resolution is needed to observe individual flexible polymer chains since the typical sizes are in the order of 10–100 nm.

SNOM is an emerging scanning probe technique, which allows optical measurement with a high resolution beyond the diffraction limit.[68–73] The principle of SNOM imaging is illustrated in Figure 1.3. When object A is illuminated by light, there arises not only the propagating scattering light but also the optical near-field around the surface of A, which is a non-propagating component of the light. The dimension of the optical near-field depends on the size and the shape of A. When another object B is put in the region where the energy of the optical near-field is concentrated, the optical near-field is scattered by B. In this way, the non-propagating optical near-field can be detected in the far-field as the propagating light scattered by B. In the actual SNOM system, A and B correspond to a SNOM probe and a sample, respectively. The SNOM probe has a sub-wavelength aperture at the end. When the incident light reaches the aperture, the optical near-field generates at the back of the aperture. The interaction between the probe and the sample through the optical near-field is observed as the resulting propagating light such as scattering. Because the dimension of the near-field is as small as the size of the aperture, the optical response from the nanometric area can be obtained. The high-resolution map of the optical response is obtained by scanning the sample surface with the probe. SNOM can be combined with various spectroscopic measurements: Raman scattering,
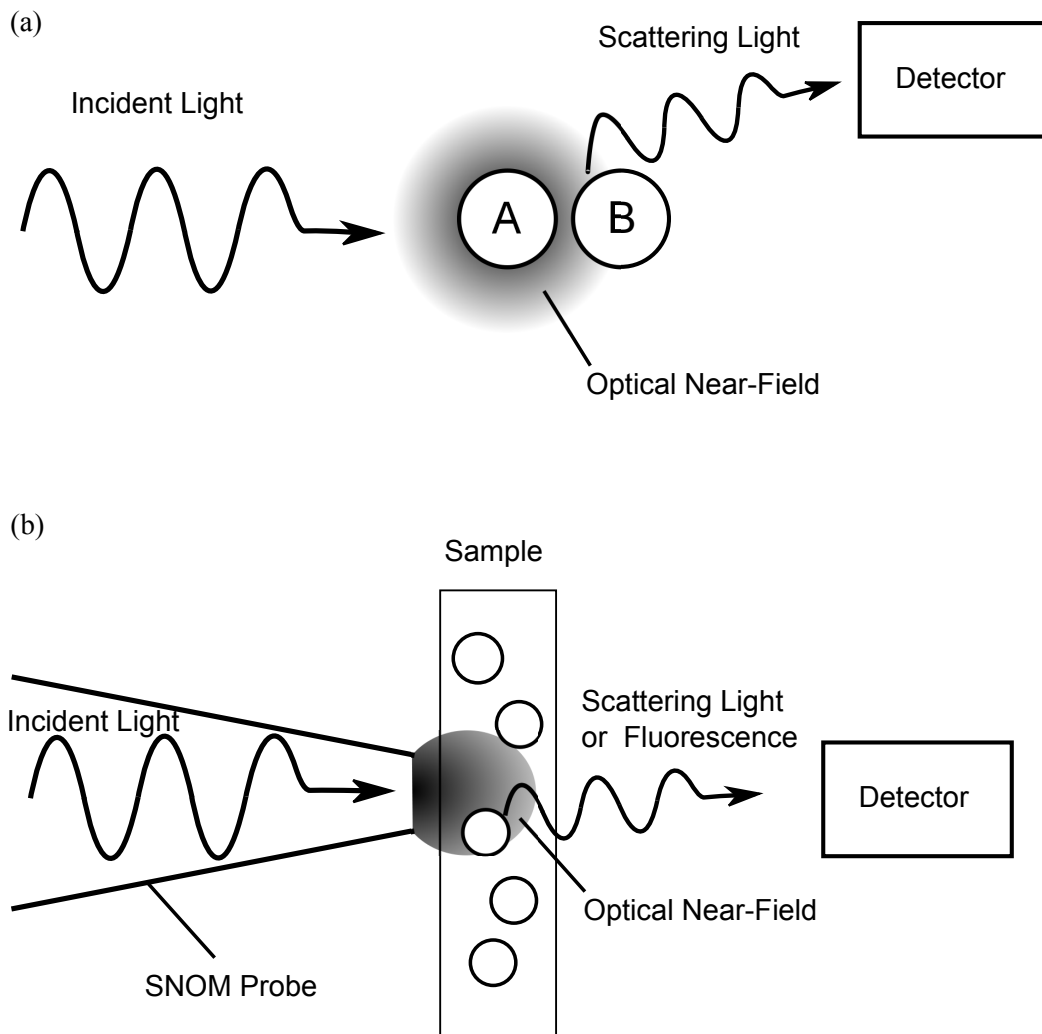
Figure 1.3: Schematic illustration of the optical near-field system. (a) Light illumination to object A generates optical near-field. Object B scatters the optical near-filed around A and make it detectable at far-field. (b) The actual SNOM system. The SNOM probe and the sample correspond to objects A and B in panel a, respectively.

infrared and fluorescence spectroscopy. In the case that the sample contains fluorescence dyes, the fluorescence is excited by the optical near-filed. The spatial distribution of the fluorescence dye can be imaged by detecting the fluorescence. Therefore, SNOM enables us to directly observe the conformation of the single chain, which is fluorescently labeled and silhouetted against the surrounding unlabeled polymers.[74–80] Furthermore, the orientation of the fluorescence dye can be evaluated by the use of polarized light because the absorption and fluorescence anisotropies reflect the orientation of the transition dipole.[81–83] The microscopic polarization measurements reveal the spatial distribution of the orientational anisotropy.[84] The direct observation through these techniques will help clarify the structure and dynamics of the single polymer chain.

1.2 Outline of This Thesis

This thesis consists of six chapters. The first chapter describes the background and motivation of this thesis. The historical development of theories and experiments on the structure and dynamics of the polymer chain under the external force is mentioned. The following chapters deal with the direct observation of single poly(methyl methacrylate) (PMMA) chain under the external forces.

In chapter 2, the application of SNOM to the observation of a single polymer chain in a bulk film under the uniaxial extension is demonstrated. The quantitative analysis of the chain conformation is introduced. The microscopic chain extension at the molecular level during the plastic deformation is investigated.

Chapter 3 deals with the uniaxial extension well above the glass transition temperature. The molecular extension ratio of the single chain is compared with the macroscopic extension ratio. The validity of the affine deformation is investigated in terms of the average and distribution function of the chain dimension. The extension behavior of a long probe chain in short matrix chains is also discussed.

Chapter 4 describes the chain conformation during the stress relaxation process after

the uniaxial extension. The relaxation in the dimension of the single chain is compared with that in the macroscopic stress and birefringence. The observed chain behavior is compared with the Doi–Edwards model. The individual chain behavior is discussed in terms of the distribution function of the whole chain dimension.

Chapter 5 deals with the relaxation behavior of the long probe chain in the blend matrix of long and short chains after the uniaxial extension. The effect of the disentanglement between the long and short chains on the conformation of the long chain is investigated; Observed is the whole chain relaxation depending on the blend ratio and molecular weight. The segmental orientation of the long probe chain is also evaluated from the single chain observation through the excitation polarization modulation microscopy. The relaxation at the scales of the segment and the whole chain is compared with the predictions of the slip-link simulation based on the Doi–Takimoto model.[43]

In chapter 6, the effect of the surface rubbing on the conformation of the chain in the thin film is investigated. The rubbed film is well known for the functionality to align the liquid crystal molecules.[85] The conformational change induced by the rubbing process is studied in terms of the segmental orientation and the dimension of the whole chain, which are evaluated by excitation polarization modulation microscopy and SNOM, respectively.

References

[1] Flory, P. J. *Principles of Polymer Chemistry*; Cornell University Press: New York, 1953.

[2] Flory, P. J. *Statistical Mechanics of Chain Molecules*; Wiley-Interscience: New York, 1969.

[3] de Gennes, P. G. *Scaling Concepts in Polymer Physics*; Cornell University Press: New York, 1979.

[4] Graessley, W. W. *Polymeric Liquids and Networks: Structure and Properties*; Garland Books: New York, 2004.

[5] Graessley, W. W. *Polymeric Liquids and Networks: Dynamics and Rheology*; Garland Books: New York, 2008.

[6] Watanabe, H. *Prog. Polym. Sci.* **1999**, *24*, 1253–1403.

[7] McLeish, T. C. B. *Adv. Phys.* **2002**, *51*, 1379–1527.

[8] Garbassi, F.; Morra, M.; Occhiello, E. *Polymer Surfaces: From Physics to Technology*; Wiley: Chichester, 1998.

[9] Karim, A.; Kumar, S. *Polymer surfaces, interfaces and thin films*; World Scientific: Singapore, 2000.

[10] Brown, H. R.; Russell, T. P. *Macromolecules* **1996**, *29*, 798–800.

[11] Guth, E.; Mark, H. *Monatsh.* **1934**, *65*, 93–121.

[12] Kuhn, W. *Kolloid Z.* **1934**, *68*, 2–15.

[13] Debye, P. *J. Appl. Phys.* **1944**, *15*, 338–342.

[14] Zimm, B. H. *J, Chem. Phys.* **1948**, *16*, 1099–1116.

[15] Cotton, J. P.; Decker, D.; Benoit, H.; Farnoux, B.; Higgins, J.; Jannink, G.; Ober, R.; Picot, C.; des Cloizeaux, J. *Macromolecules* **1974**, *7*, 863–872.

[16] Kuhn, W. *Kolloid Z.* **1936**, *76*, 258–271.

[17] Wall, F. T. *J. Chem. Phys.* **1942**, *10*, 485–488.

[18] Treloar, L. R. G. *Trans. Faraday Soc.* **1943**, *39*, 36–41.

[19] James, H. M.; Guth, E. *J. Chem. Phys.* **1943**, *11*, 455–481.

[20] Treloar, L. R. G. *The Physics of Rubber Elasticity*, 3rd ed.; Clarendon: Oxford, 1975.

[21] Rouse, P. E. *J. Chem. Phys.* **1953**, *21*, 1272–1280.

[22] Graessley, W. W. *Adv. Polym. Sci.* **1974**, *47*, 1–179.

[23] de Gennes, P. G. *J. Chem. Phys.* **1971**, *55*, 572–579.

[24] Doi, M.; Edwards, S. F. *J. Chem. Soc. Faraday Trans. II* **1978**, *74*, 1789–1801.

[25] Doi, M.; Edwards, S. F. *J. Chem. Soc. Faraday Trans. II* **1978**, *74*, 1802–1817.

[26] Doi, M.; Edwards, S. F. *J. Chem. Soc. Faraday Trans. II* **1978**, *74*, 1818–1832.

[27] Doi, M.; Edwards, S. F. *The Theory of Polymer Dynamics*, 3rd ed.; Clarendon: Oxford, 1986.

[28] Doi, M. *J. Polym. Sci., Polym. Lett. Ed.* **1981**, *19*, 265–273.

[29] Doi, M. *J. Polym. Sci., Polym. Phys. Ed.* **1983**, *21*, 667–684.

[30] Milner, S. T.; McLeish, T. C. B. *Phys. Rev. Lett.* **1998**, *81*, 725–728.

[31] Graessley, W. W. *Adv. Polym. Sci.* **1982**, *47*, 67–117.

[32] Klein, J. *Macromolecules* **1978**, *11*, 852–858.

[33] Daoud, M.; Gennes, P. G. D. *J. Polym. Sci., Polym. Phys. Ed.* **1979**, *17*, 1971–1981.

[34] Klein, J. *Macromolecules* **1986**, *19*, 105–118.

[35] Ianniruberto, G.; Marrucci, G. *J. Non-Newtonian Fluid Mech.* **1996**, *65*, 241–246.

[36] Mead, D. W.; Larson, R. G.; Doi, M. *Macromolecules* **1998**, *31*, 7895–7914.

[37] Ianniruberto, G.; Marrucci, G. *J. Rheol.* **2001**, *45*, 1305–1318.

[38] Graham, R. S.; Likhtman, A. E.; McLeish, T. C. B.; Milner, S. T. *J. Rheol.* **2003**, *47*, 1171–1200.

[39] Marrucci, G. *J. Polym. Sci., Polym. Phys. Ed.* **1985**, *23*, 159–177.

[40] Ball, R. C.; McLeish, T. C. B. *Macromolecules* **1989**, *22*, 1911–1913.

[41] Milner, S. T.; McLeish, T. C. B.; Young, R. N.; Hakiki, A.; Johnson, J. M. *Macromolecules* **1998**, *31*, 9345–9353.

[42] Hua, C. C.; Schieber, J. D. *J. Chem. Phys.* **1998**, *109*, 10018–10027.

[43] Doi, M.; Takimoto, J. *Philos. Trans. R. Soc. London, Ser. A* **2003**, *361*, 641–652.

[44] Masubuchi, Y.; Takimoto, J.; Koyama, K.; Ianniruberto, G.; Marrucci, G.; Greco, F. *J. Chem. Phys.* **2001**, *115*, 4387–4394.

[45] Ferry, J. D. *Viscoelastic Properties of Polymers*, 3rd ed.; Wiley: New York, 1980.

[46] Picot, C.; Duplessix, R.; Decker, D.; Benoit, H.; Boué, F.; Cotton, J. P.; Daoud, M.; Farnoux, B.; Jannink, G.; Nierlich, M.; de Vries, A. J.; Pincus, P. *Macromolecules* **1977**, *10*, 436–442.

[47] Boué, F.; Nierlich, M.; Jannink, G.; Ball, R. *J. Phys. (Paris)* **1982**, *43*, 137–148.

[48] Boué, F. *Adv. Polym. Sci.* **1987**, *82*, 47–101.

[49] Bent, J.; Hutchings, L.; Richards, R. W.; Gough, T.; Spares, R.; Coates, P. D.; Grillo, I.; Marien, O. G.; Read, D. J.; Graham, R. S.; Likhtman, A. E.; Groves, D. J.; Nicholson, T. M.; McLeish, T. C. B. *Science* **2003**, *301*, 1691–1695.

[50] Graham, R. S.; Bent, J.; Hutchings, L. R.; Richards, R. W.; Groves, D. J.; Embery, J.; Nicholson, T. M.; McLeish, T. C. B.; Likhtman, A. E.; Harlen, O. G.; Read, D. J.; Gough, T.; Spares, R.; Coates, P. D.; Grillo, I. *Macromolecules* **2006**, *39*, 2700–2709.

[51] Blanchard, A.; Graham, R.; Heinrich, M.; Pyckhout-Hintzen, W.; Richter, D.; Likhtman, A.; McLeish, T.; Read, D.; Straube, E.; Kohlbrecher, J. *Phys. Rev. Lett.* **2005**, *95*, 166001.

[52] Graham, R. S.; Bent, J.; Clarke, N.; Hutchings, L. R.; Richards, R. W.; Gough, T.; Hoyle, D. M.; Harlen, O. G.; Grillo, I.; Auhl, D.; McLeish, T. C. B. *Soft Matter* **2009**, *5*, 2383–2389.

[53] Watanabe, H. *Macromol. Rapid Commun.* **2001**, *22*, 127–175.

[54] Kajiyama, T.; Tanaka, K.; Ge, S. R.; Takahara, A. *Prog. Surf. Sci.* **1996**, *52*, 1–52.

[55] Tanaka, K.; Takahara, A.; Kajiyama, T. *Macromolecules* **2000**, *33*, 7588–7593.

[56] Toney, M. F.; Russell, T. P.; Logan, J. A.; Kikuchi, H.; Sands, J. M.; Kumar, S. K. *Nature* **1995**, *374*, 709–711.

[57] Kumaki, J.; Nishikawa, Y.; Hashimoto, T. *J. Am. Chem. Soc.* **1996**, *118*, 3321–3322.

[58] Kumaki, J.; Hashimoto, T. *J. Am. Chem. Soc.* **2003**, *125*, 4907–4917.

[59] Kiriy, A.; Gorodyska, G.; Minko, S.; Stamm, M.; Tsitsilianis, C. *Macromolecules* **2003**, *36*, 8704–8711.

[60] Houseal, T. W.; Bustamante, C.; Stump, R. F.; Maestre, M. F. *Biophys. J.* **1989**, *56*, 507–516.

[61] Morikawa, K.; Yanagida, M. *J. Biochem.* **1981**, *89*, 693–696.

[62] Chu, S. *Science* **1991**, *253*, 861–866.

[63] Perkins, T. T.; Smith, D. E.; Chu, S. *Science* **1994**, *264*, 819–822.

[64] Smith, D. E.; Chu, S. *Science* **1998**, *281*, 1335–1340.

[65] Maier, B.; Rädler, J. O. *Phys. Rev. Lett.* **1999**, *82*, 1911–1914.

[66] Maier, B.; Rädler, J. O. *Macromolecules* **2001**, *34*, 5723–5724.

[67] Teixeira, R. E.; Dambal, A. K.; Richter, D. H.; Shaqfeh, E. S. G.; Chu, S. *Macromolecules* **2007**, *40*, 2461–2476.

[68] Betzig, E.; Trautman, J. K. *Science* **1992**, *257*, 189–195.

[69] Ohtsu, M. *Near-field Nano/Atom Optics and Technology*; Springer: Tokyo, 1998.

[70] Dunn, R. C. *Chem. Rev.* **1999**, *99*, 2891–2928.

[71] Aoki, H.; Ito, S. *J. Phys. Chem. B* **2001**, *105*, 4558–4564.

[72] Aoki, H.; Kunai, Y.; Ito, S.; Yamada, H.; Matsushige, K. *Appl. Surf. Sci.* **2002**, *188*, 534–538.

[73] Ito, S.; Aoki, H. *Bull. Chem. Soc. Jpn.* **2003**, *76*, 1693–1705.

[74] Ito, S.; Aoki, H. *Adv. Polym. Sci.* **2005**, *182*, 131–169.

[75] Aoki, H.; Anryu, M.; Ito, S. *Polymer* **2005**, *46*, 5896–5902.

[76] Yang, J.; Sekine, R.; Aoki, H.; Ito, S. *Macromolecules* **2007**, *40*, 7573–7580.

[77] Aoki, H.; Morita, S.; Sekine, R.; Ito, S. *Polym. J.* **2008**, *40*, 274–280.

[78] Sekine, R.; Aoki, H.; Ito, S. *J. Phys. Chem. B* **2009**, *113*, 7095–7100.

[79] Tamai, Y.; Sekine, R.; Aoki, H.; Ito, S. *Macromolecules* **2009**, *42*, 4224–4229.

[80] Aoki, H.; Sekine, R.; Iwamoto, T.; Ito, S. *Polym. J.* **2009**, *42*, 124–130.

[81] Nishijima, Y. *J. Polym. Sci. Part C: Polym. Symp.* **1970**, *31*, 353–373.

[82] Valeur, B.; Monnerie, L. *J. Poly. Sci., Polym. Phys. Ed.* **1976**, *14*, 11–27.

[83] Lee, H.; Paeng, K.; Swallen, S. F.; Ediger, M. D. *Science* **2009**, *323*, 231–234.

[84] Gupta, V. K.; Kornfield, J. A.; Ferencz, A.; Wegner, G. *Science* **1994**, *265*, 940–942.

[85] Geary, J. M.; Goodby, J. W.; Kmetz, A. R.; Patel, J. S. *J. Appl. Phys.* **1987**, *62*, 4100–4108.

Chapter 2

Conformation of Single PMMA Chain in Uniaxially Stretched Film

Studied by SNOM

2.1 Introduction

The variation of the conformation of a polymer chain is the origin of the unique physical properties of polymer materials such as the entropic elasticity. The chain morphology induced by uniaxial elongation has been extensively investigated so far from both theoretical and experimental points of view. The orientation of the polymer chain in the stretched state has been studied by various methods such as birefringence and infrared absorption dichroism. Whereas these techniques examine the average orientation of the chain segments, the conformation of the whole chain contour has been investigated by SANS.[1–9] Both uncross-linked[3,4,9] and cross-linked[5–8] polymer systems have been analyzed by SANS measurements. In these studies, the deformation of the deuterated polymer chains was examined in terms of the chain dimensions in the directions parallel and perpendicular to the elongation axis. The conformation of the single polymer chain under uniaxial deformation is complicated, and has not been completely described by the model.

The direct observation of the single polymer chain provides detailed information on the shape of each polymer chain and would be great help to understand the rheological properties at the molecular level. Several studies on the direct observation of single polymer chains have been reported using AFM so far.[10–12] Since AFM probes the surface topography, it has been applied to the isolated polymer chains adsorbed on a flat substrate. It cannot be used to observe a single polymer chain embedded in a bulk medium. Fluorescence labeling technique is an established method to distinguish such a single polymer chain from its surroundings.[13,14] However, the conventional
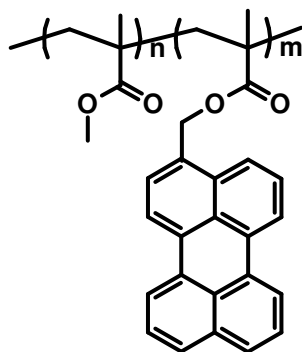
17

Figure 2.1: Chemical structure of PMMA-Pe.

fluorescence microscopy suffers from the diffraction-limited resolution of a half of the wavelength of light. Therefore, the application of the optical microscopy to single macromolecular imaging has been limited to the observation of huge biomacromolecules such as DNA.[13,14]

SNOM is an emerging scanning probe technique, which allows optical measurement with high resolution beyond the diffraction limit of light.[15–19] The light incidence to the sub-wavelength-sized aperture generates an optical near-field restricted in the space of the aperture size. This allows one to illuminate the specimen and to obtain the optical response from the nanometric area. Therefore, SNOM is a promising tool to directly observe the conformation of the single chain of the fluorescently labeled polymer.[20,21] Since the optical near-field illuminates the region beneath the surface by 200 nm, SNOM enables us to observe the chain conformation in the bulk system.

In the current chapter, the single polymer chain in the uniaxially elongated film is directly observed by SNOM. The conformational change of PMMA chain induced by the macroscopic stretching is quantitatively evaluated.

2.2 Experiments

Perylene-labeled PMMA (PMMA-Pe, Figure 2.1) was synthesized by bulk free radical copolymerization of methyl methacrylate and 3-perylenylmethyl methacrylate initiated by azoisobutyronitrile. The fraction of the labeled unit was evaluated to be 0.77% by UV–Vis absorption (U3500, Hitachi). The obtained polymer was purified by the fractional precipitation in methanol from toluene solution to achieve a relatively narrow molecular weight distribution. The weight- and number-averaged molecular weights, M_w and M_n, were determined by gel permeation chromatography (GPC) (D-7000G, Hitachi) using a column with the exclusion limit of 2×10^7 (Shodex KF806) with the eluent of THF, which was calibrated by the PMMA standards (Scientific Polymer Products, Inc.): $M_w = 1.99 \times 10^6$, $M_n = 1.58 \times 10^6$, and $M_w/M_n = 1.26$.

In order to observe the isolated single labeled chains in the PMMA bulk, the PMMA thin film containing a trace amount of PMMA-Pe was prepared by the spin-coating method. The mixed toluene solution of the unlabeled PMMA ($M_w = 1.89 \times 10^6$) and PMMA-Pe (0.005 wt % to the unlabeled polymer) was spin-coated onto a glass substrate to form a film with a thickness of 80 nm. The thin film was floated onto a water surface and picked up on a self-standing film of the unlabeled PMMA (the size was 25mm $\times$ 7mm, and the thickness was 300 μm), which was prepared by the solution casting of the unlabeled PMMA. The conformation of PMMA-Pe may be affected by the shear flow in the spin-coating process and the confinement effect of the thin film.[22] Therefore the sample film was annealed for 48 h at 180 °C in vacuum to reach the equilibrium. The later investigation was not affected by the further annealing at 200 °C, which indicates that the annealing time was sufficient. The GPC measurement of the film after annealing confirmed that the thermal cleavage of the polymer chains did not occur.

A tensile tester (RTM-500, Orientec) with a 10 kg load cell was used for stretching of the films. The length between the clamps was 20 mm. The stretching was carried out at 140 °C with a crosshead speed of 50 mm/min. The force and displacement were

monitored on a chart recorder. After the stretching, the film was rapidly quenched to room temperature in the stretched state. The extension ratio λ was calculated as l/l_0, where l_0 and l are the lengths of the film along the stretching direction before and after the elongation, respectively. The engineering stress σ_e was evaluated as

$$\sigma_e = \frac{F}{A_0},\tag{2.1}$$

where F is the force applied to the sample, and A_0 is the sample cross section before stretching. The birefringence measurement was carried out by Senarmont method.

The SNOM measurement was performed by a commercially available instrument (α-SNOM, WITec) with the hollow cantilever probe with a sub-wavelength aperture of 60 nm. The laser beam at a wavelength of 438 nm was focused onto the backside of the aperture to generate the optical near-field. The perylene fluorescence was collected by a microscope objective (0.80NA, $60\times$, Nikon) from the backside of the substrate and guided to a photomultiplier (H8631, Hamamatsu Photonics). The SNOM measurement was carried out in an ambient condition.

2.3   Results and Discussion

2.3.1   Stress and Birefringence

Figure 2.2a shows the stress – extension ratio curve of the PMMA film. This indicates the stress yielding at $\lambda = 1.1$ followed by the necking of the film. The necking spread over the whole specimen at the range of $\lambda = 1.1$–2.5, and the stress increased again until the film fracture at $\lambda = 3.3$. Figure 2.2b shows the result of the birefringence measurement. The birefringence Δn increased with the macroscopic extension ratio of the film. This suggests that the orientation of the chain backbone increased with the extension of the film.
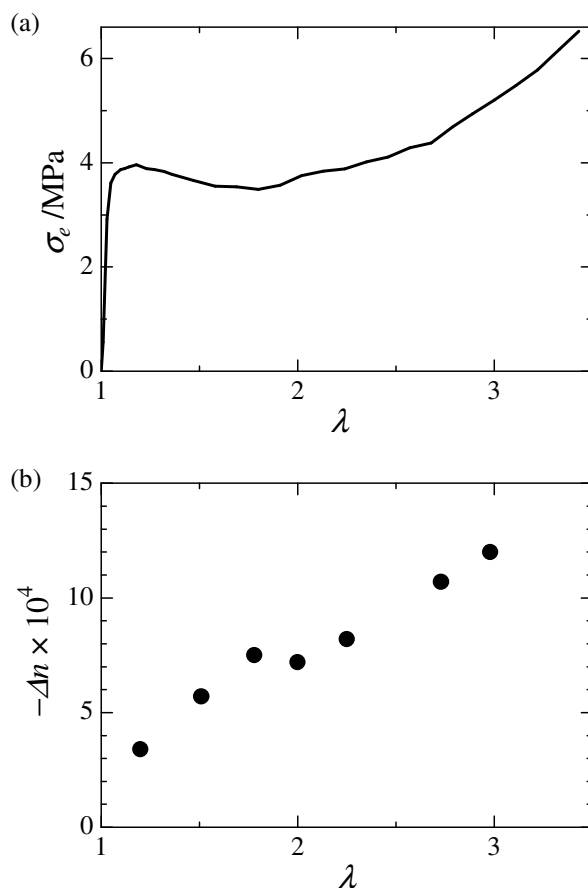
Figure 2.2: (a) Engineering stress – extension ratio curve for the PMMA film stretched at 140 °C. (b) Birefringence of the stretched PMMA films plotted against the extension ratio.

2.3.2 SNOM Image

Figure 2.3a shows the fluorescence SNOM image of the initial PMMA film before stretching. The perylene-labeled PMMA chains embedded in the unlabeled PMMA bulk film were observed as the bright spots in the fluorescence image. Each fluorescence spot was confirmed to be corresponding to the individual PMMA-Pe chain from the statistical analysis.[18] Since the optical near-field penetrates into the sample film by a few hundred nm, the shape of the PMMA chain observed in the SNOM image corresponds to the two-dimensional projection of the chain conformation. The ratio of the fluorescent monomer unit in PMMA-Pe was very small (0.77%); therefore, the effect of the dyes on
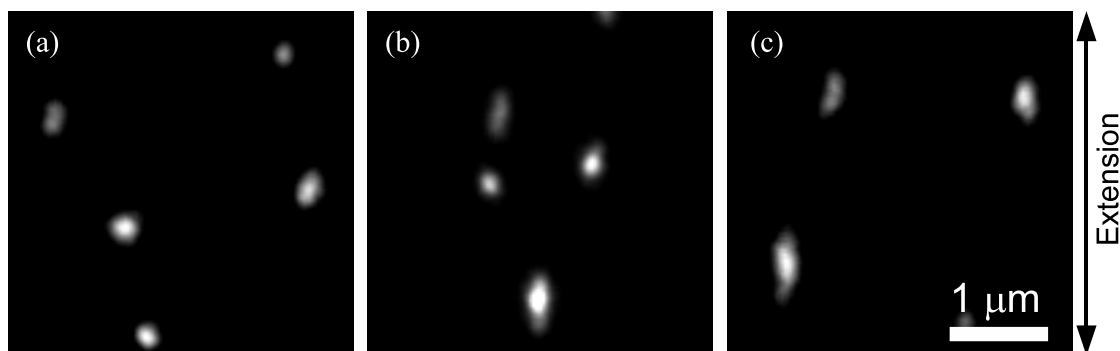
Figure 2.3: Fluorescence SNOM images of single polymer chains in the PMMA films (a) before stretching, and after stretching to the extension ratio of (b) 2.0 and (c) 3.0.

the chain conformation is considered to be negligible. The single PMMA-Pe chains with the same molecular weight were observed in various forms, indicating the flexibility of the PMMA chain. Figure 2.3b and c depict the SNOM images of the films after stretching to the extension ratio of 2.0 and 3.0, respectively. These images clearly show the polymer chains in the elongated conformation along the macroscopic stretching direction. When the author observed the same stretched film by SNOM 1 h, 6 h, and 24 h after stretching, any conformational change was not observed. Therefore the effect of the relaxation at room temperature is negligible because of the resolution of SNOM on the order of ten nm.

2.3.3   Analysis of the Single Chain Conformation

The conformation of the single PMMA chain was quantitatively evaluated from the fluorescence intensity distribution.[14] The fluorescence intensity is proportional to the number of fluorescence dye molecules randomly introduced to the PMMA-Pe chain; therefore, the intensity at each pixel is proportional to the number of the chain segment therein. The first moment of the fluorescence intensity distribution denotes the position of the center of mass:

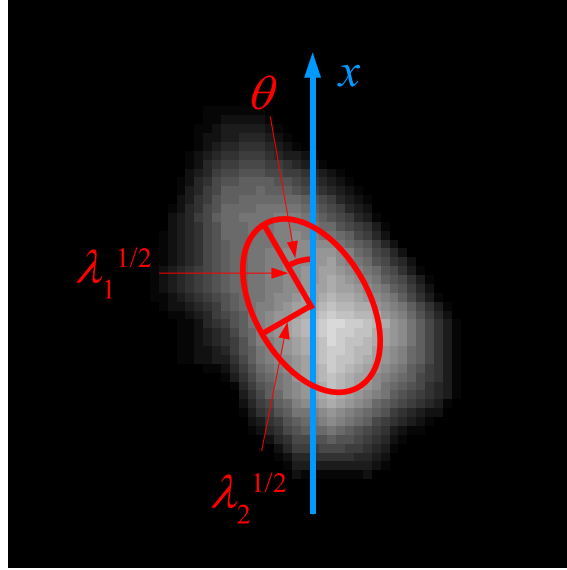$$\mathbf{r}_0 = \frac{1}{I} \sum_i \mathbf{r}_i I_i, \tag{2.2}$$

Figure 2.4: An example of the analysis of a single fluorescence spot. The red curve shows the most appropriate ellipsoid for the segmental distribution.

where I_i is the fluorescence intensity at the i-th pixel, $\mathbf{r}_i$ is the position vector, and I is the total fluorescence intensity from the single chain. The second moment of the fluorescence intensity distribution is calculated as

$$R_{xx}^2 = \frac{1}{I}\sum_i (x_i - x_0)^2 I_i, \tag{2.3}$$

$$R_{yy}^2 = \frac{1}{I}\sum_i (y_i - y_0)^2 I_i, \tag{2.4}$$

$$R_{xy}^2 = R_{yx}^2 = \frac{1}{I}\sum_i (x_i - x_0)(y_i - y_0)I_i, \tag{2.5}$$

where (x_i, y_i) and (x_0, y_0) are the position of the i-th pixel and the center of mass in the orthogonal coordinate system. The x axis is defined as the macroscopic extension axis of the film. R_{xx} and R_{yy} indicate the dimensions of the fluorescence spot along the x and y
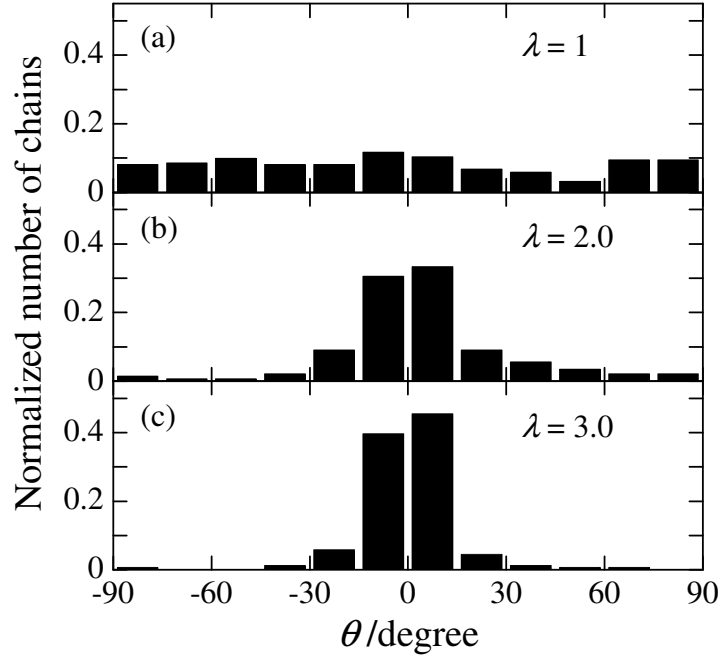
23

Figure 2.5: Histograms of the orientation angle of the PMMA chain to the stretching direction of the film: (a) before stretching, and after stretching to the extension ratio of (b) 2.0 and (c) 3.0.

axes, respectively. The tensor $\mathbf{R}$ is a parameter related to the polymer conformation:[23]

$$\mathbf{R} = \begin{pmatrix} R^2_{xx} & R^2_{xy} \\ R^2_{yx} & R^2_{yy} \end{pmatrix}.$$

(2.6)

The eigenvalues λ_1 and λ_2 $(\lambda_1 > \lambda_2)$ of $\mathbf{R}$ correspond to the squared lengths of the long and short axes, respectively, of the most appropriate ellipsoid for the segmental distribution as shown in Figure 2.4. The angle, θ, between the extension axis and the long axis of the ellipsoid is given by

$$\theta = \arctan\left(\frac{\lambda_1 - R^2_{xx}}{R^2_{xy}}\right).$$

(2.7)

Figure 2.5 shows the histogram of θ for the 150 PMMA-Pe chains. It clearly shows that before stretching each chain was randomly oriented. After stretching, the orientation
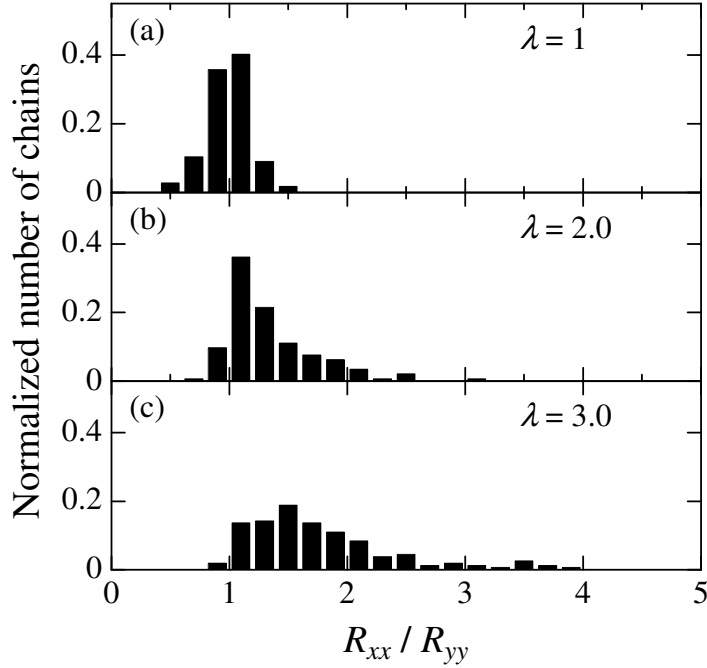
Figure 2.6: Histograms of the chain aspect ratio R_{xx}/R_{yy} in the film (a) before stretching, and after stretching to the extension ratio of (b) 2.0 and (c) 3.0.

angle shows the narrow distribution with a peak at $\theta \sim 0°$. This indicates that the PMMA chains in the elongated films take stretched conformations along the elongation axis. The distribution narrowed with strain. None of the PMMA chains showed the orientation of $|\theta| > 45°$ at $\lambda = 3.0$, indicating that all the chains deformed to the stretching direction.

Not only the direction of the orientation, the asphericity of the single chain is discussed in terms of the aspect ratio R_{xx}/R_{yy}, which is the ratio of the chain dimensions along the parallel and perpendicular axes to the stretching direction. Figure 2.6 shows the distribution of R_{xx}/R_{yy} in the films before and after stretching. Before stretching, the PMMA chain did not show the circular form due to the conformational distribution. However, the orientation of the chain conformation was random, resulting in the homogeneous distribution of the orientational angle θ and the distribution of R_{xx}/R_{yy} in the range of 0.5–1.5 with the maximum probability at unity: $\langle R_{xx}/R_{yy}\rangle = 1.00 \pm 0.18$. On the other hand, the asphericity of the PMMA chains increased by the macroscopic

elongation and its distribution spread: $\langle R_{xx}/R_{yy} \rangle = 1.35 \pm 0.38$ and 1.78 ± 0.63 in the films of $\lambda = 2.0$ and 3.0, respectively. Few chains showed the asphericity less than unity after stretching, indicating that most of the chains were deformed by the macroscopic elongation.

The deformation at the single chain level is compared with the macroscopic extension ratio. In order to compare the conformational change of the polymer chains with the macroscopic extension ratio, the author defined the extension ratio at the single chain level, λ_{c}, as

$$\lambda_{c}^{2} = \frac{\langle R_{xx}^{*}{}^{2} \rangle}{\langle R_{xx}^{*}{}^{2} \rangle_{0}}, \tag{2.8}$$

where $\langle R_{xx}^{*}{}^{2} \rangle_{0}$ and $\langle R_{xx}^{*}{}^{2} \rangle$ denote the average of the true dimension of chains along the x axis before and after stretching as follows,

$$R_{xx}^{*}{}^{2} = \frac{1}{N} \sum_{j}^{N} (x_{j} - x_{0})^{2}, \tag{2.9}$$

where N is the number of segments and x_{j} is the x-coordinate of the position of the j-th segment of the chain.[23] SNOM shows much higher resolution than conventional microscopy; however, it still suffers from the limit of finite resolution of ~ 100 nm, which is caused by finite dimension of the aperture. Therefore, the observed value of R_{xx} is somewhat larger than the true value, R_{xx}^{*}. The point spread function in fluorescence SNOM measurement is well approximated as a Gauss function, which was determined from the observation of a quantum dot.[24] The fluorescence image is expressed by the convolution of the distribution function of the chain segment and the point spread function. The second moment of the convoluted function is a sum of the second moments of the original functions.[25] Therefore,

$$R_{xx}^{2} = R_{xx}^{*}{}^{2} + a^{2}, \tag{2.10}$$

where a^{2} is the variance of the point spread function. As for the direction perpendicular to
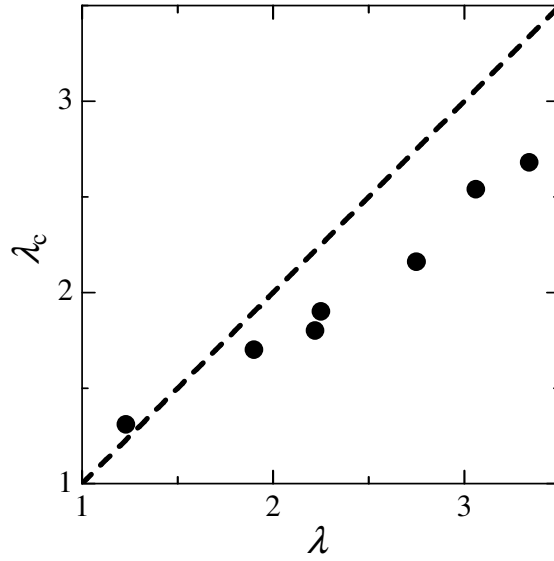
Figure 2.7: Average chain extension ratio plotted against the macroscopic extension ratio of the film. The broken line indicates the case of the affine deformation ($\lambda_\mathrm{c} = \lambda$).

the stretching axis, the change in the dimension was too small for the precise evaluation. Therefore, the author focused on the direction parallel to the stretching axis.

Figure 2.7 shows the relationship between the microscopic and macroscopic extension ratio. The macroscopic strain is not homogeneous through the whole film because the plastic deformation occurs. For this reason, the macroscopic extension ratio in Figure 2.7 was estimated from the change in the width of the film at the position observed by SNOM assuming the constant volume during the deformation. The average chain extension ratio was smaller than the macroscopic extension ratio, showing the deviation from affine deformation at the single chain level. Under the condition that the plastic deformation occurs, the thermal motion of the polymer chain is not sufficient to follow the mechanical deformation. It is suggested that the chains slip along the adjacent chains during the plastic deformation.

2.4 Conclusion

The conformation of the single polymer chain in uniaxially stretched PMMA was studied by SNOM. The direct observation of the individual elongated single polymer chain was succeeded. The conformation of the single PMMA chain was quantitatively evaluated from the fluorescence intensity distribution. The chain showed smaller deformation than that expected from the affine deformation, suggesting the presence of chain slip in the film. The further study using SNOM is expected to reveal the mechanical property of polymer solids from the level of single polymer chain.

References

[1] Benoit, H.; Duplessix, B.; Ober, R.; Daoud, M.; Cotton, J. P.; Farnoux, B.; Jannink, G. *Macromolecules* **1975**, *8*, 451–453.

[2] Sperling, L. H. *Polym. Eng. Sci.* **1984**, *24*, 1–21.

[3] Hammouda, B.; Bubeck, R. A.; Mildner, D. F. *Polymer* **1986**, *27*, 393–397.

[4] Schroeder, J. R.; Hammouda, B.; Bubeck, R. A.; Chang., J. W. *J. Polym. Sci. B, Polym. Phys.* **1991**, *29*, 1607–1612.

[5] Benoit, H.; Decker, D.; Duplessix, R.; Picot, C.; Rempp, P.; Cotton, J. P.; Farnoux, B.; Jannink, G.; Ober, R. *J. Polym. Sci., Polym. Phys. Ed.* **1976**, *14*, 2119–2128.

[6] Hinkley, J. A.; Han, C. C.; Mozer, B.; Yu, H. *Macromolecules* **1978**, *11*, 836–838.

[7] Clough, S. B.; Maconnachie, A.; Allen, G. *Macromolecules* **1980**, *13*, 774–775.

[8] Tsay, H. M.; Ullman, R. *Macromolecules* **1988**, *21*, 2963–2972.

[9] Picot, C.; Duplessix, R.; Decker, D.; Benoit, H.; Boué, F.; Cotton, J. P.; Daoud, M.; Farnoux, B.; Jannink, G.; Nierlich, M.; de Vries, A. J.; Pincus, P. *Macromolecules* **1977**, *10*, 436–442.

[10] Kumaki, J.; Nishikawa, Y.; Hashimoto, T. *J. Am. Chem. Soc.* **1996**, *118*, 3321–3322.

[11] Kumaki, J.; Hashimoto, T. *J. Am. Chem. Soc.* **2003**, *125*, 4907–4917.

[12] Kiriy, A.; Gorodyska, G.; Minko, S.; Stamm, M.; Tsitsilianis, C. *Macromolecules* **2003**, *36*, 8704–8711.

[13] Maier, B.; Rädler, J. O. *Phys. Rev. Lett.* **1999**, *82*, 1911–1914.

[14] Maier, B.; Rädler, J. O. *Macromolecules* **2001**, *34*, 5723–5724.

[15] Betzig, E.; Trautman, J. K. *Science* **1992**, *257*, 189–195.

[16] Ohtsu, M. *Near-field Nano/Atom Optics and Technology*; Springer: Tokyo, 1998.

[17] Aoki, H.; Ito, S. *J. Phys. Chem. B* **2001**, *105*, 4558–4564.

[18] Aoki, H.; Kunai, Y.; Ito, S.; Yamada, H.; Matsushige, K. *Appl. Surf. Sci.* **2002**, *188*, 534–538.

[19] Ito, S.; Aoki, H. *Bull. Chem. Soc. Jpn.* **2003**, *76*, 1693–1705.

[20] Ito, S.; Aoki, H. *Adv. Polym. Sci.* **2005**, *182*, 131–169.

[21] Aoki, H.; Anryu, M.; Ito, S. *Polymer* **2005**, *46*, 5896–5902.

[22] Kraus, J.; Müller-Buschbaum, P.; Kuhlmann, T.; Schubert, D. W.; Stamm, M. *Europhys. Lett.* **2000**, *49*, 210–216.

[23] Rudnick, J.; Gaspari, G. *Science* **1987**, *237*, 384–389.

[24] Yang, J.; Sekine, R.; Aoki, H.; Ito, S. *Macromolecules* **2007**, *40*, 7573–7580.

[25] Laury-Micoulaut, C. A. *Astron. Astrophys.* **1976**, *51*, 343–346.

Chapter 3

Affine Deformation of Single Polymer Chain in PMMA Films

under Uniaxial Extension Observed by SNOM

3.1   Introduction

The microscopic molecular structures of polymer chains such as orientation and conformation are closely related with macroscopic properties of polymer materials. Observing and controlling the chain structures are significant from both scientific and practical points of view. The stress induced by external deformation gives rise to the segmental orientation, which is observed by birefringence[1,2] and infrared absorption dichroism.[1,3] The stress–optical rule ensures the relationship between the chain motion and viscoelastic quantities. Abundant rheological studies have contributed to the developments of molecular models for the chain dynamics.[4,5] One of the most successful models for the entangled polymer system is the tube model developed by Doi and Edwards.[6] In this model, a tube along a certain chain is introduced to represent the topological constraint from the neighboring chains. It assumes the affine deformation under step strain and reptation along the tube. The segmental orientation simulated under these microscopic assumptions well describes viscoelastic behavior. Further improvement of the model is performed by considering the relaxation of surrounding chains in terms of constraint release and dynamic tube dilation.

The theoretical models predict the chain motion not only in the segmental scale but also in the length scale of the whole single chain, which is characterized by parameters such as radius of gyration. The radius of gyration of a polymer chain in bulk systems has been experimentally investigated by SANS.[7] Boué et al. studied the conformational change of polystyrene chains under uniaxial extension, concluding that the radius of gyration changes according to affine deformation soon after stretching for

31

large enough chains.[8–10] The complementary observation in different length scales gives further insights of polymer dynamics. However, the segmental orientation and the radius of gyration obtained by the above methods are the averaged value for the numerous chains in the system, whereas the theoretical models are based on the behavior of single polymer chains. The observation of single polymer chains enables us to discuss the motion of individual chains in association with the variety of the chain conformation. The assumptions about the chain motion in the theoretical models are more clearly tested by observing individual properties of single polymer chains, which do not suffer from blur by averaging over a large number of chains.

In order to detect in-situ features of polymer chains locating inside a bulk medium, a single chain must be distinguished from its surroundings. Fluorescence labeling is an established method, which has been applied to observe single DNA molecules. Chu et al. studied the conformational change of single DNA molecules under elongational flow.[11] However, the conventional fluorescence microscopy suffers from the low spatial resolution due to the diffraction limit to a half of the wavelength of light. Therefore, the application of the optical microscopy to single macromolecular imaging has been limited to the observation of huge biomacromolecules such as DNA. SNOM is an emerging scanning probe technique, which allows optical measurement with a high resolution beyond the diffraction limit of light. This enables us to directly observe the conformation of the single chain, which is fluorescently labeled and silhouetted against surrounding unlabeled polymers.

In the previous chapter, the author showed that SNOM is a promising method to observe the elongated conformation of single polymer chains under the uniaxial deformation. The chain conformation of PMMA was examined under the plastic deformation. It was shown that the microscopic strain of the single chain was smaller than the macroscopic strain, suggesting the presence of slipping of polymer chain on the course of stretching. In the current chapter, the author reports the case of the elastic deformation. The PMMA films were uniaxially stretched well above the glass transition temperature,

quenched to room temperature, and then the conformation of the whole single chain was observed by SNOM. The chain deformations in different molecular weight matrices are discussed with the results of SNOM and birefringence.

3.2 Experiments

Sample preparation. The synthesis of perylene-labeled PMMA (PMMA-Pe, Figure 2.1) is described elsewhere.[12,13] The fraction of the labeled unit was evaluated to be 0.77% by UV–Vis absorption (U3500, Hitachi). The unlabeled PMMAs with high and low molecular weights (denoted as PMMA-*h* and PMMA-*l*, respectively) were synthesized by atom transfer radical polymerization.[14] Methyl methacrylate was polymerized with *p*-toluenesulfonyl chloride in conjunction with copper(I) chloride and 4,4'-dinonyl-2,2'-dipyridyl at 70 °C in vacuum. The weight- and number-averaged molecular weights, M_w and M_n, were determined by GPC measurement as shown in Table 3.1.

In order to observe the single labeled chains in the PMMA bulk by SNOM, the sample containing a trace amount of PMMA-Pe near the surface was prepared in the following procedure. A mixed toluene solution of the unlabeled PMMA (PMMA-*h* or PMMA-*l*) and PMMA-Pe (0.005 wt % to the unlabeled polymer) was spin-coated onto a glass substrate to form a film with a thickness of 80 nm. The thin film was floated onto a water surface and scooped up on a self-standing thick film of the unlabeled PMMA (the size was 25 mm × 7 mm, and the thickness was 300 μm), which was prepared separately

Table 3.1: Characterization of PMMA.

Sample	$M_w/10^6$	$M_n/10^6$	M_w/M_n
PMMA-Pe	1.99	1.58	1.26
PMMA-*h*	1.89	1.53	1.24
PMMA-*l*	0.176	0.132	1.33

by the solution casting. The conformation of PMMA-Pe may be affected by the shear flow in the spin-coating process and the confinement effect of the thin film. Therefore, the sample film was annealed for 48 h at 200 °C, which is longer than the relaxation time estimated from the literature,[15] in vacuum to reach the equilibrium.

Tensile deformation. A tensile tester (RTM-500, Orientec) with a 10 kg load cell was used for stretching the films. The length between the clamps was 20 mm. The stretching was carried out at 160 °C with a crosshead speed of 5 mm/min. The force and displacement were monitored on a chart recorder. The extension ratio, λ, was calculated as l/l_0, where l_0 and l are the lengths of the film along the stretching direction before and after the elongation, respectively. The true stress, σ, was evaluated as follows assuming the constant volume of the film:

$$\sigma = \frac{F}{A} = \frac{F}{A_0}\lambda. \tag{3.1}$$

where F is the force applied to the sample, A is the sample cross section at the extension ratio of λ, A_0 is the cross section at $\lambda = 1$. After the stretching to the various extension ratios, the thermostatic chamber was opened and the film was rapidly cooled by the blow of air at room temperature. In this quenching procedure, the film was returned to the glassy state within 10 s.

Birefringence measurement. The birefringence measurement was carried out by Senarmont method. The optical system was composed of a laser, a polarizer, a quarterwave plate, an analyzer, and a photo detector. The axes of the polarizer and the quarterwave plate were set at 45° to the strain axis. After passing through the oriented sample, the plane polarized light becomes elliptically polarized. The quarterwave plate converts elliptical polarization into linear polarization with the azimuthal angle, φ, which was determined by rotating the analyzer. The retardation, Γ, was evaluated as $\Gamma = \lambda_L(\varphi/\pi)$, where λ_L is the incident wavelength. The birefringence, Δn, was

determined as $\Delta n = \Gamma/d$, where d is the sample thickness.

SNOM measurement. The SNOM measurement was performed by a commercially available instrument (α-SNOM, WITec) using a hollow cantilever probe with a sub-wavelength aperture of 60 nm. The laser beam at a wavelength of 438 nm (BCL-015-440, CrystaLaser) was focused onto the backside of the aperture to generate the optical near-field. While scanning the sample surface in the contact mode with the cantilever, the perylene fluorescence was collected by a microscope objective (0.80NA, 60×, Nikon) from the backside of the substrate, passed through a long-pass filter (AELP454, Omega Optical), and detected with a photomultiplier (H8631, Hamamatsu Photonics). The SNOM measurement was carried out in an ambient condition. All the SNOM images were taken by the same probe.

3.3   Results and Discussion

3.3.1   Stress and Birefringence

Figure 3.1 shows the true stress – extension ratio curves of the PMMA films stretched at 160 °C. Since the extension was carried out much above the glass transition temperature, the stress monotonously increased with the extension ratio. Figure 3.2 shows the birefringence of the quenched film plotted against the extension ratio. Birefringence is related to the orientation of the chain segment as

$$\Delta n = \Phi \Delta n_0, \tag{3.2}$$

where Δn_0 is the intrinsic birefringence and Φ is an orientational order parameter

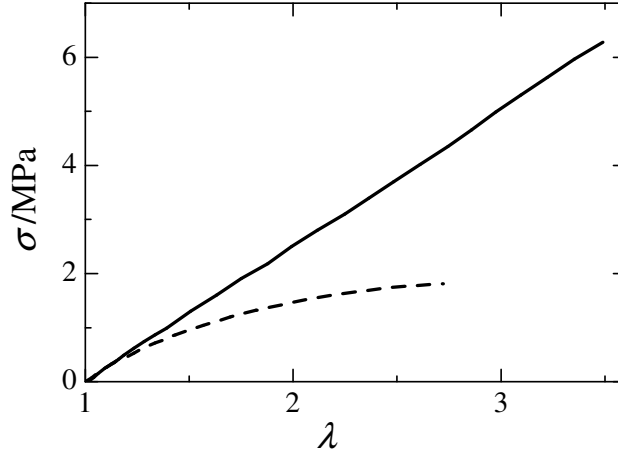$$\Phi = (3\langle \cos^2 \phi \rangle - 1)/2, \tag{3.3}$$

Figure 3.1: True stress – extension ratio curves of PMMA-*h* and PMMA-*l* films (solid and dashed curves, respectively) stretched at 160 °C with a crosshead speed of 5 mm/min.

where ϕ is the angle between the stretching direction and the main axis of the structural unit, and $\langle \ \rangle$ represents the statistical average. The random orientation gives $\Phi = 0$, whereas the perfect uniaxial orientation gives $\Phi = 1$. The intrinsic birefringence of PMMA is reported as $\Delta n_0 = -0.0043$.[16] Applying this value to the birefringence data, the author calculated the orientational order parameter, which is shown in the right axis of Figure 3.2. Under the assumption that each entanglement point changes its position affinely by the macroscopic deformation, the extension ratio dependence of Φ after the step strain is given from the rubber elasticity theory:[17,18]

$$\Phi = \frac{1}{5n_e}\left(\lambda^2 - \frac{1}{\lambda}\right),\tag{3.4}$$

where n_e denotes the number of segment between entanglements. The value of n_e is determined from the experimental data of Φ at the early stage of the deformation. The dashed curve in Figure 3.2 shows the theoretical curve obtained from eq 3.4 with $n_e = 6.7$. For the PMMA-*h* film, the experimental values of Δn ($\Phi = \Delta n/\Delta n_0$) almost agreed with the theoretical values based on the affine network model. The deviation at high extension ratios suggests that the segmental orientation of the polymer chain was somewhat relaxed
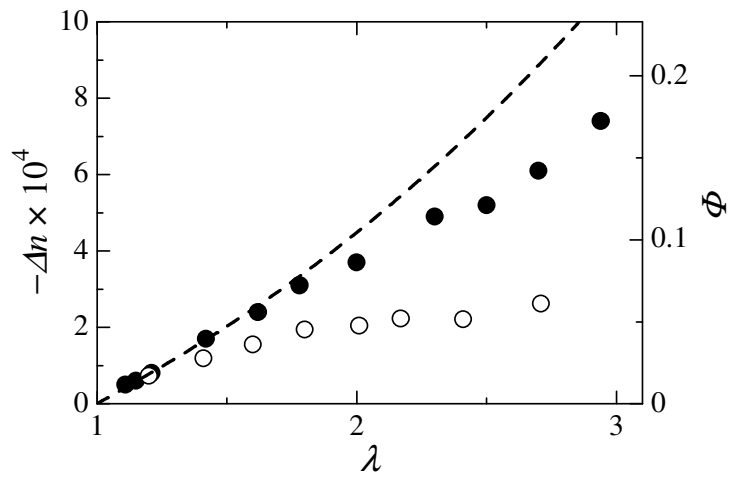
Figure 3.2: Birefringence of the stretched PMMA films plotted against the extension ratio. Closed and open circles represent PMMA-*h* and PMMA-*l*, respectively. The right axis shows the orientational order parameter, and the dashed curve shows the calculated Φ value based on the affine network model (eq 3.4).
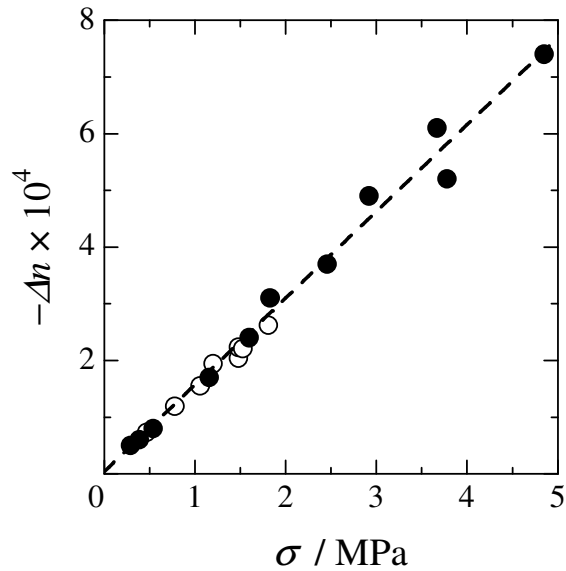

Figure 3.3: Birefringence of the stretched PMMA films plotted against stress. Closed and open circles represent PMMA-*h* and PMMA-*l*, respectively.
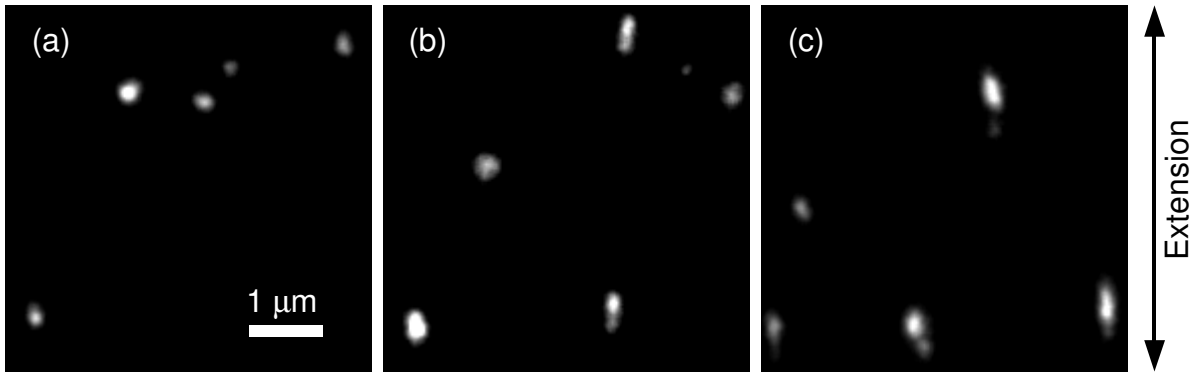
37

Figure 3.4: Fluorescence SNOM images of single polymer chains in the PMMA-*h* films (a) before stretching, and after stretching to the extension ratio of (b) 2.0 and (c) 3.0.

during the extension process. The PMMA-*l* film showed smaller stress and birefringence compared with the PMMA-*h* film because the shorter chains relax more rapidly.

Figure 3.3 shows the birefringence plotted against the stress. The birefringence was proportional to the stress according to the stress–optical rule,[6]

$$\Delta n = C\sigma, \tag{3.5}$$

where C is the stress–optical coefficient. This indicates that the stress is directly related to the orientation of the chain segment, not affected by the finite extensibility of the chain[19] and the glassy component[20] in the current experimental condition. From Figure 3.3, C was evaluated to be -1.5×10^{-10} Pa^{-1} , which is in good agreement with the values reported in the literature.[1,2]

3.3.2 SNOM Image

Figure 3.4 shows the fluorescence SNOM images of the PMMA films under the uniaxial extension. The perylene-labeled PMMA chains embedded in the unlabeled bulk film were observed as the bright spots in the fluorescence image. Each fluorescence spot was confirmed to be individual PMMA-Pe chain from the statistical analysis.[21] Since

38

the optical near-field penetrates into the sample film by a few hundred nm, the shape of the PMMA chain observed in the SNOM image is given as a two-dimensional projection of the chain conformation. In Figure 3.4a, the single PMMA-Pe chains with the same molecular weight were observed in various forms, indicating the flexibility of the PMMA chain. Figures 3.4b and 3.4c depict the SNOM images of the films after stretching at the extension ratio of 2.0 and 3.0, respectively. These images clearly show the polymer chains with elongated conformations along the macroscopic stretching direction. It was confirmed that the conformation of the whole single chain does not change after relaxation periods of 10–60 s, therefore the conformation was not disturbed by the quenching process.

3.3.3 Average Chain Extension Ratio

The conformation of the single PMMA chain was quantitatively evaluated from the fluorescence intensity distribution in terms of the true dimension along the stretching direction R_{xx}^* (eq 2.9), the angle θ between the extension axis and the long axis of the most appropriate ellipsoid for the segmental distribution (eq 2.7), and the average chain extension ratio λ_c (eq 2.8) by the procedure shown in chapter 2. Figure 3.5 shows the relationship between the extension ratio λ_c at the single chain level and the ratio λ at the macroscopic level. As for the samples with the high molecular weight matrix, λ_c was almost equal to λ. This indicates the affine deformation of the single polymer chain in the sense that the dimension of the whole single chain changes in the same ratio as the macroscopic deformation of the film. It should be noted that SNOM and the birefringence have different length scale of the observation: SNOM measures the dimension of the whole contour of the single chain whereas the birefringence measures the orientation of the segment. As shown in Figure 3.2, some parts of the segmental orientation is relaxed by the rearrangement in a relatively small length scale, which occurs within the time scale of the extension process. On the other hand, the relaxation of the chain dimension occurs by the motion of the whole chain contour, which is described as contraction and reptation
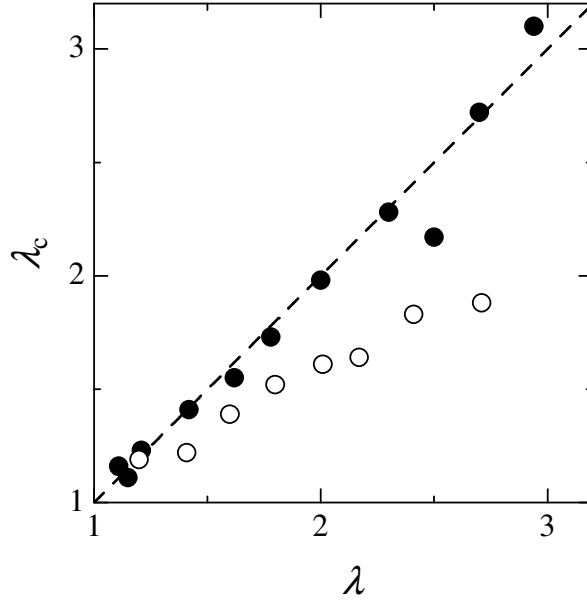
39

Figure 3.5: Average chain extension ratio λ_c plotted against the macroscopic extension ratio λ of the film. Closed and open circles represent the samples with PMMA-*h* and PMMA-*l* matrices, respectively. The dashed line indicates the affine deformation ($\lambda_c = \lambda$).

in the tube model.[6] In the current condition of the tensile deformation, the relaxation of the whole single chains hardly occurs during the extension process because of the large molecular weight of $M_w \simeq 2 \times 10^6$ compared with the molecular weight between entanglements, M_e, of PMMA; $M_e \simeq 4\text{--}10 \times 10^3$.[22-24]

Next, the extension of the chains embedded in the low molecular weight bulk medium is considered. The labeled chains in the PMMA-*l* matrix showed smaller λ_c than λ. This is caused by the disentanglement of the matrix chain from the probe chain during the stretching of the film. Thus, the degree of the chain deformation depends on the molecular weight of the surrounding chains. The affine deformation of a whole chain is observed only when the rate of the disentanglement is much slower than the extension of the film.
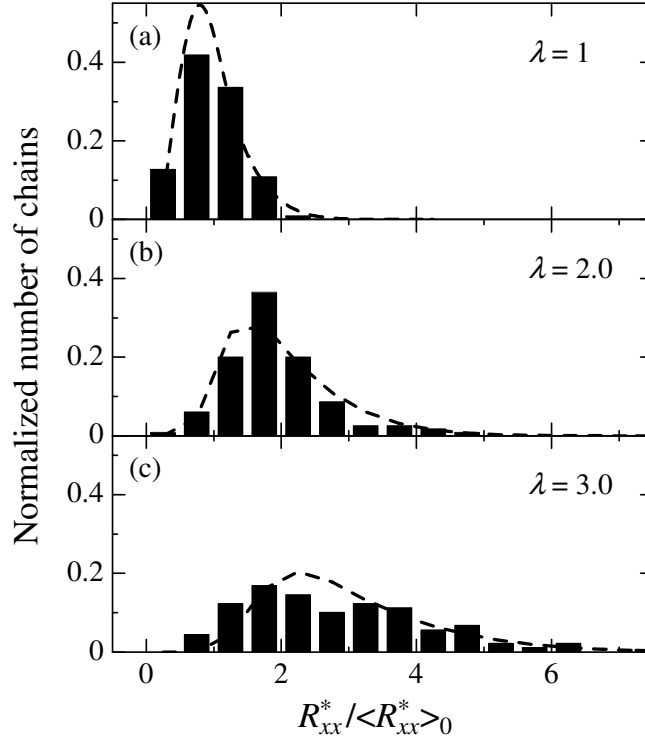
Figure 3.6: Histograms of the chain dimension parallel to the stretching direction normalized by the initial average value in the film (a) before stretching, and after stretching to the extension ratio of (b) 2.0 and (c) 3.0. The matrix is PMMA-*h*. The dashed lines indicate the results of random walk simulation followed by affine deformation.

3.3.4 Distribution of the Chain Conformation

The author next focuses on the conformation of individual polymer chains, taking the advantage of the single chain observation. Since the author could not observe the same polymer chain before and after stretching due to the experimental difficulty, the conformational change is discussed in terms of the distribution of the chain dimension along the extension axis normalized by its initial average, $R_{xx}^*/\langle R_{xx}^*\rangle_0$, and the angle θ between the main axis of the whole chain and the extension axis. Figure 3.6 shows histograms of $R_{xx}^*/\langle R_{xx}^*\rangle_0$ for the samples with PMMA-*h* matrix ($\lambda = 1, 2.0,$ and 3.0). The variety of the values results from the conformational distribution of the PMMA chains. The standard deviations of $R_{xx}^*/\langle R_{xx}^*\rangle_0$ were 0.43, 0.78, and 1.32 for the samples with $\lambda = 1, 2.0$ and 3.0, respectively.
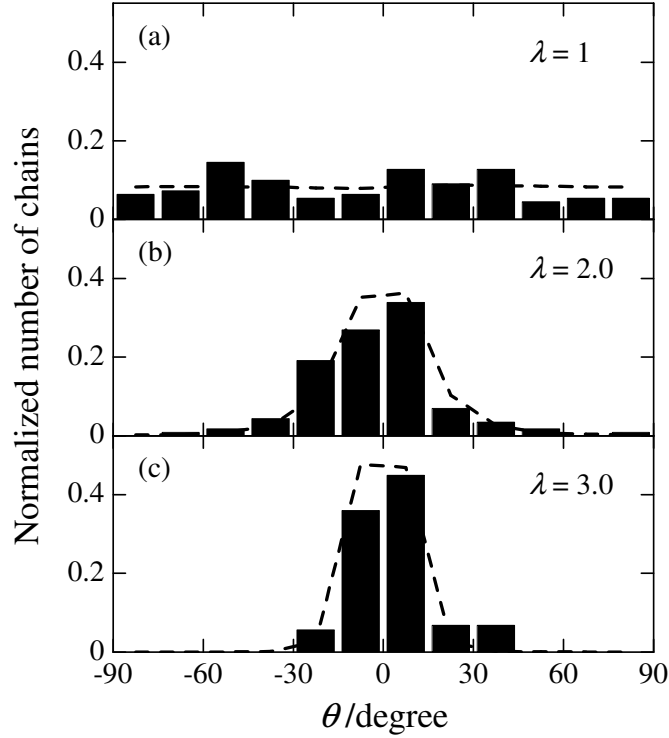
Figure 3.7: Histograms of the orientation angle of the PMMA chain to the stretching direction of the film (a) before stretching, and after stretching to the extension ratio of (b) 2.0 and (c) 3.0. The matrix is PMMA-*h*. The dashed lines indicate the results of random walk simulation followed by affine deformation.

Figure 3.7 shows histograms of θ for the same samples. It clearly shows that before stretching each chain was randomly oriented. After stretching, the orientation angle shows the narrow distribution with a peak at $\theta \sim 0°$. This indicates that the PMMA chains in the elongated film takes a stretched conformation along the elongation axis. The distribution of θ narrowed with the increase of the macroscopic strain. The standard deviations of θ were 48.1, 21.8, 12.5 for the samples with $\lambda = 1$, 2.0 and 3.0, respectively.

The experimental values of $R_{xx}^*/\langle R_{xx}^*\rangle_0$ and θ are compared with those obtained from the random walk simulation. The freely-jointed chains were generated in three dimensional space by Monte Carlo method. In the simulation of the uniaxial extension of the film, the affine deformation of the all segment was assumed. R_{xx}^* was calculated from eq 2.9 for each generated chain. The angle θ was also determined by the same

procedure as eq 2.7. The dashed lines in Figures 3.6 and 3.7 show the results of the random walk simulation. Both of the experimentally obtained histograms for $R_{xx}^*/\langle R_{xx}^*\rangle_0$ and θ were in good agreement with the random walk simulation on the basis of the affine deformation not only for the average value but also for the distribution function. This indicates that the polymer chain with a large molecular weight deforms according to the affine transformation at the single chain level.

3.4   Conclusion

SNOM was applied to observe the single polymer chains embedded in the PMMA films, which were stretched much above the glass transition temperature. For the samples with the high molecular weight matrix, the average chain extension ratio coincided with the macroscopic extension ratio, showing the affine deformation of the whole chain, whereas the segmental orientation evaluated from birefringence was smaller than that expected from the affine network model. Thus, the extension of the polymer chain depends on its length scale of the observation. In the low molecular weight matrix, the chain extension ratio was smaller than the macroscopic extension ratio, which is caused by the disentanglement of the short matrix chain from the probe chain. The variety of the single chain conformation was analyzed in terms of the chain dimension along the extension axis, and the angle between the main axis of the whole chain and the extension axis. For the sample with high molecular weight matrix, these parameters almost agreed with those obtained from random walk simulation followed by affine deformation not only for the average value but also for the distribution.

References

[1] Kahar, N.; Duckett, R. A.; Ward, I. M. *Polymer* **1978**, *19*, 136–144.

[2] Marrucci, G.; de Cindio, B. *Rheol. Acta.* **1980**, *19*, 68–75.

[3] Zhao, Y.; Jasse, B.; Monnerie, L. *Makromol. Chem. Macromol. Symp.* **1986**, *5*, 87–97.

[4] Watanabe, H. *Prog. Polym. Sci.* **1999**, *24*, 1253–1403.

[5] McLeish, T. C. B. *Adv. Phys.* **2002**, *51*, 1379–1527.

[6] Doi, M.; Edwards, S. F. *The Theory of Polymer Dynamics*, 3rd ed.; Clarendon: Oxford, 1986.

[7] Cotton, J. P.; Decker, D.; Benoit, H.; Farnoux, B.; Higgins, J.; Jannink, G.; Ober, R.; Picot, C.; des Cloizeaux, J. *Macromolecules* **1974**, *7*, 863–872.

[8] Boué, F. *Adv. Polym. Sci.* **1987**, *82*, 47–101.

[9] Picot, C.; Duplessix, R.; Decker, D.; Benoit, H.; Boué, F.; Cotton, J. P.; Daoud, M.; Farnoux, B.; Jannink, G.; Nierlich, M.; de Vries, A. J.; Pincus, P. *Macromolecules* **1977**, *10*, 436–442.

[10] Boué, F.; Nierlich, M.; Jannink, G.; Ball, R. *J. Phys. (Paris)* **1982**, *43*, 137–148.

[11] Smith, D. E.; Chu, S. *Science* **1998**, *281*, 1335–1340.

[12] Aoki, H.; Tanaka, S.; Ito, S.; Yamamoto, M. *Macromolecules* **2000**, *33*, 9650–9656.

[13] Aoki, H.; Morita, S.; Sekine, R.; Ito, S. *Polym. J.* **2008**, *40*, 274–280.

[14] Grimaud, T.; Matyjaszewski, K. *Macromolecules* **1997**, *30*, 2216–2218.

[15] Masuda, T.; Kitagawa, K.; Onogi, S. *Polym. J.* **1970**, *1*, 418–424.

[16] Kashiwagi, M.; Folkes, M. J.; Ward, I. M. *Polymer* **1971**, *12*, 697–710.

[17] Roe, R. J.; Krigbaum, W. R. *J. Appl. Phys.* **1964**, *35*, 2215–2219.

[18] Treloar, L. R. G. *The Physics of Rubber Elasticity*, 3rd ed.; Clarendon: Oxford, 1975.

[19] Matsumoto, T.; Bogue, D. C. *J. Polym. Sci., Polym. Phys. Ed.* **1977**, *15*, 1663–1674.

[20] Inoue, T.; Okamoto, H.; Osaki, K. *Macromolecules* **1991**, *24*, 5670–5675.

[21] Aoki, H.; Kunai, Y.; Ito, S.; Yamada, H.; Matsushige, K. *Appl. Surf. Sci.* **2002**, *188*, 534–538.

[22] Fetters, L. J.; Lohse, D. J.; Richter, D.; Witten, T. A.; Zirkel, A. *Macromolecules* **1994**, *27*, 4639–4647.

[23] Fuchs, K.; Friedrich, C.; Weese, J. *Macromolecules* **1996**, *29*, 5893–5901.

[24] Ferry, J. D. *Viscoelastic Properties of Polymers*, 3rd ed.; Wiley: New York, 1980.

Chapter 4

Relaxation of Single Polymer Chain in PMMA Films

under Uniaxial Extension Observed by SNOM

4.1   Introduction

The relaxation behavior of polymer melts has long been investigated because of its importance both in scientific and industrial fields. The stress induced by an external strain is relaxed through the motion of deformed polymer chains to the equilibrium conformations. In entangled polymer systems, the relaxation is slow because of the mutual uncrossability of the chains. The dynamics in such systems has been explained by the molecular models based on the tube model by de Gennes,[1] Doi and Edwards.[2–5] In the Doi–Edwards model, the chain motion is constrained in a tube-like region surrounding the chain backbone. When the system is deformed by a step strain, the chain changes in conformation according to affine deformation. Then, these chains relax through the motions along the tube: the contraction of the chain contour and the reptation. The stress is calculated under these assumptions of the chain dynamics. The tube model has been improved to explain the viscoelastic properties of various systems by considering the contour length fluctuation and the relaxation of surrounding chains.[6,7] While theoretical molecular models express the mechanical properties and have been compared with rheological experiments, they also predict the time evolution of the chain conformation. The observations of the polymer chain at the various length scales are essential to evaluate the chain motion, which is assumed in theoretical models. The average dimension of a whole single chain under external stress has been measured by SANS in concentrated polymer systems.[8–12] The recent improvement of the SANS instrument enabled the detection of the conformational relaxation consistent with the contraction of the chain contour.[12] The scattering measurement has great advantage in the high resolution; but the

variety of chain conformations is canceled in the value averaged over the bulk sample. The observation of individual single polymer chains could reveal the exact behavior of real chains, which possibly depends on initial chain conformations and surrounding conditions. The understanding of the distribution of the chain motion will lead to the improvement of theoretical models, which have been based on the pre-averaged chain dynamics.[7]

The direct observation of single polymer chain has been performed for fluorescently labeled DNA molecules. Chu et al. succeeded in the direct observation of the tube-like motion of DNA chains by fluorescence microscopy.[13] The conformational changes of DNA molecules in a dilute and entangled solution under flow have also been studied.[14,15] However, the conventional fluorescence microscopy has a low spatial resolution of ~ 250 nm due to the diffraction-limit of light. Therefore, the application of optical microscopy to single macromolecular imaging has been limited to the observation of huge biomacromolecules such as DNA. SNOM is an emerging scanning probe technique, which allows optical measurement with a high resolution beyond the diffraction limit. This enables us to directly observe the in-situ conformation of the single chain in a concentrated system.

In the previous chapters, the author observed a deformation of PMMA chains in the films under uniaxial deformation. It was revealed that the dimension of the whole single chain increased affinely with the macroscopic strain when the film is stretched well above the glass transition temperature. In the current chapter, the chain conformation during the stress relaxation process is investigated by SNOM in contrast with the stress and the birefringence. Furthermore, the experimental results are compared with the theoretical prediction by the Doi–Edwards model.

4.2 Experiments

Sample preparation. Perylene-labeled PMMA (PMMA-Pe, Figure 2.1) was synthesized as described elsewhere.[16,17] The fraction of the labeled unit was evaluated to be 0.77% by UV–Vis absorption (U3500, Hitachi). The unlabeled PMMA was synthesized by atom transfer radical polymerization.[18] Methyl methacrylate was polymerized with p-toluenesulfonyl chloride in conjunction with copper(I) chloride and 4,4'-dinonyl-2,2'-dipyridyl at 70 °C in vacuum. The weight- and number-averaged molecular weights, M_w and M_n, were determined by GPC measurement as shown in Table 4.1.

In order to observe single labeled chains in the PMMA bulk by SNOM, the author prepared the sample containing a trace amount of PMMA-Pe near the surface by the following procedure. A mixed toluene solution of unlabeled PMMA and PMMA-Pe (0.005 wt % to the unlabeled polymer) was spin-coated onto a glass substrate to form an 80-nm-thick film. The thin film was floated on water and deposited on a self-standing thick film of unlabeled PMMA (the size was 25 mm × 7 mm, and the thickness was 300 μm), which was prepared separately by the solution casting. The conformation of PMMA-Pe may be affected by the shear flow in the spin-coating process and the confinement effect of the thin film. Therefore, the sample film was annealed for 48 h at 200 °C, which is longer than the relaxation time estimated from the literature,[19] in vacuum to reach the equilibrium.

Table 4.1: Characterization of PMMA.

Sample	$M_w/10^6$	$M_n/10^6$	M_w/M_n
PMMA-Pe	1.99	1.58	1.26
PMMA	1.89	1.53	1.24

Tensile deformation. A tensile tester (RTM-500, Orientec) with a 10 kg load cell was used for stretching the films. The length between the clamps was 20 mm. The stretching was carried out at 160–200 °C with a crosshead speed of 50 mm/min. After the stretching, the clamp gap was kept constant for time t. Then the films were immediately quenched to room temperature. The force was monitored on a chart recorder throughout the stretching and relaxation processes. The extension ratio, λ, was calculated as l/l_0 where l_0 and l are the lengths of the film along the stretching direction before and after the elongation, respectively. The true stress, σ, was evaluated as follows assuming the constant volume of the film:

$$\sigma = \frac{F}{A} = \frac{F}{A_0}\lambda, \tag{4.1}$$

where F is the force applied to the sample, A is the sample cross section at the extension ratio of λ, A_0 is the cross section at $\lambda = 1$.

Birefringence measurement. The birefringence measurement was carried out by the Senarmont method. The optical system was composed of a laser, a polarizer, a quarterwave plate, an analyzer, and a photo detector. The axes of the polarizer and the quarterwave plate were set at 45° to the strain axis. After passing through the oriented sample, the plane polarized light becomes elliptically polarized. The quarterwave plate converts it into linearly polarized light, the direction of which is different from the initial polarization by an angle φ. The retardation, Γ, was evaluated as $\Gamma = \lambda_{\mathrm{L}}(\varphi/\pi)$, where λ_{L} is the incident wavelength. The accuracy of Γ in this measurement was better than 3 nm. The birefringence, Δn, was determined as $\Delta n = \Gamma/d$, where d is the sample thickness.

SNOM measurement. The SNOM measurement was performed by a commercially available instrument (α-SNOM, WITec) using a hollow cantilever probe with a sub-wavelength aperture of 60 nm. The laser beam at a wavelength of 438 nm (BCL-015-440, CrystaLaser) was focused onto the backside of the aperture to generate the optical near-field. While scanning the sample surface in the contact mode with the cantilever, the perylene fluorescence was collected by a microscope objective (0.80NA,

60×, Nikon) from the backside of the substrate, passed through a long-pass filter (AELP454, Omega Optical), and detected with a photomultiplier (H8631, Hamamatsu Photonics). The SNOM measurement was carried out in an ambient condition. All the SNOM images were taken by the same probe.

4.3   Results and Discussion

4.3.1   Stress and Birefringence

Figure 4.1a shows a stress relaxation curve of the PMMA film after the tensile deformation of $\lambda = 2.0$. The author applied the time–temperature superposition principle to obtain the master curve at a reference temperature $T_r = 160\,°C$. The stress monotonously decreased with time. The shift factor, a_T, used to obtain the master curve is shown in Figure 4.1b. The solid curve in Figure 4.1b represents the WLF equation:

$$\log a_T = -\frac{9.78(T - T_r)}{130 + T - T_r},\tag{4.2}$$

which is consistent with the literature.[19]

The strain dependence of the stress relaxation was investigated in terms of the apparent Young's modulus defined by $E_a = 3\sigma/(\lambda^2 - \lambda^{-1})$.[20] Figure 4.2 shows E_a of the PMMA films stretched to λ = 1.3–2.5 plotted against time. If the strain is within the linear regime, E_a would be independent of strain. In the time range of this experiment, E_a depended on the strain and the curves were not parallel: the larger the strain was, the faster E_a decreased. This fast relaxation is attributed to the contraction presented in the Doi–Edwards theory. In the rest of this paper, the case of $\lambda = 2.0$ is investigated.

Figure 4.3 shows the birefringence plotted against the stress, in which the data for the extension process (open circles) from chapter 3 are also shown. The birefringence was in proportion to the stress in both the extension and relaxation processes according to the
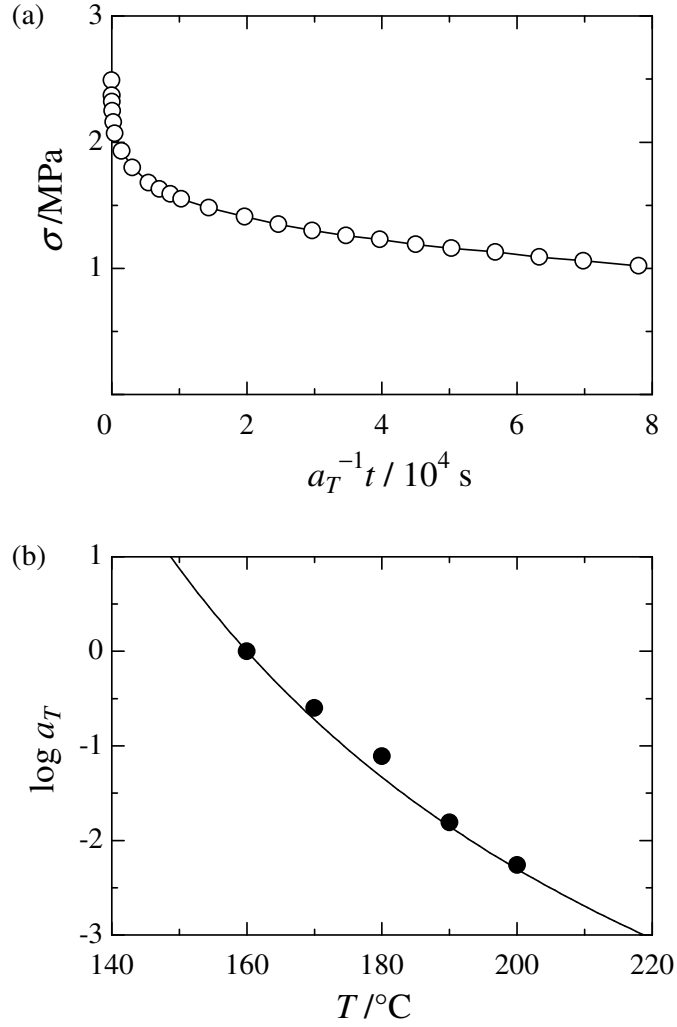
Figure 4.1: (a) Stress relaxation master curve for the PMMA film with $\lambda = 2.0$ at 160°C. (b) Shift factor of PMMA to form the master curve. The solid curve represents the WLF equation (eq 4.2).

stress–optical rule,[5]

$$\Delta n = C\sigma, \tag{4.3}$$

where C is the stress–optical coefficient. The value of C was evaluated to be -1.5×10^{-10} Pa^{-1}. Since the birefringence arises from the orientational anisotropy of the monomers, the stress is directly related to the orientation of the chain backbone.
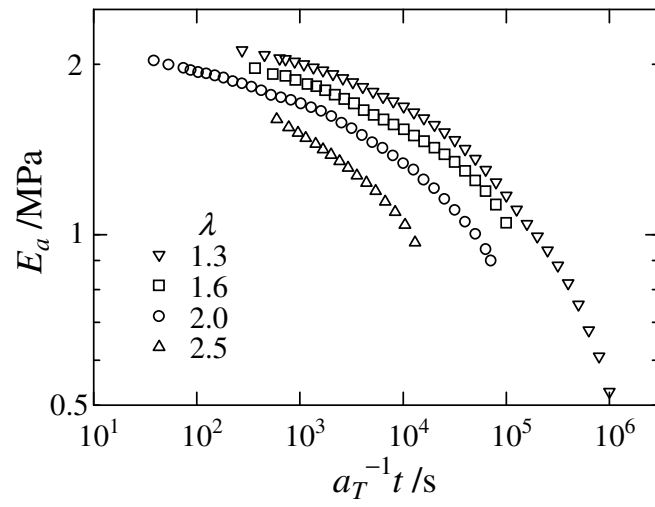
Figure 4.2: Apparent Young's modulus plotted against time, which was reduced to 160 °C.
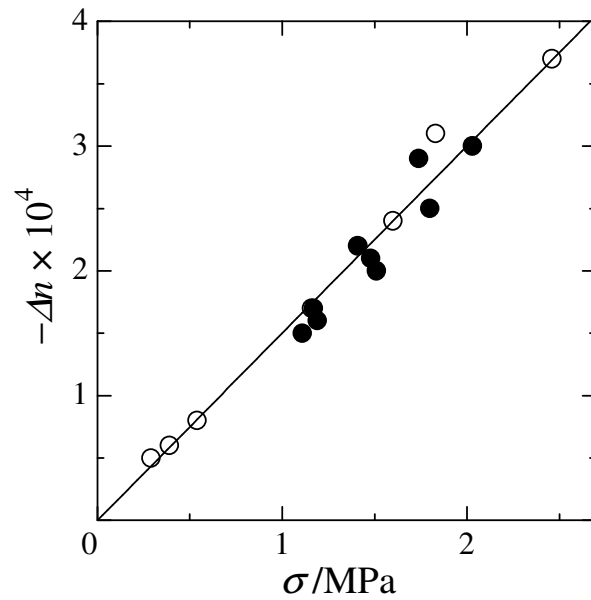

Figure 4.3: Birefringence plotted against stress. Open and closed circles represent the extension and relaxation processes, respectively.
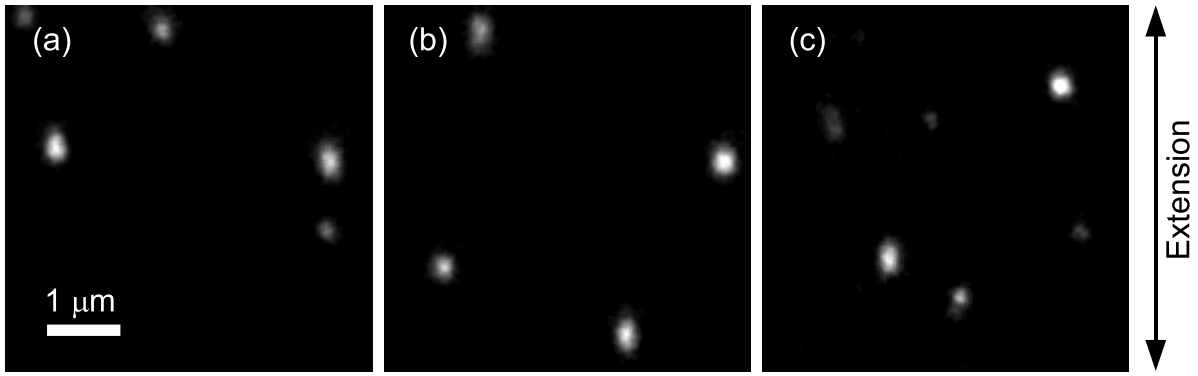
Figure 4.4: Fluorescence SNOM images of single polymer chains in the PMMA films, which were quenched immediately after the stretching (a), and after the relaxation periods, $a_T^{-1}t$, of 3.6×10^3 s (b), and 7.1×10^4 s (c). The macroscopic extension ratio is 2.0.

4.3.2 Chain Conformation during the Relaxation Process

Figure 4.4 shows the fluorescence SNOM images of the PMMA films immediately after stretching (a) and during the stress relaxation process (b, c). The perylene-labeled PMMA chains embedded in the unlabeled bulk film were observed as bright spots in the fluorescence image. Each fluorescence spot was confirmed to be individual PMMA-Pe chain from the statistical analysis.[16,21] Since the optical near-field penetrates into the sample film by a few hundred nm, the shape of the PMMA chain observed in the SNOM image is given as a two-dimensional projection of the chain conformation. These images clearly show the polymer chains with elongated conformations along the macroscopic stretching direction. The stresses of the samples in Figures 4.4a, b, and c were 2.46, 1.74, and 1.17 MPa, respectively. Even during this stress relaxation process, many of the chains showed elongated conformations as shown in panels b and c of Figure 4.4.

The conformation of the single PMMA chain was quantitatively evaluated from the fluorescence intensity distribution in terms of the true dimension along the stretching direction R_{xx}^* (eq 2.9) by the procedure shown in chapter 2. The results of the single chain analysis of the SNOM images are summarized in Figure 4.5, which shows histograms for the dimension of the chain along the stretching direction normalized by the initial
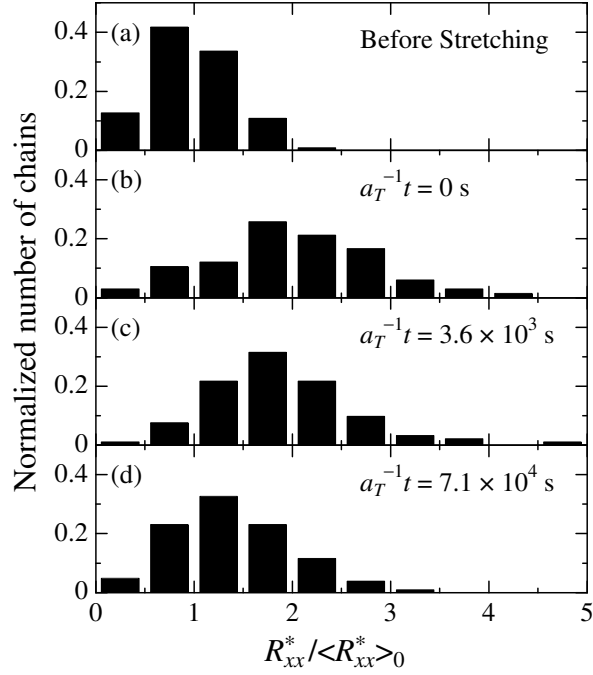
Figure 4.5: Histograms of the chain dimension parallel to the stretching direction, which was normalized by the initial average value, in the films before stretching (a), quenched immediately after the stretching (b), and after the relaxation periods, $a_T^{-1}t$, of 3.6×10^3 s (c), and 7.1×10^4 s (d).

average, $\langle R_{xx}^* \rangle_0$. Figure 4.5a shows the conformational distribution of flexible PMMA chains in the equilibrium state. The dimension of each chain increased by the stretching of the film (Figure 4.5b). The distribution of $R_{xx}^*/\langle R_{xx}^* \rangle_0$ did not significantly change at the early stage of the relaxation process (Figure 4.5c). The chain dimension clearly decreased for the samples with a longer relaxation period (Figure 4.5d).

The author first focuses on the time evolution of the average value in terms of the molecular extension ratio at the single chain level, λ_c, which is defined by eq 2.8. Figure 4.6 shows λ_c and the stress plotted against time. Soon after the stretching, λ_c was equal to the macroscopic extension ratio of the film, λ, showing the affine deformation. The macroscopic stress decreased over the whole time range of the observation. On the other hand, λ_c almost kept the initial value of 2.0 at the early stage of the stress relaxation process ($a_T t^{-1} < 1 \times 10^4$ s). This indicates that the whole chain kept a stretched
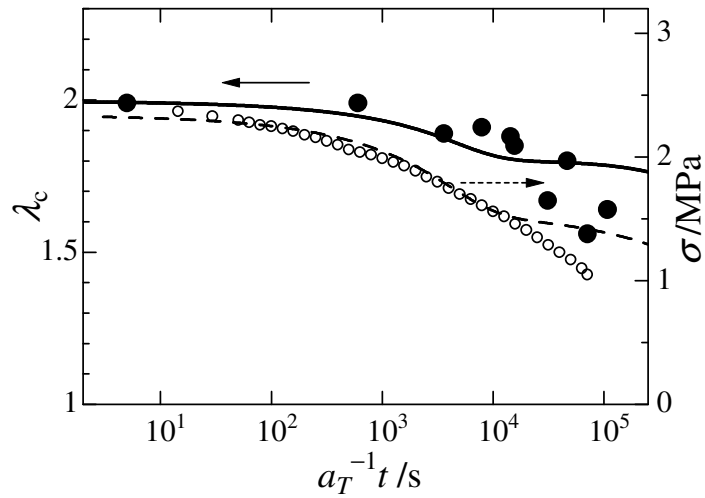
Figure 4.6: Chain extension ratio (closed circles) and stress (open circles) plotted against time, which was reduced to 160 °C. The macroscopic extension ratio is 2.0. Solid and dashed curves indicate the chain extension ratio and stress calculated from the Doi–Edwards model, respectively.
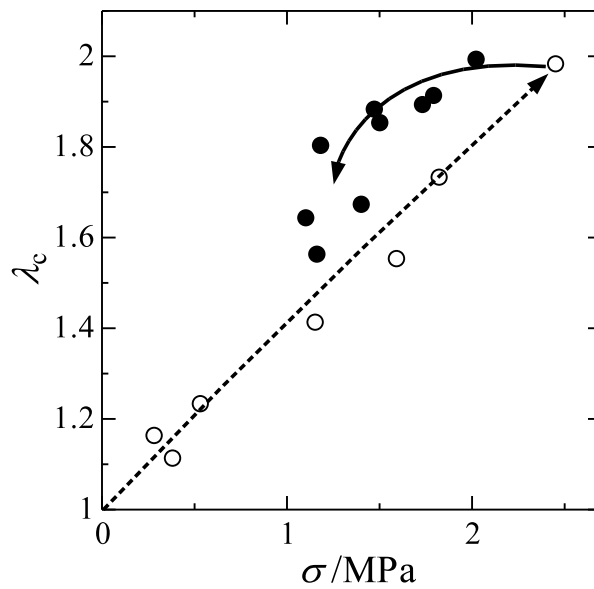

Figure 4.7: Chain extension ratio plotted against stress. Open and closed circles represent the extension and relaxation processes, respectively.

conformation in the short time scale in spite of the decrease in the stress.

Figure 4.7 shows λ_c plotted against the stress during the extension (data from chapter 3) and relaxation processes. In the extension process, λ_c increased with the stress. At the early stage of the relaxation process, however, the extension ratio of the single chain was not dependent on the decrease in the stress. λ_c does not directly correspond with the stress, whereas the birefringence is related to the stress (Figure 4.3).

4.3.3 Comparison with Doi–Edwards Model

The experimental data are compared with the Doi–Edwards model. First, the affine deformation is assumed for a step strain. The contour length, L, and the orientation of the primitive chain are increased by the deformation. Then, the relaxation takes place through following three steps: (A) the redistribution of monomers between the entanglements, (B) the contraction of the chain contour, and (C) the reptation of the entire chain with the relaxation times of τ_A, τ_B, and τ_C, respectively.

In step A, the stress decreases according to $\sigma \propto t^{-1/2}$. In the time scale of the current experiment, this fast relaxation was not observed. Since step A does not affect the conformation of the whole chain, $\langle R_{xx}^{*2} \rangle$ and $\langle L \rangle$ are the same with those after the affine deformation: $\langle R_{xx}^{*2} \rangle = \lambda^2 \langle R_{xx}^{*2} \rangle_0$, and $\langle L \rangle = \alpha \langle L_0 \rangle$, where α is the average stretch ratio of the contour length of the primitive chain, and L_0 is L at the equilibrium. α is a monotonically increasing function with strain: $\alpha = 1.23$ for the uniaxial extension of $\lambda = 2.0$.[5] At step B, where L reduces to L_0, the stress decreases by a factor of $1/\alpha^2$ through the decrease in the contour length and the increase in the number of monomers between entanglements. When the Rouse model is applied to step B, the time evolution of $\langle L \rangle$ is given by $\langle L \rangle = \langle L_0 \rangle \mu_B$,[2,5] where

$$\mu_B = \sum_{p=1,3,5,\cdots}^{\infty} \frac{8}{p^2 \pi^2} \left\{ 1 + (\alpha - 1) \exp\left(-\frac{t p^2}{\tau_B} \right) \right\}. \tag{4.4}$$

57

Under this assumption, the stress is expressed as

$$\sigma = \frac{15}{4} G_N^0 Q \mu_B^2, \tag{4.5}$$

where G_N^0 is plateau modulus, and Q denotes the orientation immediately after the step strain ($Q = 0.580$ for $\lambda = 2$).[5] On the other hand, $\langle R_{xx}^{*\,2} \rangle$ decreases by a factor of $1/\alpha$ in proportion to $\langle L \rangle$:[4,22]

$$\langle R_{xx}^{*\,2} \rangle = \langle R_{xx}^{*\,2} \rangle_0 \frac{\lambda^2}{\alpha} \mu_B. \tag{4.6}$$

The relaxation time of step B is $\tau_B = \tau_A (M/M_e)^2$, where M_e is the molecular weight between entanglements: $M_e = \rho R T / G_N^0$, where ρ is the density, R is the gas constant, and T is the temperature. At step C, the conformation is relaxed to the equilibrium through reptation. The stress and $\langle R_{xx}^{*\,2} \rangle$ are related to the fraction of the primitive chain segment in the original tube:[2,3,22]

$$\sigma = \frac{15}{4} G_N^0 Q \mu_B^2 \mu_{C1}, \tag{4.7}$$

$$\langle R_{xx}^{*\,2} \rangle = \langle R_{xx}^{*\,2} \rangle_0 \left\{ \left(\frac{\lambda^2}{\alpha} \mu_B - 1 \right) \mu_{C2} + 1 \right\}, \tag{4.8}$$

where

$$\mu_{C1} = \sum_{p=1,3,5,\cdots}^{\infty} \frac{8}{p^2 \pi^2} \exp\left(-\frac{t p^2}{\tau_C} \right), \tag{4.9}$$

$$\mu_{C2} = \sum_{p=1,3,5,\cdots}^{\infty} \frac{96}{p^4 \pi^4} \exp\left(-\frac{t p^2}{\tau_C} \right). \tag{4.10}$$

From eq 4.8,

$$\lambda_c = \left\{ \left(\frac{\lambda^2}{\alpha} \mu_B - 1 \right) \mu_{C2} + 1 \right\}^{\frac{1}{2}}. \tag{4.11}$$

The relaxation time of the step C is $\tau_C = 3 \tau_A (M/M_e)^3$.

The author fitted the stress relaxation curve using eq 4.7 with τ_A and the plateau modulus G_N^0 as the fitting parameters. The theoretical stress relaxation curve is shown as a dashed curve in Figure 4.6. The best fit values were $\tau_A = 4.0 \times 10^{-2}$ s and $G_N^0 = 0.72$ MPa. These values are consistent with the experimental values obtained

from shear measurements in the literature.[20,23] The relaxation times of steps B and C were calculated as $\tau_B = 4.5 \times 10^3$ s and $\tau_C = 4.5 \times 10^6$ s, respectively. Therefore, the stress relaxation is mainly caused by step B in the time range of this experiment. This is consistent with the strain-dependent decrease of the relaxation modulus shown in Figure 4.2, because step B is a strain-dependent process. The inconsistency between the experimental and theoretical values at the longer time ($a_T t^{-1} > 1 \times 10^4$ s) may be caused by the motion of the matrix chains, which leads to disentanglement. Using the parameters obtained from the analysis of the stress relaxation, the author calculated the theoretical curve for λ_c from eq 4.11 (solid curve in Figure 4.6). The theoretical prediction was consistent with the experimental data in the time range of $a_T^{-1} t < 1 \times 10^4$ s, showing the slow reduction of λ_c. At step B, the reduction of λ_c originates from the decrease in the tube length. On the other hand, the stress reduces through not only the decrease in the tube length but also the increase in the number of monomers between entanglements. The faster relaxation in stress is caused by the conformational change at the short length scale, which hardly affects the dimension of the whole chain level.

4.3.4 Distribution of the Chain Relaxation

The author next focuses on the distribution function of R_{xx}^*. In the contraction process, the degree of relaxation could be different for each chain because the stretch ratio of the chain contour, L/L_0, could be different for each chain: the chain with a larger L/L_0 shows a larger relaxation through the contraction.[7] This leads to a change in the shape of the distribution function for R_{xx}^*. In order to focus on the shape of the distribution function, the histograms of R_{xx}^* in Figure 4.5 were redrawn to Figure 4.8 in terms of the chain dimension normalized by the average value of each sample, $R_{xx}^*/\langle R_{xx}^* \rangle$. In the film immediately after stretching (panel b in Figure 4.8), the shape of the distribution function of $R_{xx}^*/\langle R_{xx}^* \rangle$ did not significantly change from that before stretching (panel a). This is consistent with the picture of the affine deformation. Every chain is stretched with a given molecular extension ratio λ_c, which is equal to the macroscopic extension ratio.
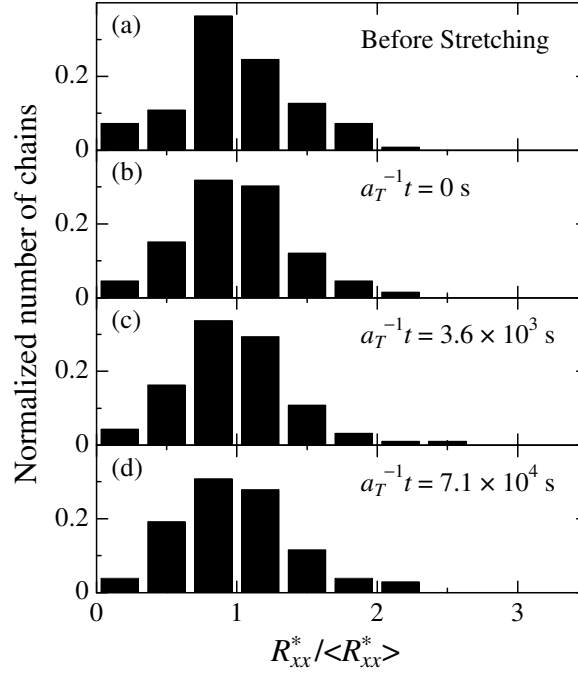
Figure 4.8: Histograms of the chain dimension parallel to the stretching direction, which was normalized by the average value for each sample, in the films before stretching (a), quenched immediately after the stretching (b), and after the relaxation periods, $a_T^{-1}t$, of 3.6×10^3 s (c), and 7.1×10^4 s (d).

In the stress relaxation process (panels c and d), the distribution functions retained the shape. This implies that each chain has a similar stretch ratio of the chain contour L/L_0 and also shows similar relaxation behavior in the contraction process. This is probably due to the high molecular weight of the sample. In the present case, the number of entanglement segments per chain is large: $M_w/M_e \approx 340$. Therefore, the orientation of the primitive chain segment was well averaged over the whole single chain. This intramolecular statistics leads to the similar L/L_0 values of every chains, consequently the homogeneous relaxation during the contraction process.

4.4   Conclusion

The relaxation of single PMMA chains in a uniaxially stretched film was directly observed by SNOM in real space. It was found that the whole chain kept an elongated conformation in spite of the decrease in stress at the early stage of the relaxation process. The experimental data was consistent with the contraction process in the Doi–Edwards model. This suggests that the faster relaxation in stress is caused by the conformational change at the small length scale, which hardly affects the conformation at the whole chain scale. The shape of the distribution function of the chain dimension did not change significantly during the relaxation process, implying homogeneous chain relaxation on a whole chain scale for the well entangled system. Thus direct observation of the single chain enables us to investigate the polymer physics considering the individual behaviors of polymer chains.

References

[1] de Gennes, P. G. *J. Chem. Phys.* **1971**, *55*, 572–579.

[2] Doi, M. *J. Polym. Sci., Polym. Phys. Ed.* **1980**, *18*, 1005–1020.

[3] Doi, M.; Edwards, S. F. *J. Chem. Soc. Faraday Trans. II* **1978**, *74*, 1789–1801.

[4] Doi, M.; Edwards, S. F. *J. Chem. Soc. Faraday Trans. II* **1978**, *74*, 1802–1817.

[5] Doi, M.; Edwards, S. F. *The Theory of Polymer Dynamics*, 3rd ed.; Clarendon: Oxford, 1986.

[6] Watanabe, H. *Prog. Polym. Sci.* **1999**, *24*, 1253–1403.

[7] McLeish, T. C. B. *Adv. Phys.* **2002**, *51*, 1379–1527.

[8] Boué, F.; Nierlich, M.; Jannink, G.; Ball, R. *J. Phys. (Paris)* **1982**, *43*, 137–148.

[9] Boué, F. *Adv. Polym. Sci.* **1987**, *82*, 47–101.

[10] Bent, J.; Hutchings, L.; Richards, R. W.; Gough, T.; Spares, R.; Coates, P. D.; Grillo, I.; Marien, O. G.; Read, D. J.; Graham, R. S.; Likhtman, A. E.; Groves, D. J.; Nicholson, T. M.; McLeish, T. C. B. *Science* **2003**, *301*, 1691–1695.

[11] Graham, R. S.; Bent, J.; Hutchings, L. R.; Richards, R. W.; Groves, D. J.; Embery, J.; Nicholson, T. M.; McLeish, T. C. B.; Likhtman, A. E.; Harlen, O. G.; Read, D. J.; Gough, T.; Spares, R.; Coates, P. D.; Grillo, I. *Macromolecules* **2006**, *39*, 2700–2709.

[12] Blanchard, A.; Graham, R.; Heinrich, M.; Pyckhout-Hintzen, W.; Richter, D.; Likhtman, A.; McLeish, T.; Read, D.; Straube, E.; Kohlbrecher, J. *Phys. Rev. Lett.* **2005**, *95*, 166001.

[13] Perkins, T. T.; Smith, D. E.; Chu, S. *Science* **1994**, *264*, 819–822.

[14] Smith, D. E.; Chu, S. *Science* **1998**, *281*, 1335–1340.

[15] Teixeira, R. E.; Dambal, A. K.; Richter, D. H.; Shaqfeh, E. S. G.; Chu, S. *Macromolecules* **2007**, *40*, 2461–2476.

[16] Aoki, H.; Morita, S.; Sekine, R.; Ito, S. *Polym. J.* **2008**, *40*, 274–280.

[17] Aoki, H.; Tanaka, S.; Ito, S.; Yamamoto, M. *Macromolecules* **2000**, *33*, 9650–9656.

[18] Grimaud, T.; Matyjaszewski, K. *Macromolecules* **1997**, *30*, 2216–2218.

[19] Masuda, T.; Kitagawa, K.; Onogi, S. *Polym. J.* **1970**, *1*, 418–424.

[20] Ferry, J. D. *Viscoelastic Properties of Polymers*, 3rd ed.; Wiley: New York, 1980.

[21] Aoki, H.; Kunai, Y.; Ito, S.; Yamada, H.; Matsushige, K. *Appl. Surf. Sci.* **2002**, *188*, 534–538.

[22] Viovy, J. L.; Monnerie, L.; Tassin, J. F. *J. Polym. Sci., Polym. Phys. Ed.* **1983**, *21*, 2427–2444.

[23] Fuchs, K.; Friedrich, C.; Weese, J. *Macromolecules* **1996**, *29*, 5893–5901.

Chapter 5

Relaxation of Single Polymer Chain

in Binary Molecular Weight Blends Observed by SNOM

5.1   Introduction

The relaxation behavior of a polymer chain has long been investigated through both theoretical and experimental approaches because of its importance in various applications such as polymer processing and material design. Most of the molecular models describing the behavior of a polymer chain in an entangled system are based on the tube model by de Gennes,[1] Doi and Edwards.[2–5] In the original Doi–Edwards model, dynamic properties of monodisperse linear polymers are calculated from the motion of a single chain in a fixed network. The motion of a polymer chain is assumed to be restricted by a tube surrounding the chain backbone, which represents the entanglements among the neighboring chains. The tube model has been improved to explain the viscoelastic properties of various systems.[6,7] The assumption of the fixed network cannot be applied to polydisperse systems because of the fast relaxation of the short chains, which leads to the disentanglement between the long and short chains and allows the local motion of the long chain in a lateral direction to its backbone. The relaxation caused by the disentanglement from the surrounding chains has been considered theoretically with the picture of the constraint release.[8] Both analytical calculations[9,10] and stochastic simulations[11–15] have been used to express entangled chain dynamics, which contains the effect of constraint release. The slip-link models are able to simulate the dynamics of the polymer chains with molecular weight distributions and have used to describe the polydisperse systems. Experimentally, the binary blend of the same chemical species with different molecular weights has been studied as the most simple model system of the polydispersity through various methods such as rheological measurement,[16–18] optical

measurement,[19] infrared absorption dichroism,[20] dielectric measurement,[21] and neutron scattering.[22,23] The contrast enhancement techniques by introducing the deuterium and fluorescent moiety are powerful approach to reveal the dynamics of a selective component in blend systems. However, previous experiments provide physical values averaged over a large number of chains. The direct observation of the single chain would be a more effective approach to reveal the chain dynamics in blend systems because the disentanglement depends on the surrounding conditions of individual chains.

The fluorescence labeling is an established method to distinguish a polymer chain from its surroundings. This has been applied to the observation of single DNA molecules under the fluorescence microscopy.[24–26] However, the conventional fluorescence microscopy suffers from the low spatial resolution of a half of the wavelength of light due to the diffraction limit. The higher resolution is needed to observe individual flexible polymer chains since their typical sizes are in the order of 10–100 nm. SNOM is an emerging scanning probe technique, which allows optical measurement with a high resolution beyond the diffraction limit. The combination of fluorescence labeling and SNOM enables us to directly observe the in-situ conformation of the single chain. Furthermore, the orientation of the dye in the fluorescently labeled polymer can be evaluated by the use of polarized light because the absorption and fluorescence anisotropies reflect the orientation of the transition dipole. The polarization measurements under near- and far-field microscopy reveal the spatial distribution of the orientational anisotropy.[27]

In the previous chapters, the author observed a deformation of PMMA chains in the nearly monodisperse PMMA films under uniaxial deformation during the extension and relaxation processes. It was found that the dimension of the whole single chain increased affinely with the macroscopic strain when the film is stretched well above the glass transition temperature, and the whole chain keeps the elongated conformation in spite of the decrease in the stress at the early stage of the relaxation process. The observed chain behavior was successfully explained by the contraction process of the Doi–Edwards

model.[3,5] The assumption of the fixed network is reasonable to describe the chain relaxation at the early stage in the well-entangled monodisperse system. In the current study, the effect of the disentanglement with surrounding chains on the conformational relaxation is investigated through the direct observation of the single polymer chain in PMMA blend films of long and short chains (*L*- and *S*-chains, respectively) during the stress relaxation process. The relaxation process for the conformation of the whole chain contour and the segmental orientation was directly observed for the individual *L*-chains by near-field and polarization modulation microscopy. The experimental results were discussed in comparison with the prediction from the slip-link simulation based on the Doi–Takimoto model.[14,28]

5.2 Experiments

Sample preparation. The synthesis of perylene-labeled PMMA (L-Pe, Figure 2.1) is described elsewhere.[29,30] The fraction of the labeled unit was evaluated to be 0.77% by UV–Vis absorption (U3500, Hitachi). The unlabeled PMMA was synthesized by atom transfer radical polymerization.[31] Methyl methacrylate was polymerized with *p*-toluenesulfonyl chloride in conjunction with copper(I) chloride and 4,4'-dinonyl-2,2'-dipyridyl at 70 °C in vacuum. The weight- and number-averaged molecular weights, M_w and M_n, were determined by GPC measurement as shown in Table 5.1.

Table 5.1: Characterization of PMMA.

Code	$M_\mathrm{w}/10^4$	$M_\mathrm{n}/10^4$	$M_\mathrm{w}/M_\mathrm{n}$
L-Pe	199	158	1.26
L	212	133	1.60
S17	17.6	13.2	1.33
S07	7.10	6.22	1.14
S03	2.93	2.61	1.12

Sample films were prepared by the blends of long (L) and short (S17, S07, or S03) PMMAs where a trace amount of the probe L-Pe chain was dispersed. In the SNOM measurement, the fluorescent moiety far below the surface cannot be observed; therefore, the probe chain should exist within ~200 nm beneath the surface. The sample films prepared in the following procedure. A mixed toluene solution of unlabeled and labeled PMMA (0.005 wt % to the unlabeled polymer) was spin-coated onto a glass substrate to form a film with a thickness of 80 nm. The self-standing thick film of unlabeled PMMA (the size was 25 mm × 7 mm, and the thickness was 300 μm) with the same blend composition as the matrix of the thin film was prepared separately by solution casting. The thin film was floated onto a water surface and scooped up on a thick film. The conformation of L-Pe may be affected by the shear flow in the spin-coating process and the confinement effect of the thin film. Therefore, the sample film was annealed for 48 h at 200 °C, which is longer than the relaxation time estimated from the literature,[32] in vacuum to reach the equilibrium.

Tensile deformation. A tensile tester (RTM-500, Orientec) with a 10 kg load cell was used to stretch the films. The length between the clamps was 20 mm. The stretching was carried out at 160–200 °C with a crosshead speed of 50 mm/min. After the stretching, the clamp gap was kept constant for time t. Then the films were immediately quenched to room temperature. The force was monitored on a chart recorder throughout the stretching and relaxation processes. The extension ratio, λ, was calculated as l/l_0 where l_0 and l are the lengths of the film along the stretching direction before and after the elongation, respectively. The true stress, σ, was evaluated as follows assuming the constant volume of the film:

$$\sigma = \frac{F}{A} = \frac{F}{A_0}\lambda, \tag{5.1}$$

where F is the force applied to the sample, A is the sample cross section at the extension ratio of λ, A_0 is the cross section at $\lambda = 1$.

Birefringence measurement. The birefringence measurement was carried out by Senarmont method. The optical system was composed of a laser at a wavelength $\lambda_L = 532$ nm, a polarizer, a quarterwave plate, an analyzer, and a photo detector. The axes of the polarizer and the quarterwave plate were set at $45°$ to the strain axis of the oriented sample. After passing through the oriented sample, the plane polarized light becomes elliptically polarized. The quarterwave plate converts it into linearly polarized light, the direction of which is different from the initial polarization by an angle φ. The retardation, Γ, was evaluated as $\Gamma = \lambda_L(\varphi/\pi)$. The accuracy of Γ in this measurement was better than 3 nm. The birefringence, Δn, was determined as $\Delta n = \Gamma/d$, where d is the sample thickness.

Excitation polarization modulation microscopy. The orientation anisotropy of fluorescence dye was measured under an inverted fluorescence microscope (TE-2000, Nikon) equipped with an EMCCD camera (Cascade II, Roper Scientific). A 442 nm laser beam was passed through an electro-optic modulator (EOM) (EO-AM-NR-C4, THORLABS), and focused on the sample through an objective lens (100×, 1.4 NA, Nikon). The fluorescence signal was collected through a filter cube (BV-2A, Nikon), which contains a dichroic mirror (455 nm) and a longpass filter (470 nm). The direction of the linearly polarized excitation beam was alternately modulated in the parallel and perpendicular direction to the stretching axis at a frequency of 0.25 Hz by the EOM.

SNOM measurement. The SNOM measurement was performed by a commercially available instrument (α-SNOM, WITec) using a hollow cantilever probe with a sub-wavelength aperture of 60 nm. The laser beam at a wavelength of 438 nm (BCL-015-440, CrystaLaser) was focused onto the backside of the aperture to generate the optical near-field. While scanning the sample surface in the contact mode with the cantilever, the perylene fluorescence was collected by a microscope objective (0.80NA, 60×, Nikon) from the backside of the substrate, passed through a long-pass filter (AELP454, Omega Optical), and detected with a photomultiplier (H8631, Hamamatsu

Photonics). The SNOM measurement was carried out in an ambient condition. All the SNOM images were taken by the same probe.

5.3   Results and Discussion

5.3.1   Stress and Birefringence

Figure 5.1 shows stress relaxation curves of PMMA films after the tensile deformation of $\lambda = 2.0$. The author applied the time–temperature superposition principle to obtain master curves at 160 °C. The shift factor, a_T, used to obtain the master curves is shown in Figure 5.1c. The solid curve in Figure 5.1c represents the WLF equation:

$$\log a_T = -\frac{9.78(T - T_{\mathrm{r}})}{130 + T - T_{\mathrm{r}}}, \tag{5.2}$$

which is consistent with the literature.[32] The shift factor was almost the same among the samples used in this study. Figure 5.1a shows the blend ratio dependence of the stress relaxation curves for the L/S17 blends. The lower the fraction of the L-chain (w_L) was, the faster the stress decreased, reflecting the faster relaxation of the S-chains. Figure 5.1b shows the dependence of the stress on the molecular weight of the S-chains, M_S, for the samples with $w_L = 0.50$. The lower the molecular weight of the S-chain was, the faster the stress decreased at the early stage of the relaxation process. This is caused by the faster relaxation of the shorter chains. The L/S07 and L/S03 blends showed plateau-like region, where the stress was almost independent of M_S. In this region, the stress relaxation curves for the blend films were similar to that for the monodisperse system, suggesting that the relaxation behavior is dominated by the entanglements among L-chains.

Figure 5.2 shows the birefringence plotted against the stress. The birefringence was proportional to the stress regardless of the blend composition according to the stress–optical rule,[5]

$$\Delta n = C\sigma, \tag{5.3}$$
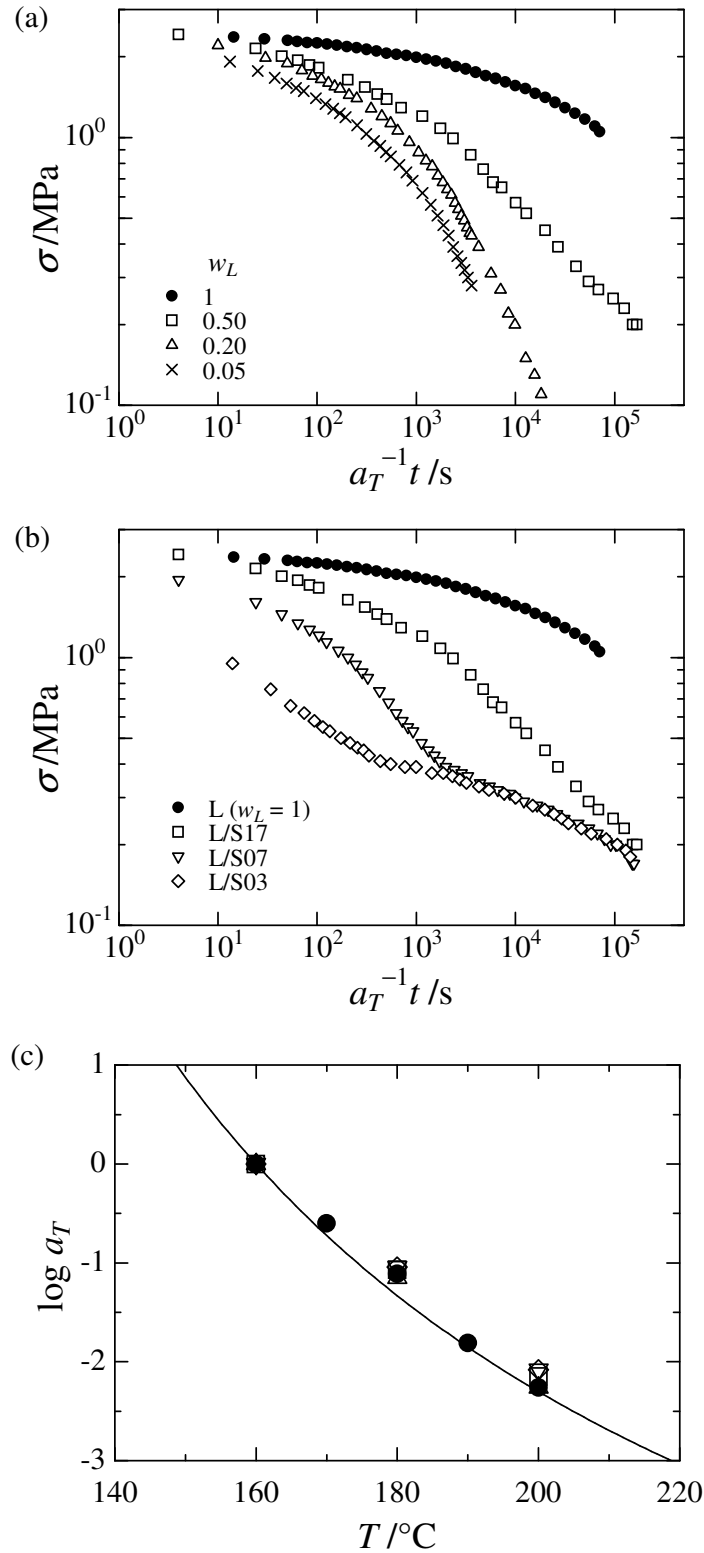
Figure 5.1: Stress relaxation master curves for the PMMA films with $\lambda = 2.0$ at 160°C: (a) L/S17 blends, and (b) blends with $w_L = 0.50$. (c) Shift factor of PMMA to form the master curves. The solid curve represents the WLF equation (eq 5.2).
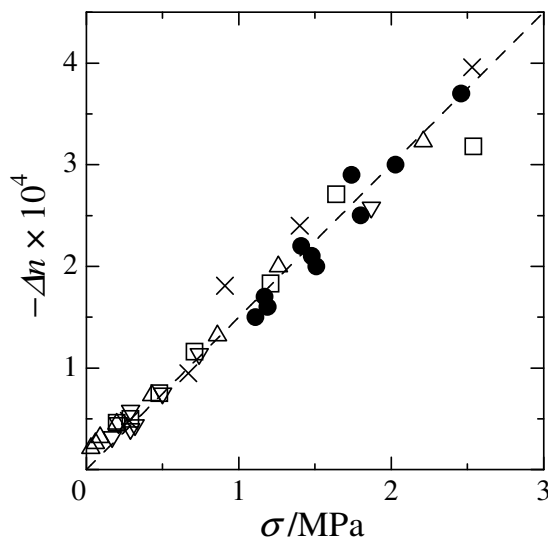
Figure 5.2: Birefringence plotted against stress. The symbols are the same as those in Figure 5.1.

where C is the stress–optical coefficient. The value of C was evaluated to be -1.5×10^{-10} Pa^{-1}. Since the birefringence arises from the orientation of the chain segment, the stress relaxation is directly related to the relaxation of the segmental orientation. In the binary blend films, the birefringence indicates the segmental orientation averaged over the all components.

5.3.2 Orientation of Fluorescence Dye

In order to evaluate the segmental orientation of the single L-chains, the orientation of the dye molecule in the labeled polymer was measured through the excitation polarization modulation microscopy. When a fluorescent molecule is excited by linearly polarized light, the excitation probability is proportional to $\cos^2 \chi$, where χ is the angle between the electric vector of the polarized light and the absorbing axis of the molecule. Because the fluorescence intensity is proportional to the excitation probability, the orientation of the molecule can be determined by measuring the dependence of the fluorescence intensity on the polarization state of the excitation light. The orientation of the dye molecules in
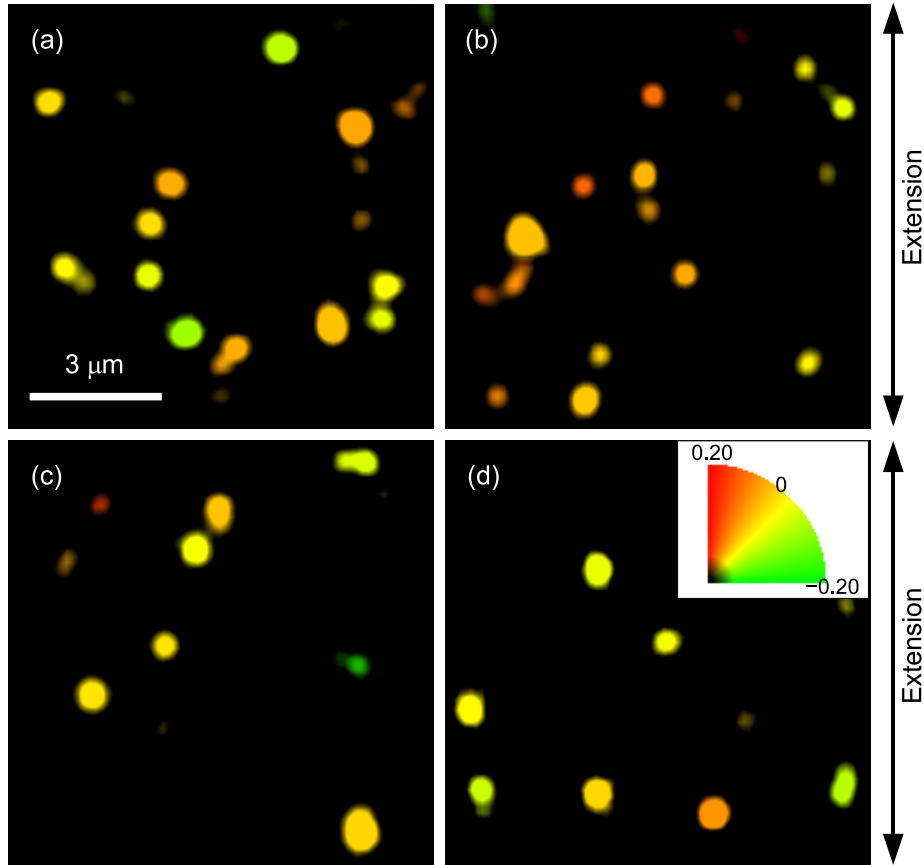
72

Figure 5.3: Anisotropy images of single polymer chains obtained by excitation polarization modulation microscopy in the PMMA films before stretching (a), immediately after the stretching (b), and after the relaxation periods $a_T^{-1}t = 3.6 \times 10^3$ s (c,d). The matrices are (a–c) L, and (d) L/S17 ($w_L = 0.20$).

each labeled chain was examined in terms of the excitation anisotropy $(I_x - I_y)/(I_x + I_y)$, where I_x and I_y are the intensities of the fluorescence from each labeled chain excited by linearly polarized light in x and y directions, respectively. The x axis is defined as the macroscopic extension axis of the film and y axis perpendicular to it. Figure 5.3 shows anisotropy images of the labeled polymers in PMMA films obtained by excitation polarization modulation microscopy. Each fluorescence spot was confirmed to be an individual L-Pe chain from the statistical analysis.[33] Since each chain was observed in a circular shape due to the diffraction limit in the image obtained by the far-field set up, the excitation anisotropy indicates the segmental orientation averaged for the single
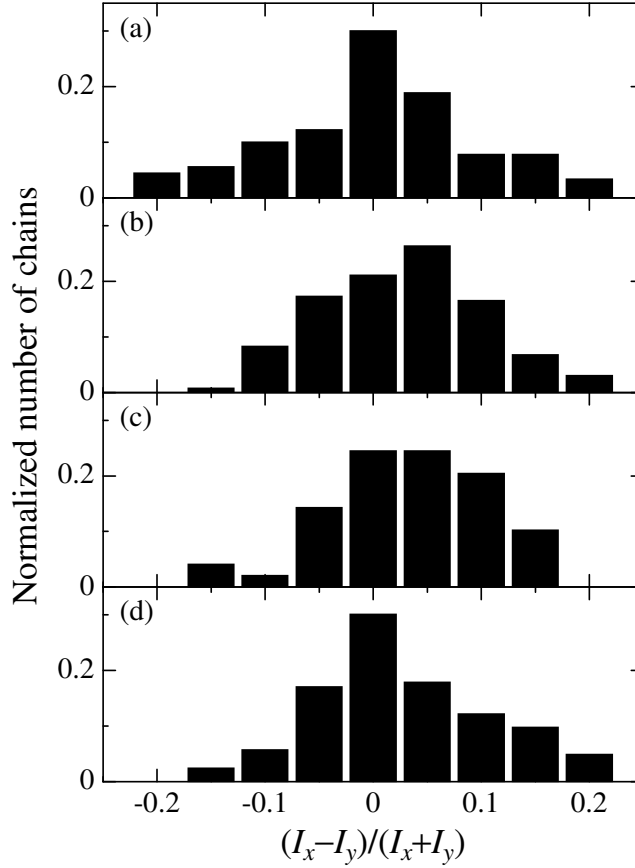
73

Figure 5.4: Histograms of excitation anisotropy of chains obtained by excitation polarization modulation microscopy for the films before stretching (a), immediately after the stretching (b), and after the relaxation periods $a_T^{-1}t = 3.6 \times 10^3$ s (c,d). The matrices are (a–c) L, and (d) L/S17 ($w_L = 0.20$).

chain. Figure 5.4 shows histograms of $(I_x - I_y)/(I_x + I_y)$. In the film before stretching, $(I_x - I_y)/(I_x + I_y)$ was symmetrically distributed around zero, indicating the isotropic orientation. The anisotropy increased with the stretching of the film, and decreased in the stress relaxation regime.

The orientational order parameter of the fluorescence dye in each chain is defined as

$$p = (3\langle\cos^2\phi_d\rangle - 1)/2, \tag{5.4}$$

where ϕ_d is the angle between x axis and the molecular axis of the dye, and $\langle\ \rangle$ represents

the statistical average for each chain. The value of p can be evaluated from the excitation anisotropy as

$$p = \frac{I_x - I_y}{I_x + 2I_y}. \tag{5.5}$$

The averaged value of p weighted by the signal intensity corresponds to the orientational order parameter of the dye in all the observed chains:

$$\bar{p} = \frac{\sum (I_x + 2I_y)p}{\sum (I_x + 2I_y)} = (3\langle \cos^2 \phi_\mathrm{d} \rangle - 1)/2, \tag{5.6}$$

where the summation and the average are taken over the observed chains and dyes, respectively. On the other hand, the orientational order parameter of the main chain,

$$\Phi = (3\langle \cos^2 \phi_\mathrm{c} \rangle - 1)/2, \tag{5.7}$$

where ϕ_c is the angle between x axis and the main axis of the structural unit, is evaluated from the birefringence:

$$\Phi = \Delta n / \Delta n_0, \tag{5.8}$$

where Δn_0 is the intrinsic birefringence of PMMA ($\Delta n_0 = -0.0043$).[34]

Figure 5.5a shows $\bar{p}$ plotted against the birefringence for the monodisperse film during the extension and relaxation processes. In this film, $\bar{p}$ was proportional to the birefringence. The excitation anisotropy corresponds to the orientation of the dye moiety labeled on the PMMA chain. The proportionality between $\bar{p}$ and Δn indicates that the dye moiety reflects the orientation of the main chain. Thus, the segmental orientation of the PMMA chain can be examined in terms of the excitation anisotropy. The value of Φ is shown in the upper axis of Figure 5.5. The orientational order parameter of the dye was smaller than that of the main chain evaluated by the birefringence, whereas they showed a proportionality in the range of this experiment. The dye moiety was introduced in the side chain ester group; therefore, the relaxation of the ester bond results in the decrease of the orientational order parameter of the dye compared to that of the main chain. Figure 5.5b
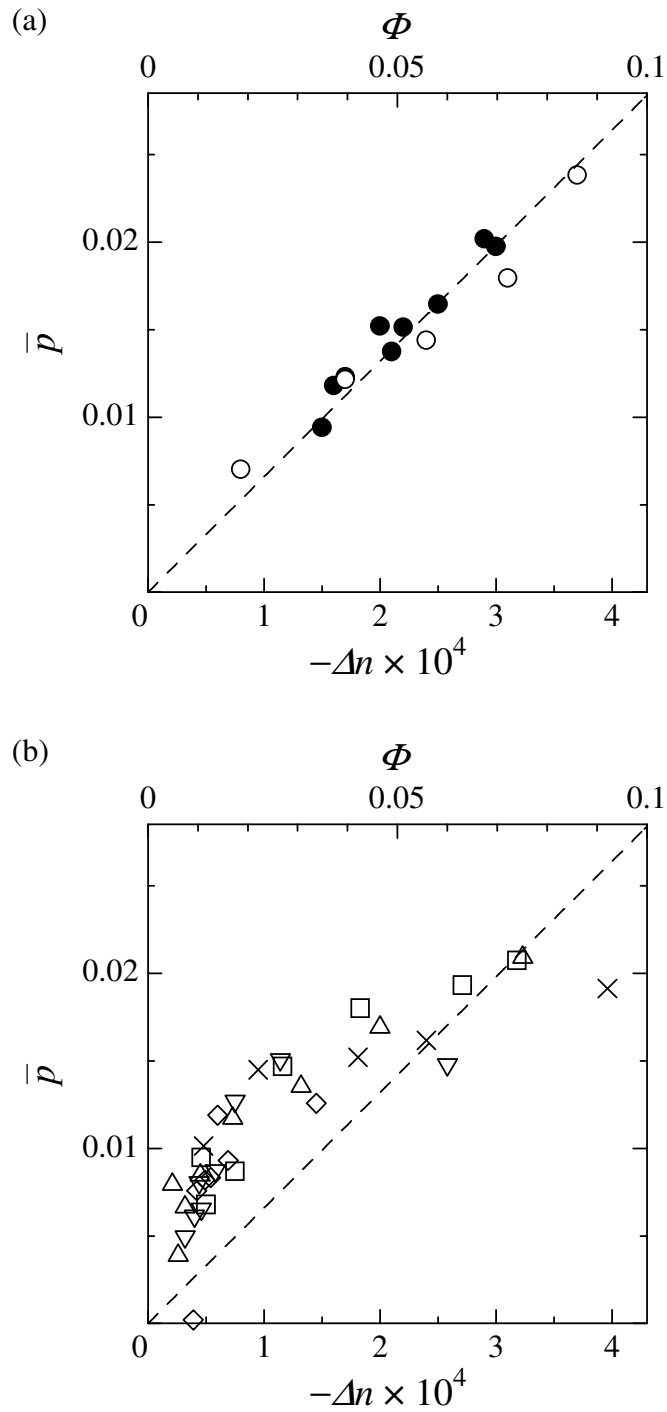
Figure 5.5: Average excitation anisotropy plotted against birefringence. (a) The monodisperse system of L. Open and closed circles indicate the extension and relaxation processes, respectively. (b) The blend system of the *L*- and *S*-chains. The symbols are the same as those in Figure 5.1. The upper axis shows the orientational order parameter of main chain.
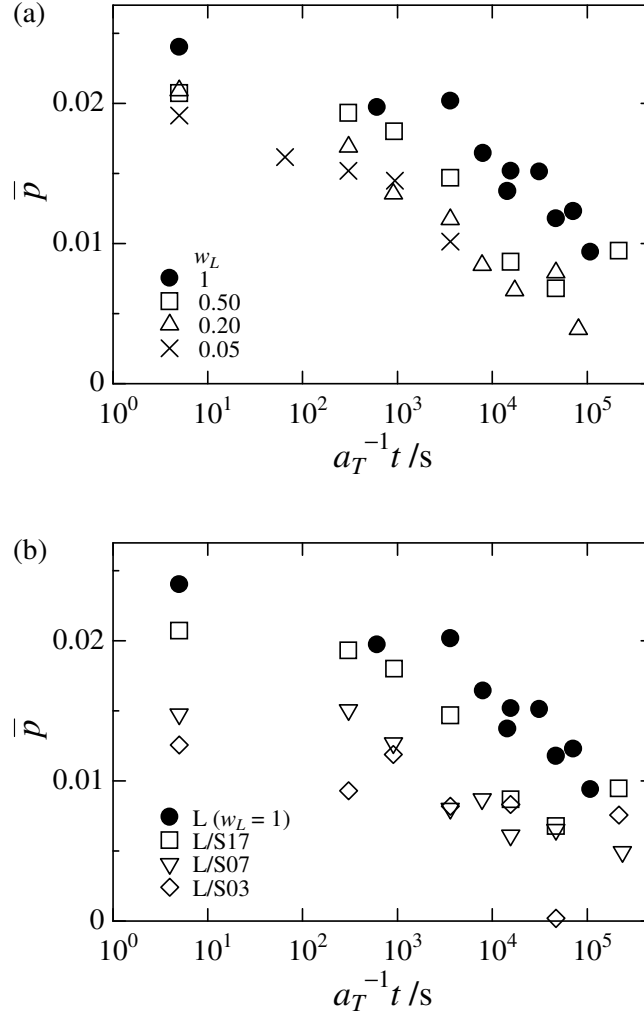
Figure 5.6: Average excitation anisotropy of PMMA films plotted against time for (a) L/S17 blends, and (b) blends with $w_L = 0.50$.

shows $\bar{p}$ plotted against the birefringence in the blend films during the stress relaxation process. In these samples, $\bar{p}$ and the birefringence showed the different relationship from the monodisperse system. In the blend films, $\bar{p}$ reflects the segmental orientation of the *L*-chains, whereas the birefringence originates from the segmental orientation of the all components. The faster relaxation in the birefringence than $\bar{p}$ during the relaxation process is caused by the faster relaxation of the *S*-chains than the *L*-chains.

Figure 5.6a shows $\bar{p}$ for L/S17 blends plotted against time. The anisotropy decreased faster with the decrease in w_L. This indicates that the segmental relaxation of the *L*-chains

were accelerated by the addition of the *S*-chains. Figure 5.6b shows M_S dependence of $\bar{p}$. The faster decrease in $\bar{p}$ was observed in the lower M_S samples at the early stage of the relaxation, whereas $\bar{p}$ reaches plateau and almost independent of M_S in the longer time region. This is consistent with the theoretical molecular picture of the constraint release. When an *S*-chain relaxes, its entanglements with the *L*-chains disappear. This releases a part of the *L*-chain from the constraint, resulting in the segmental relaxation by the local motion of the *L*-chain. With lower w_L or M_S, the frequency of the constraint release event increases, and therefore the relaxation rate increases in the short time region. On the other hand, the reptation of the *L*-chains is needed to fully relax because the *L*-chains mutually entangle in these systems.

5.3.3 Conformation of Single Polymer Chain

Figure 5.7 shows the fluorescence SNOM images of the PMMA films. The perylene-labeled PMMA chains embedded in the unlabeled bulk film were observed as the bright spots in the fluorescence image. Each fluorescence spot corresponds to single polymer chain. Since the optical near-field penetrates into the sample film by a few hundred nm, the shape of the PMMA chain observed in the SNOM image is given as a two-dimensional projection of the chain conformation. For the film immediately after the stretching (Figure 5.7b), the image clearly shows the polymer chains with elongated conformations along the macroscopic stretching direction. Even during the stress relaxation process in the monodisperse system (Figure 5.7c), many of the chains showed elongated conformations. In the blend film (Figure 5.7d), the degrees of extension of the chains were somewhat smaller than those in the monodisperse system, indicating the fast conformational relaxation.

The conformation of the single PMMA chain was quantitatively evaluated from the fluorescence intensity distribution in terms of the true dimension along the stretching direction R^*_{xx} (eq 2.9) and the average chain extension ratio λ_c (eq 2.8) by the procedure shown in chapter 2. Figure 5.8 shows the chain extension ratio in the blend films plotted
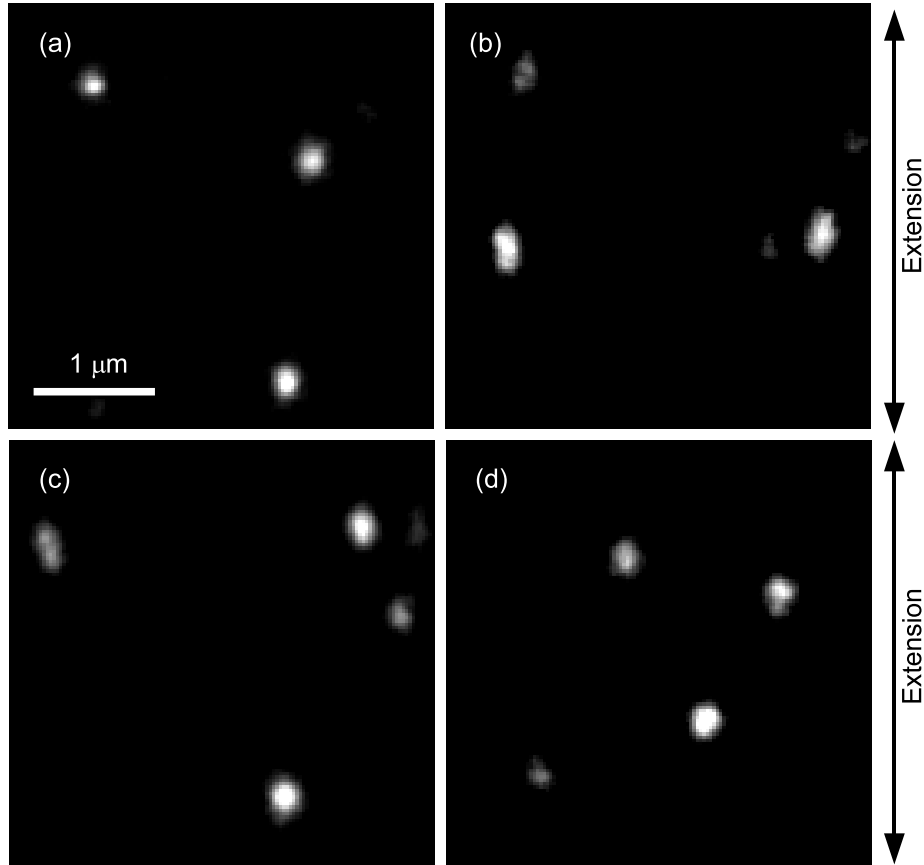
Figure 5.7: Fluorescence SNOM images of single polymer chains in the PMMA films before stretching (a), immediately after the stretching (b), and after the relaxation periods $a_T^{-1}t = 3.6 \times 10^3$ (c,d). The matrices are (a–c) L, (d) L/S17 ($w_L = 0.20$).

against time. λ_c indicates the extension ratio of the labeled L-chains in the blend films. Figure 5.8a shows the blend ratio dependence of λ_c. In the monodisperse sample of the L-chain, λ_c almost kept the initial value of 2.0 at the early stage of the relaxation process as shown in chapter 4. In the blend films, the lower w_L samples showed the smaller values of λ_c in the early time region. This indicates that not only the segmental relaxation but also the relaxation of the whole chain is accelerated by the addition of the S-chains. Even in the samples quenched immediately after the stretching, λ_c was smaller than the macroscopic extension ratio of 2.0, implying that the fast relaxation proceeds even during the extension process. Figure 5.8b shows the M_S dependence of λ_c. The lower M_S samples
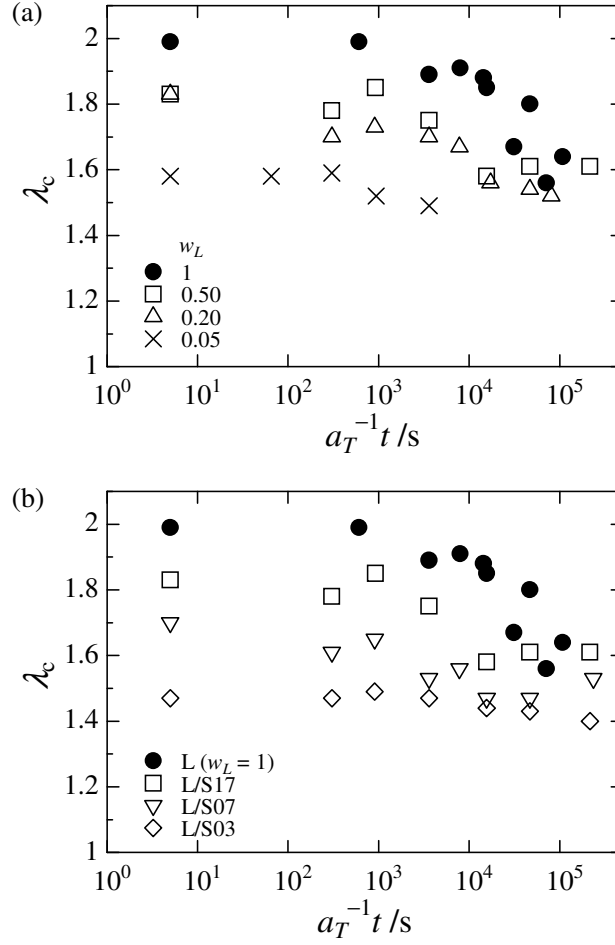
Figure 5.8: Chain extension ratio of *L*-chains plotted against time for (a) L/S17 blends, and (b) blends with $w_L = 0.50$.

showed the faster decrease in λ_c. These dependencies of λ_c on w_L and M_S suggests that the fast relaxation of λ_c is caused by the disentanglement between the *L*-chain and the *S*-chain. In the longer time region, λ_c hardly decreased with time after the fast relaxation in stress had been completed ($a_T^{-1}t > 5 \times 10^2$, 2×10^3, and 5×10^4 s for L/S03, L/S07, and L/S17, respectively). The complete conformational relaxation is restricted by the entanglement among the *L*-chains. The further decrease in λ_c is expected to proceed by the motion of *L*-chains, which was not observed in the time range of this experiment.

Figure 5.9 shows histograms of the chain dimension parallel to the stretching direction normalized by the average value before stretching, $\langle R_{xx}^* \rangle_0$. Figure 5.9a shows the result
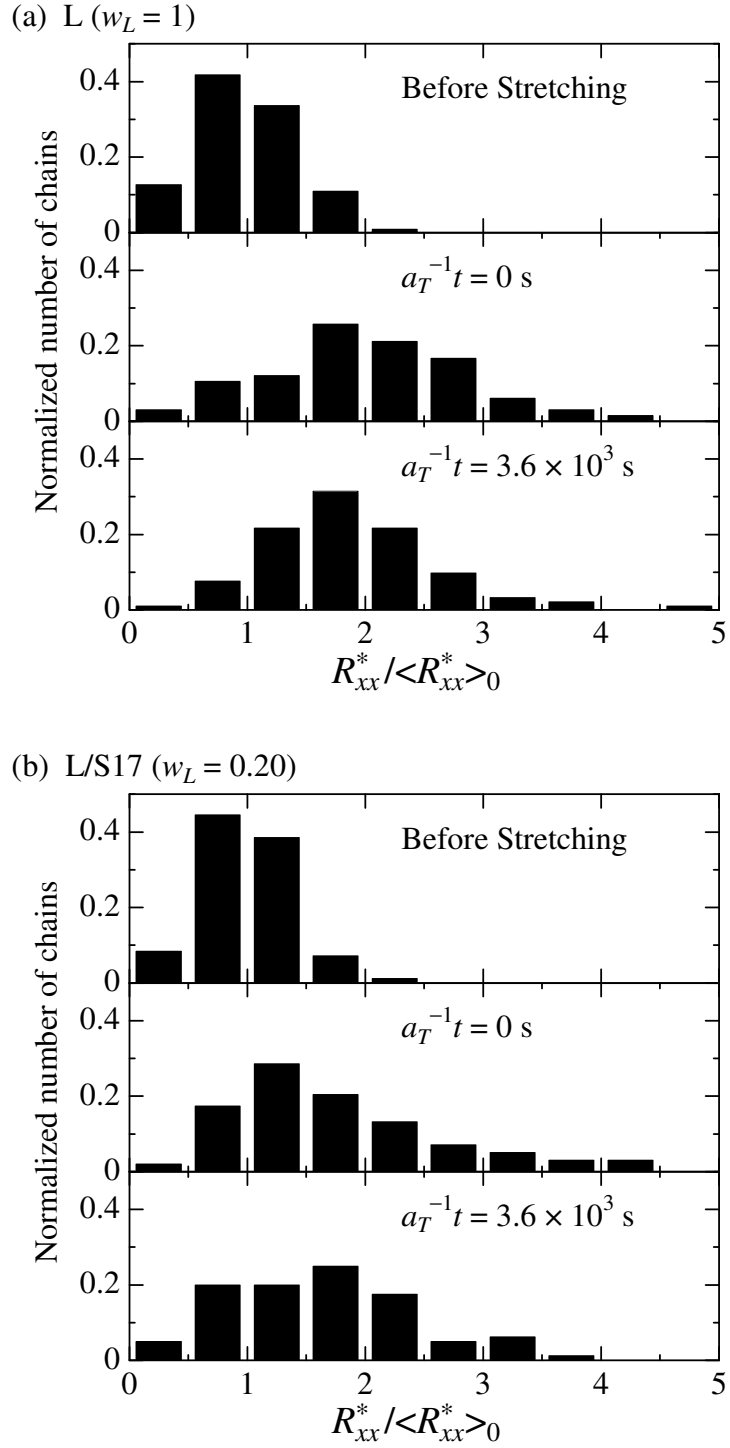
Figure 5.9: Histograms of the chain dimension parallel to the stretching direction, which was normalized by the initial average value, for the films before stretching, quenched immediately after the stretching, and after the relaxation periods $a_T^{-1}t = 3.6 \times 10^3$ s. The matrices are (a) L, and (b) L/S17 ($w_L = 0.20$).

for the monodisperse film. The dimension of each chain increased by the stretching of the film. The distribution function of $R^*_{xx}/\langle R^*_{xx}\rangle_0$ did not significantly change at the early stage of the relaxation process ($a_T^{-1}t = 3.6 \times 10^3$ s). An example of the result for the blend is shown in Figure 5.9b. In this system, the distribution function of $R^*_{xx}/\langle R^*_{xx}\rangle_0$ immediately after the stretching was peaked at the smaller value compared with monodisperse system, and it showed the tail in the large $R^*_{xx}/\langle R^*_{xx}\rangle_0$ region. The broad distribution was also seen in the relaxation process. This implies that each chain shows different extension and relaxation behaviors in the blend films. This would happen because the state of the entanglement with the surrounding chains, and therefore the effect of the disentanglement, is different chain by chain.

5.3.4 Comparison with the Slip-Link Simulation

The experimental data was compared with the slip-link simulation based on Doi–Takimoto model using a PASTA system.[14,28] In this model, the polymer system consists of chains virtually linked to other chains by pairwise slip links. These slip links represent the constraints by the entanglement with the other chains. The number of the slip links in a chain is equal to the number of entanglement, Z, and the average distance between the slip links equals to the average distance between entanglements, a_e. Each chain is deformed affinely by the macroscopic strain of the sample. Then the chain is relaxed though the contour length fluctuation and the reptation. If the end of the chain passes through the last slip link of the chain in these relaxation processes, the slip link and its partner vanish. This represents the constraint release. If, on the other hand, the length of the tail at the end of the path becomes longer than a_e, a new slip link is created at the end, and its partner is created on a randomly selected chain (constraint creation). The stress is calculated through the conformations of the chains. The model parameters to fit the simulation and experimental results are the molecular weight between entanglements, M_e, and the unit time, τ_e, which is the Rouse time of the sub-chain with the molar mass M_e.
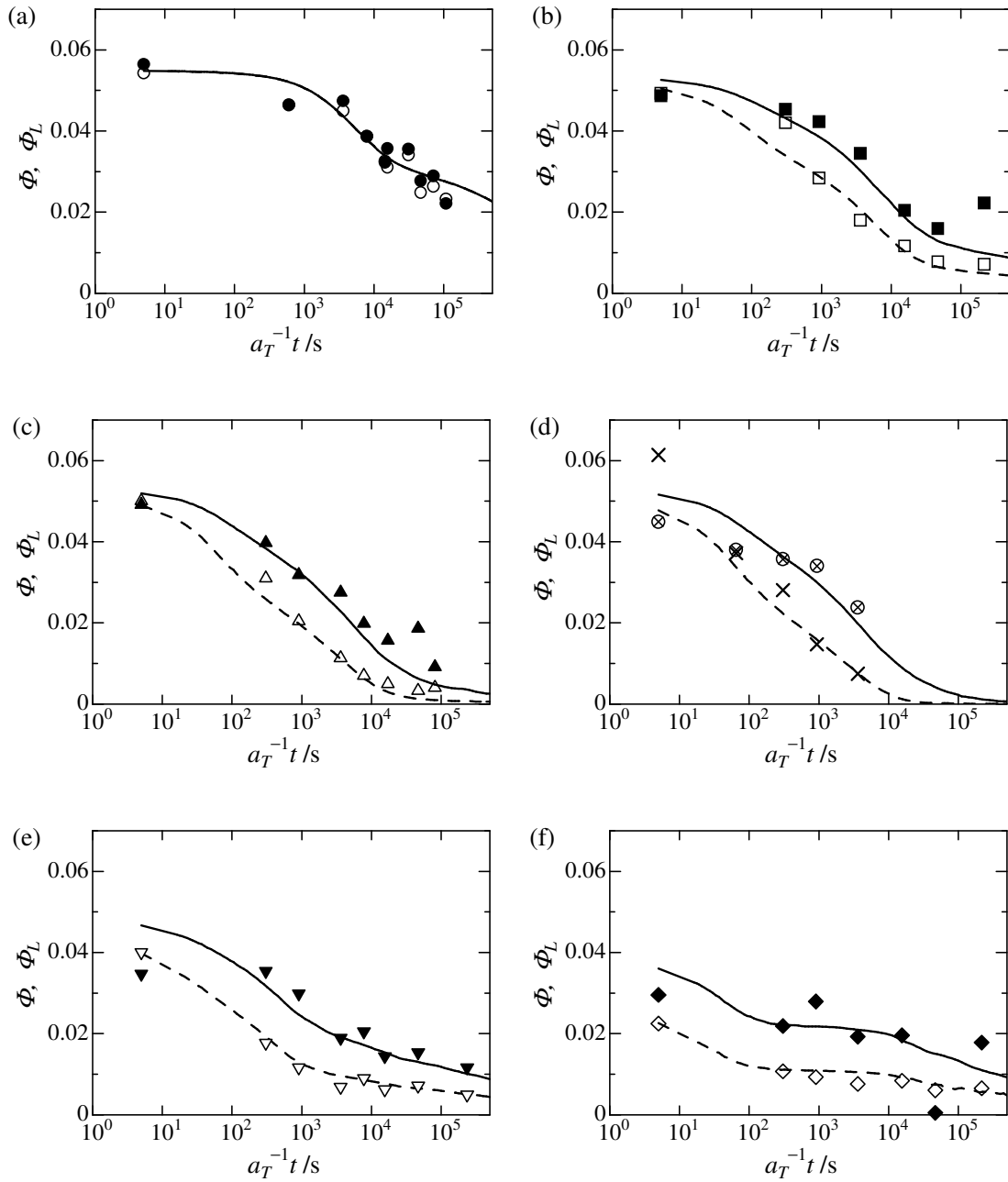
Figure 5.10: The orientational order parameters of the main chain for the entire system (open symbols and broken lines) and *L*-chains (closed symbols and solid lines) plotted against time, which were obtained from the experiment (symbols) and the simulation (lines) for (a) L, (b) L/S17 (w_L=0.50), (c) L/S17 (w_L=0.20), (d) L/S17 (w_L=0.05), (e) L/S07 (w_L=0.50), and (f) L/S03 (w_L=0.50).

Figure 5.10 shows the orientation functions for the entire system and the L-chain, Φ and Φ_L, respectively, which were obtained from the experiment and the simulation. The values of Φ_L for the experiment were evaluated from the value of $\bar{p}$ using the proportionality between the orientation function of the fluorescence dye and the main chain (Figure 5.5a). The parameters for the simulation were determined by fitting to the experimental stress relaxation curves for monodisperse L and S17: $\tau_e = 0.10$ s and $M_e = 5000$. These values are consistent with the experimental values obtained from shear measurements in the literature.[35,36] The predictions of the simulation were in good agreement with the experimental data for all the samples. The acceleration of the segmental relaxation of the L-chains by the addition of the S-chains was well described by the assumption of the constraint release.

The chain extension ratio of the L-chains predicted by the simulation is shown by curves in Figure 5.11. For the monodisperse sample, the simulation was consistent with the experiment at the early stage of the relaxation, showing the slow relaxation in λ_c. For the blends, on the other hand, the value of λ_c was inconsistent with the experimental data. The decrease in λ_c by the addition of the S-chains was not reproduced by the simulation. The acceleration of the decrease in λ_c was predicted only near the terminal relaxation time, which is out of the time range of this experiment. Although the local orientation is relaxed by constraint release, the conformation at the whole chain scale hardly changes in the simulation. This is because the simulation for the constraint release assumes the local jump within the length scale of the distance between the entanglements. As the result, the global relaxation of the whole chain proceeds mainly by the motion of the chain by itself like the contour length equilibration and reptation in the model. This is consistent with the experimental data in the long time region in the sense that the further relaxation hardly proceeds. The discrepancy in the value of λ_c mainly arises at the early stage of the relaxation process or the extension process. In this time region, the relaxation of a L-chain is expected to be dominated by the contraction of the chain contour and the disentanglement with the surrounding chains. This competition between the contraction
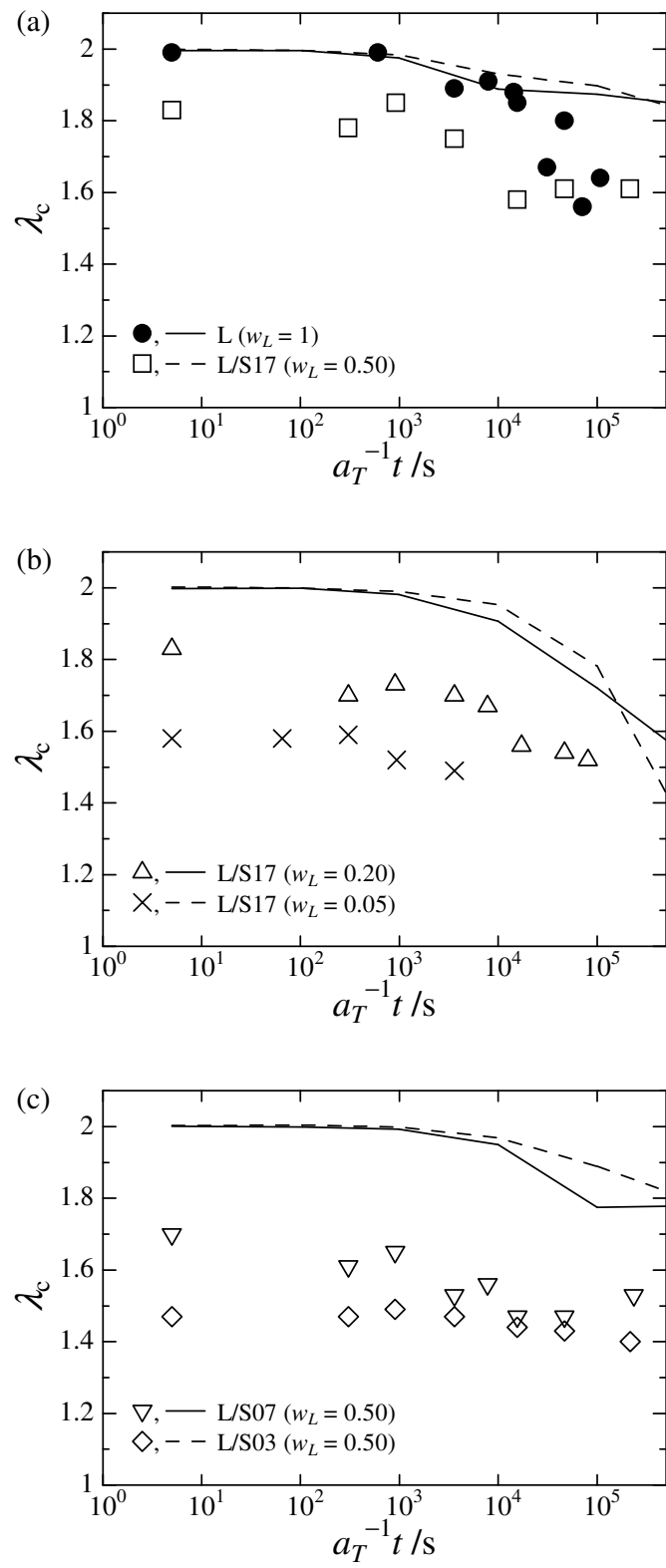
84

Figure 5.11: Chain extension ratio of *L*-chains plotted time, which was obtained from experiment (symbols) and simulation (lines).

and the constraint release in the non-linear region would be important for describing the relaxation behavior at the whole chain scale.

5.4 Conclusion

The single polymer chains in binary molecular weight blends during the stress relaxation process were observed by the excitation polarization modulation microscopy and SNOM. The relaxation in the segmental orientation of the long chain, which was evaluated by the excitation polarization microscopy, was accelerated by the addition of the short chains. The global chain dimension evaluated by SNOM also showed the smaller value from the early stage of the relaxation process in the system with short chains. This suggests that not only the segmental orientation but also the whole chain dimension decreases by the disentanglement. The distribution function of the chain dimension in the blend film was broader than that in the monodisperse film, implying that the effect of the disentanglement is different chain by chain. The fast relaxation in the whole chain dimension was inconsistent with the theoretical model, which predicts that the relaxation at the whole chain scale is not accelerated by the constraint release. The deviation mainly occurs in the non-linear region, which should be further investigated from both experimental and theoretical points of view at the various length scales.

References

[1] de Gennes, P. G. *J. Chem. Phys.* **1971**, *55*, 572–579.

[2] Doi, M.; Edwards, S. F. *J. Chem. Soc. Faraday Trans. II* **1978**, *74*, 1789–1801.

[3] Doi, M.; Edwards, S. F. *J. Chem. Soc. Faraday Trans. II* **1978**, *74*, 1802–1817.

[4] Doi, M. *J. Polym. Sci., Polym. Phys. Ed.* **1980**, *18*, 1005–1020.

[5] Doi, M.; Edwards, S. F. *The Theory of Polymer Dynamics*, 3rd ed.; Clarendon: Oxford, 1986.

[6] Watanabe, H. *Prog. Polym. Sci.* **1999**, *24*, 1253–1403.

[7] McLeish, T. C. B. *Adv. Phys.* **2002**, *51*, 1379–1527.

[8] Graessley, W. W. *Adv. Polym. Sci.* **1982**, *47*, 67–117.

[9] Ianniruberto, G.; Marrucci, G. *J. Rheol.* **2001**, *45*, 1305–1318.

[10] Graham, R. S.; Likhtman, A. E.; McLeish, T. C. B.; Milner, S. T. *J. Rheol.* **2003**, *47*, 1171–1200.

[11] Masubuchi, Y.; Watanabe, H.; Ianniruberto, G.; Greco, F.; Marrucci, G. *Macromolecules* **2008**, *41*, 8275–8280.

[12] Masubuchi, Y.; Furuichi, K.; Horio, K.; Uneyama, T.; Watanabe, H.; Ianniruberto, G.; Greco, F.; Marrucci, G. *J. Chem. Phys.* **2009**, *131*, 114906.

[13] Hua, C. C.; Schieber, J. D. *J. Chem. Phys.* **1998**, *109*, 10018–10027.

[14] Doi, M.; Takimoto, J. *Philos. Trans. R. Soc. London, Ser. A* **2003**, *361*, 641–652.

[15] Masubuchi, Y.; Takimoto, J.; Koyama, K.; Ianniruberto, G.; Marrucci, G.; Greco, F. *J. Chem. Phys.* **2001**, *115*, 4387–4394.

[16] Watanabe, H.; Kotaka, T. *Macromolecules* **1984**, *17*, 2316–2325.

[17] Struglinski, M. J.; Graessley, W. W. *Macromolecules* **1985**, *18*, 2630–2643.

[18] Auhl, D.; Chambon, P.; McLeish, T.; Read, D. *Phys. Rev. Lett.* **2009**, *103*, 136001.

[19] Tassin, J. F.; Monnerie, L. *J. Polym. Sci., Polym. Phys. Ed.* **1983**, *21*, 1981–1992.

[20] Tassin, J. F.; Baschwitz, A.; Moise, J. Y.; Monnerie, L. *Macromolecules* **1990**, *23*, 1879–1881.

[21] Watanabe, H. *Macromol. Rapid Commun.* **2001**, *22*, 127–175.

[22] Hayes, C.; Bokobza, L.; Boue, F.; Mendes, E.; Monnerie, L. *Macromolecules* **1996**, *29*, 5036–5041.

[23] Graham, R. S.; Bent, J.; Clarke, N.; Hutchings, L. R.; Richards, R. W.; Gough, T.; Hoyle, D. M.; Harlen, O. G.; Grillo, I.; Auhl, D.; McLeish, T. C. B. *Soft Matter* **2009**, *5*, 2383–2389.

[24] Perkins, T. T.; Smith, D. E.; Chu, S. *Science* **1994**, *264*, 819–822.

[25] Smith, D. E.; Chu, S. *Science* **1998**, *281*, 1335–1340.

[26] Teixeira, R. E.; Dambal, A. K.; Richter, D. H.; Shaqfeh, E. S. G.; Chu, S. *Macromolecules* **2007**, *40*, 2461–2476.

[27] Gupta, V. K.; Kornfield, J. A.; Ferencz, A.; Wegner, G. *Science* **1994**, *265*, 940–942.

[28] http://octa.jp.

[29] Aoki, H.; Morita, S.; Sekine, R.; Ito, S. *Polym. J.* **2008**, *40*, 274–280.

[30] Aoki, H.; Tanaka, S.; Ito, S.; Yamamoto, M. *Macromolecules* **2000**, *33*, 9650–9656.

[31] Grimaud, T.; Matyjaszewski, K. *Macromolecules* **1997**, *30*, 2216–2218.

[32] Masuda, T.; Kitagawa, K.; Onogi, S. *Polym. J.* **1970**, *1*, 418–424.

[33] Aoki, H.; Kunai, Y.; Ito, S.; Yamada, H.; Matsushige, K. *Appl. Surf. Sci.* **2002**, *188*, 534–538.

[34] Kashiwagi, M.; Folkes, M. J.; Ward, I. M. *Polymer* **1971**, *12*, 697–710.

[35] Ferry, J. D. *Viscoelastic Properties of Polymers*, 3rd ed.; Wiley: New York, 1980.

[36] Fuchs, K.; Friedrich, C.; Weese, J. *Macromolecules* **1996**, *29*, 5893–5901.

Chapter 6

Conformation of Single Polymer Chain in Rubbed Thin Film
Observed by SNOM

6.1 Introduction

The surface properties of polymer materials such as friction, wettability, and adhesion play an important role in the practical use. These macroscopic properties are dominated by the structure of the polymer chain near the surface. The understanding of the polymer chain near the surface is essential to control and improve the performance of polymer materials. The rubbing process is an important surface modification method. It is well known that liquid crystal molecules are strongly aligned on a rubbed polymer surface, and it has been applied to flat panel displays.[1] The orientational order of polymer chains in a film increases by the rubbing process, which has been evaluated by birefringence[2–4] and infrared absorption[3–5] measurements. In recent years, the surface sensitive experimental techniques have been developed such as grazing incidence X-ray scattering,[6] near-edge X-ray absorption fine structure,[7–9] and sum-frequency generation vibrational spectroscopy,[10] and they revealed that the rubbing induces the higher orientation near the surface than the bulk. The surface morphology of the rubbed film has been investigated by AFM.[11–14] It was shown that the groove like structure was formed during the rubbing process. Using these methods, the effect of the rubbing has been investigated in terms of the orientation at the monomeric scale and the surface morphology. However, the less information has been obtained for the behavior of polymer chains under rubbing compared with those under the tensile and shear deformations. For example, the conformation of a single polymer chain at the whole chain scale, which is characterized by parameters such as radius of gyration, has not been investigated so far for the chain in the rubbed film. The approaches from the various length scales are essential to

89

describe the exact chain behavior.[15] Furthermore, the orientation obtained from previous measurements suffers from blur by averaging over a large number of molecules. The direct observation of the single chain would be a more effective approach to reveal the response of the polymer chain to the rubbing, which could be inhomogeneous.

SNOM is an emerging scanning probe technique, which allows optical measurement with a high resolution beyond the diffraction limit of light. The fluorescence labeling technique can be combined with SNOM. This enables us to directly observe the conformation of the flexible single chain with a high resolution, which is fluorescently labeled and contrasted to surrounding unlabeled polymers. Furthermore, the topographic image is simultaneously obtained while the SNOM measurement. The chain conformation can be discussed in contrast with the surface morphology. In addition to the observation of the whole chain by SNOM, the orientation of the dye in the fluorescently labeled polymer can be evaluated by the use of polarized light because the absorption and fluorescence anisotropies reflect the orientation of the transition dipole. The polarization measurement under a microscope reveals the spatial distribution of the orientational anisotropy.[16]

In this chapter, the conformation of the single polymer chain in the rubbed PMMA film is investigated through the direct observation. The conformations at the whole chain and monomeric scales are evaluated with SNOM and excitation polarization modulation microscopy, respectively. The chain orientation induced by the rubbing below T_g is discussed in contrast with the surface morphology.

6.2 Experiments

Sample preparation. Perylene-labeled PMMA (PMMA-Pe, Figure 2.1) was synthesized as described elsewhere.[17,18] The fraction of the labeled unit was evaluated to be 0.77% by UV–Vis absorption (U3500, Hitachi). The unlabeled PMMA was synthesized by atom transfer radical polymerization.[19] The weight- and number-averaged

Table 6.1: Characterization of PMMA.

	$M_\mathrm{w}/10^6$	$M_\mathrm{n}/10^6$	$M_\mathrm{w}/M_\mathrm{n}$
PMMA-Pe	1.99	1.58	1.26
PMMA	2.12	1.33	1.60

molecular weights, M_w and M_n, were determined by GPC measurement as shown in Table 6.1. A mixed toluene solution of unlabeled PMMA and PMMA-Pe (0.02 wt % to the unlabeled polymer) was spin-coated onto a glass substrate to form a film with a thickness of 7 nm. The rubbing was performed at 30, 60, and 80 °C by unidirectionally pulling the velvet cloth for 30 cm (80 °C) or 250 cm (30 and 60 °C) at the speed of 1 cm/s under a load of 4 g/cm^2.

Excitation polarization modulation microscopy. The orientation anisotropy of fluorescence dye was measured under an inverted fluorescence microscope (TE-2000, Nikon) equipped with an EMCCD camera (Cascade II, Roper Scientific). A 442 nm laser beam was passed through an electro-optic modulator (EOM) (EO-AM-NR-C4, THORLABS), and focused on the sample through an objective lens (100×, 1.4 NA, Nikon). The fluorescence signal was collected through a filter cube (BV-2A, Nikon), which contains a dichroic mirror (455 nm) and a longpass filter (470 nm). The polarization direction of the illumination was orthogonally modulated by the EOM at a frequency of 0.25 Hz.

SNOM measurement. The SNOM measurement was performed by a commercially available instrument (α-SNOM, WITec) using a hollow cantilever probe with a sub-wavelength aperture of 60 nm. The laser beam at a wavelength of 441 nm (BCL-015-440, CrystaLaser) was focused onto the backside of the aperture to generate the optical near-field. While scanning the sample surface in the contact mode with the cantilever, the perylene fluorescence was collected by a microscope objective (0.80NA, 60×, Nikon) from the backside of the substrate and detected with a photomultiplier
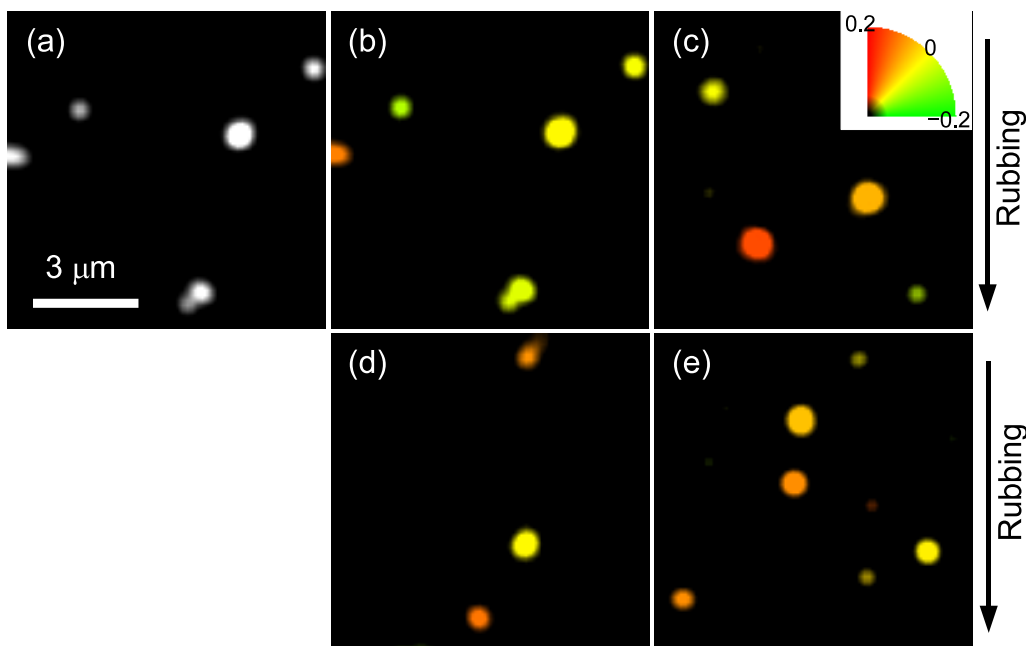
Figure 6.1: (a) Fluorescence and (b–e) anisotropy images of single polymer chains obtained by excitation polarization modulation microscopy in the PMMA films (a,b) before rubbing, and after rubbing at (c) 30 °C, (d) 60 °C, and (e) 80 °C.

(H8631, Hamamatsu Photonics) through a long-pass filter (LP02-442RS-25, Semrock). The SNOM measurement was carried out in an ambient condition. All the SNOM images were taken by the same probe.

6.3   Results and Discussion

6.3.1   Orientation of Fluorescence Dye

Figure 6.1a shows a fluorescence image of a PMMA film before rubbing obtained by the excitation polarization modulation microscopy. Each fluorescence spot was confirmed to be an individual PMMA-Pe chain from the statistical analysis.[20] The orientation of the dye molecules in each labeled chain was examined in terms of the excitation anisotropy $(I_x - I_y)/(I_x + I_y)$, where I_x and I_y are the intensities of the fluorescence from each labeled chain excited by linearly polarized light in x and y directions, respectively. The x axis is
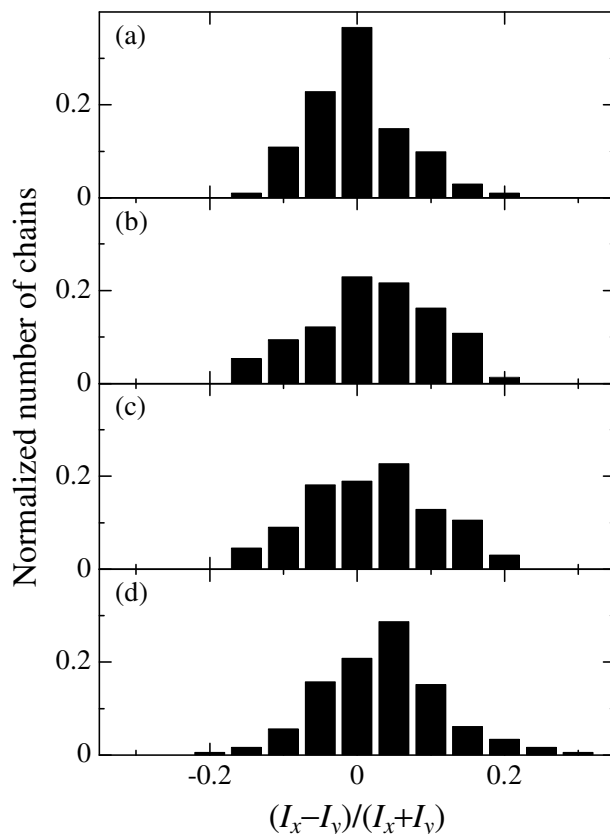
Figure 6.2: Histograms of excitation anisotropy of chains obtained by excitation polarization modulation microscopy for the films (a) before rubbing, and after rubbing at (b) 30 °C, (c) 60 °C, and (d) 80 °C.

defined as the rubbing direction of the film and y axis perpendicular to it. The excitation anisotropy of the fluorescence intensity for each labeled chain indicates the average orientation of the dye moieties. For the complete orientation in the x and y axes, the values of $(I_x - I_y)/(I_x + I_y)$ are $+1$ and -1, respectively. In the previous chapter, it was shown that the average orientation of the dye correlates with that of the segmental orientation of the main chain. The values of $(I_x - I_y)/(I_x + I_y)$ for the individual chains are represented by colors in Figures 6.1b–e. Whereas the conformation of each chain was not clearly observed in the fluorescence image due to the diffraction limit, the segmental orientation for a single PMMA chain can be examined through the excitation anisotropy.

Figure 6.2 shows the histograms of $(I_x - I_y)/(I_x + I_y)$. In the film before rubbing,
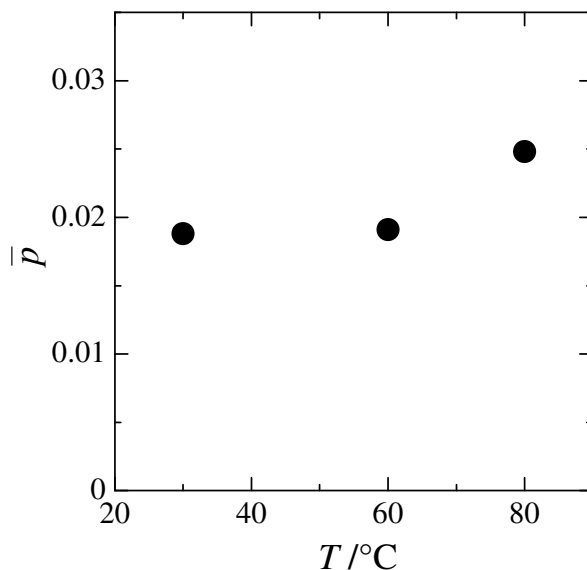
Figure 6.3: Average excitation anisotropy of PMMA films plotted against the rubbing temperature.

the excitation anisotropy showed a symmetric distribution at a peak position of zero, indicating the isotropic orientation. In the rubbed films, the distribution was shifted to higher $(I_x - I_y)/(I_x + I_y)$ value. This indicates that the orientation of the fluorescence dye in each polymer chain increased by the rubbing. The average orientational order parameter of the dye $\bar{p}$, which is defined by eq 5.6, is shown in Figure 6.3. The value of $\bar{p}$ was zero before rubbing. After rubbing, $\bar{p}$ took positive values. The film rubbed at 80 °C showed the higher anisotropy than those at 30 and 60 °C, reflecting the increased molecular mobility with the temperature. This implies the chain is more oriented by the rubbing at the higher temperature.

6.3.2 Chain Conformation Observed by SNOM

Figures 6.4a–d show the fluorescence SNOM images of the PMMA films. The perylene-labeled PMMA chains embedded in the unlabeled matrix were observed as the bright spots in the fluorescence image. The SNOM images showed much higher resolution than the fluorescence images obtained under the far-field set up (Figure 6.1).
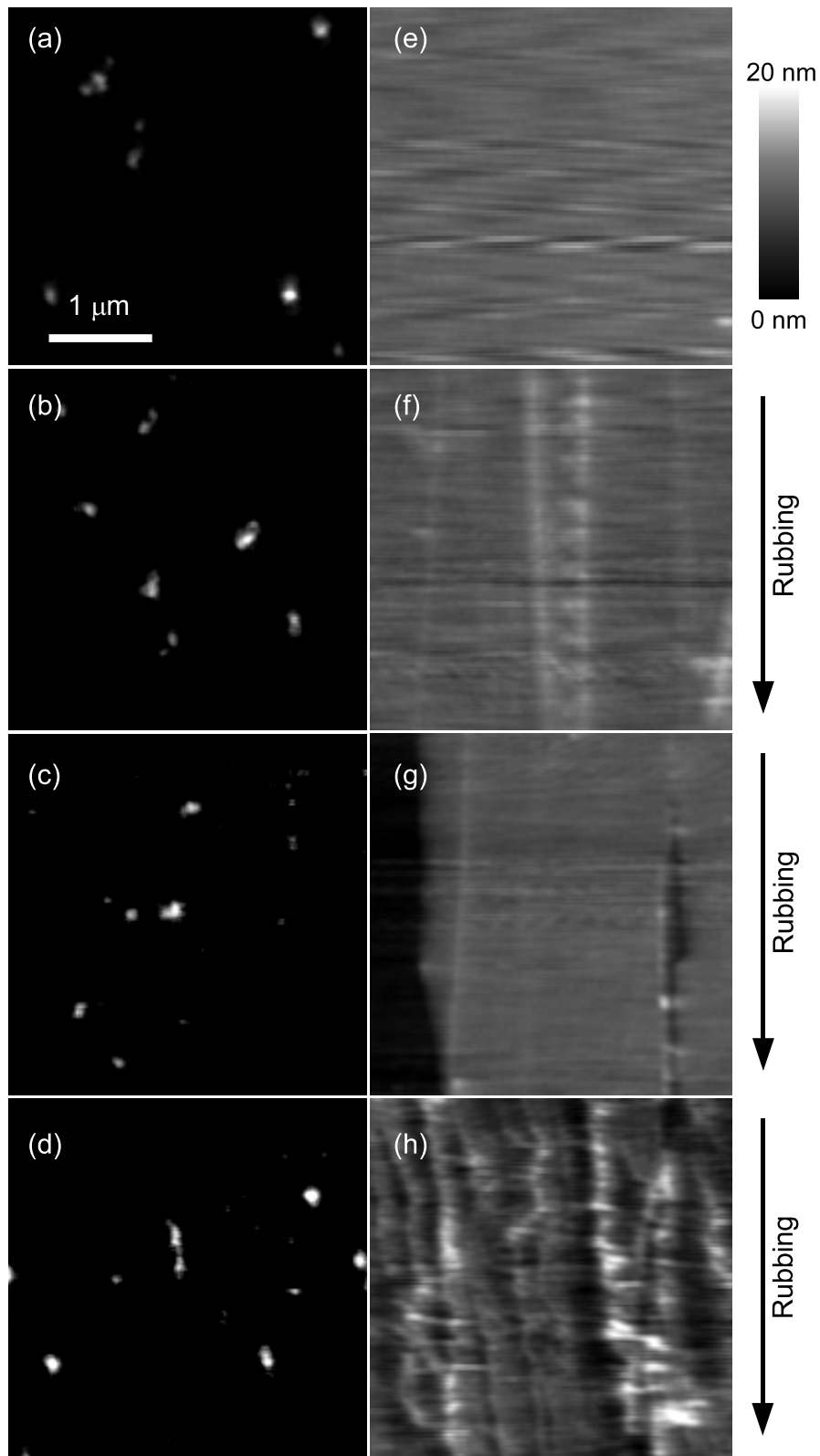
94

Figure 6.4: Fluorescence (a–d) and topographic (e–h) images of single polymer chains in the PMMA films obtained by SNOM: (a,e) Before rubbing, and after rubbing at (b,f) 30, (c,g) 60, and (d,h) 80 °C.
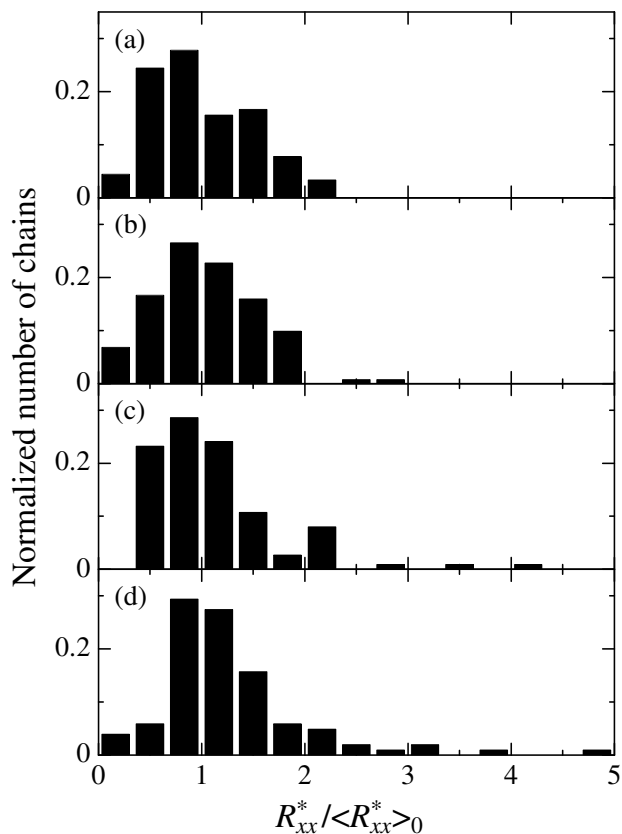
Figure 6.5: Histograms of the chain dimension parallel to the stretching direction, which was normalized by the initial average value, for the films (a) before rubbing, and after rubbing at (b) 30, (c) 60, and (d) 80 °C.

The topographic images simultaneously obtained during the SNOM measurements are shown in Figure 6.4e–h. The groove along the rubbing direction with the height of 2–5 nm was observed in the rubbed films. The films were partly scratched and peeled off by the rubbing at 60 and 80 °C. The film rubbed at 80 °C showed markedly different morphology from the others. There were fine ordered grooves with the periodicity of approximately 500 nm and the height of 3–15 nm. This suggests that the surface of the film was largely deformed by the shear force. In this film, some of the chains showed highly stretched conformation along the rubbing direction (Figure 6.4d).

In order to evaluate the chain conformation quantitatively, the fluorescence intensity distribution for each spot was analyzed by the same procedure shown in chapter 2. The
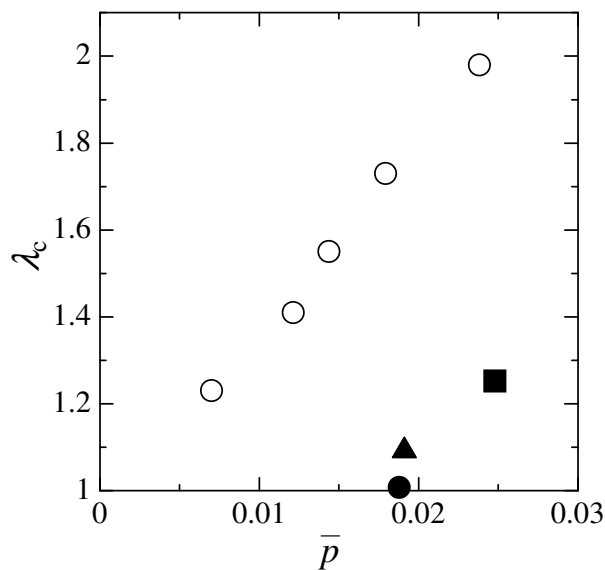
Figure 6.6: Chain extension ratio plotted against the average excitation anisotropy for (closed symbols) the thin films rubbed at (circle) 30, (triangle) 60, and (square) 80 °C. Open circles represent the bulk film uniaxially stretched at 160 °C.

conformation of the whole single chain was evaluated in terms of the chain dimension along the rubbing direction R_{xx}^*, which is defined by eq 2.9. Figure 6.5 shows histograms of R_{xx}^* normalized by the average value before rubbing, $\langle R_{xx}^* \rangle_0$. The distribution function of $R_{xx}^* / \langle R_{xx}^* \rangle_0$ was not significantly changed by the rubbing at 30 °C. This indicates that the global conformation of the whole chain was not changed by the rubbing near the room temperature. The film rubbed at 60 °C also showed the similar distribution function to that of the unrubbed film, while the weak tail appeared in the large $R_{xx}^* / \langle R_{xx}^* \rangle_0$ region. In the film rubbed at 80 °C, on the other hand, the peak shifted to the higher value and the distribution became broader. This suggests that the chains were stretched along the rubbing direction.

The average chain extension ratio, λ_c, which is defined by eq 2.8, is plotted against $\bar{p}$ in Figure 6.6. The data for the uniaxial extension of the bulk film at 160 °C in the previous chapter are also shown by the open symbols therein. In the uniaxial extension process above T_g, both of the orientation at the segmental orientation and the dimension

97

of the whole chain increased with strain. On the other hand, the rubbing process near the room temperature hardly changes the dimension of the whole chain in spite of the increase in the orientational anisotropy of the fluorescence dye. At the room temperature, the motion of the main chain is frozen. Therefore, it is unlikely that the rearrangement of the chain contour at the whole chain scale is induced by rubbing. In the rubbing process at the higher temperature, the motion of the main chain is thermally activated; therefore, the individual PMMA chains were elongated in the rubbing direction. However, the deformation of the chain conformation was observed even below the bulk T_g of PMMA. In a thin film, there are less entanglements compared to the bulk state, resulting in the higher chain mobility.[21] Furthermore, the recent study on the plastic flow of the bulk PMMA has shown that the chain mobility is also enhanced by applying the stress.[22,23] These decreased number of entanglements and the applied stress allowed the deformation at the whole chain scale below the bulk T_g. Even in this case, the value of λ_c is still smaller than that for the uniaxial extension above T_g. This indicates that rubbing process mainly induces the conformational change at the length scale of the monomer unit rather than the whole chain.

6.4 Conclusion

The conformation of the single polymer chain in the rubbed thin film was investigated through the direct observation by the excitation polarization modulation microscopy and SNOM. The orientational anisotropy of the dyes in the labeled chains increased by the rubbing, indicating that the conformation at the length scale of the monomer unit was rearranged. On the other hand, the conformation at the whole chain scale was not significantly changed by the rubbing near the room temperature. The increase in the chain dimension along the rubbing direction was observed in the film rubbed at 80 °C, associated with surface morphology with the fine ordered groove. This conformational change at the whole chain scale below the bulk T_g is expected to be caused by the reduced

number of entanglements and the stress-enhanced chain mobility. The extension ratio of the whole chain in rubbed film was much smaller than that in the uniaxially stretched film. This indicates that the rubbing process mainly changes the local conformation at the length scale of monomer unit rather than the global conformation of the whole chain.

References

[1] Geary, J. M.; Goodby, J. W.; Kmetz, A. R.; Patel, J. S. *J. Appl. Phys.* **1987**, *62*, 4100–4108.

[2] Schwab, A. D.; Agra, D. M. G.; Kim, J.; Kumar, S.; Dhinojwala, A. *Macromolecules* **2000**, *33*, 4903–4909.

[3] van Aerle, N. A. J. M.; Barmentlo, M.; Hollering, R. W. J. *J. Appl. Phys.* **1993**, *74*, 3111–3120.

[4] Lee, E. S.; Vetter, P.; Miyashita, T.; Uchida, T. *Jpn. J. Appl. Phys.* **1993**, *32*, L1339–L1341.

[5] Sakamoto, K.; Arafune, R.; Ito, N.; Ushioda, S.; Suzuki, Y.; Morokawa, S. *J. Appl. Phys.* **1996**, *80*, 431–439.

[6] Toney, M. F.; Russell, T. P.; Logan, J. A.; Kikuchi, H.; Sands, J. M.; Kumar, S. K. *Nature* **1995**, *374*, 709–711.

[7] Liu, Y.; Russell, T. P.; Samant, M. G.; Stohr, J.; Brown, H. R.; Cossy-Favre, A.; Diaz, J. *Macromolecules* **1997**, *30*, 7768–7771.

[8] Cossy-Favre, A.; Diaz, J.; Liu, Y.; Brown, H. R.; Samant, M. G.; Stohr, J.; Hanna, A. J.; Anders, S.; Russell, T. P. *Macromolecules* **1998**, *31*, 4957–4962.

[9] Stohr, J.; Samant, M. G.; Cossy-Favre, A.; Diaz, J.; Momoi, Y.; Odahara, S.; Nagata, T. *Macromolecules* **1998**, *31*, 1942–1946.

[10] Wei, X.; Zhuang, X.; Hong, S.; Goto, T.; Shen, Y. R. *Phys. Rev. Lett.* **1999**, *82*, 4256–4259.

[11] Zhu, Y.; Wang, L.; Lu, Z.; Wei, Y.; Chen, X. X.; Tang, J. H. *Appl. Phys. Lett.* **1994**, *65*, 49–51.

[12] Kikuchi, H.; Logan, J. A.; Yoon, D. Y. *J. Appl. Phys.* **1996**, *79*, 6811–6817.

[13] Kim, J.; Rosenblatt, C. *J. Appl. Phys.* **2000**, *87*, 155–158.

[14] Lee, S. W.; Yoon, J.; Kim, H. C.; Lee, B.; Chang, T.; Ree, M. *Macromolecules* **2003**, *36*, 9905–9916.

[15] McLeish, T. C. B. *Adv. Phys.* **2002**, *51*, 1379–1527.

[16] Gupta, V. K.; Kornfield, J. A.; Ferencz, A.; Wegner, G. *Science* **1994**, *265*, 940–942.

[17] Aoki, H.; Morita, S.; Sekine, R.; Ito, S. *Polym. J.* **2008**, *40*, 274–280.

[18] Aoki, H.; Tanaka, S.; Ito, S.; Yamamoto, M. *Macromolecules* **2000**, *33*, 9650–9656.

[19] Grimaud, T.; Matyjaszewski, K. *Macromolecules* **1997**, *30*, 2216–2218.

[20] Aoki, H.; Kunai, Y.; Ito, S.; Yamada, H.; Matsushige, K. *Appl. Surf. Sci.* **2002**, *188*, 534–538.

[21] Brown, H. R.; Russell, T. P. *Macromolecules* **1996**, *29*, 798–800.

[22] Lee, H.; Paeng, K.; Swallen, S. F.; Ediger, M. D. *J. Chem. Phys.* **2008**, *128*, 134902.

[23] Lee, H.; Paeng, K.; Swallen, S. F.; Ediger, M. D. *Science* **2009**, *323*, 231–234.

Summary

In this thesis, the single polymer chains in bulk and thin films under the external force were directly observed by SNOM. The conformations of polymer chains under the uniaxial extension and the surface rubbing were analyzed and compared with macroscopic mechanical properties, optical properties, and theoretical models. The summary of each chapter is presented below.

In chapter 2, the direct observation of the single polymer chain in an uniaxially stretched PMMA film was demonstrated. The elongated conformation of the single polymer chain was successfully observed. The author introduced the quantitative analysis of the chain conformation from the fluorescence intensity distribution. Observation of the plastically deformed films with various strains revealed that the microscopic extension ratio of the single chain was smaller than the macroscopic extension ratio of the film. This suggests the presence of the slip of the polymer chains on the course of the plastic deformation.

In chapter 3, the conformation of single polymer chain under the uniaxial extension well above the glass transition temperature was studied. In the high molecular weight matrix, the average extension ratio at the single chain level coincided with the macroscopic extension ratio. The distribution of the chain conformation was in good agreement with that of the freely-jointed chain followed by affine deformation. On the other hand, the probe chain embedded in the low molecular weight matrix showed the smaller extension than that expected from the affine deformation. This suggests that the conformation of the probe chain is affected by the relaxation of the short surrounding chains through disentanglement.

In chapter 4, the chain conformation during the stress relaxation process after the uniaxial extension was investigated. The extension ratio at the molecular level was

directly evaluated from the SNOM images and compared with the macroscopic stress relaxation. At the early stage of the relaxation process, the whole single chain almost kept the stretched conformation in spite of the decrease in stress. On the other hand, the birefringence, which reflects the orientation of the chain backbone in average, decreased proportionally to the stress according to the stress–optical rule. This suggests that the fast relaxation in stress is caused by the local conformational change at the length scale much smaller than the entire chain length. The experimental data was successfully explained by the contraction of the primitive chain contour in Doi–Edwards model. Furthermore, the distribution function of the chain dimension was found to retain its shape during the relaxation process, indicating that the conformational relaxation of polymer chain is rather homogeneous in the well-entangled system.

In chapter 5, the conformational relaxation of the individual PMMA chain was examined in the binary blend systems, which consist of high and low molecular weight components. The whole chain dimension and the segmental orientation were evaluated for the high molecular weight long chain with SNOM and excitation polarization modulation microscopy. At the early stage of the stress relaxation process, not only the segmental orientation but also the whole chain dimension of the long chain decreased faster in matrices with short chains. This indicates that the relaxation at the whole chain scale is accelerated by disentanglement, which is caused by the motion of the short surrounding chains. The shape of the distribution function of the chain dimension in the blend film was broader than that in the monodisperse film, implying that the effect of the disentanglement is different chain by chain. The fast relaxation in the whole chain dimension could not be explained by the constraint release picture in the theoretical model, which assumes that the disentanglement only activates the local motion of the long chain.

In chapter 6, the effect of the surface rubbing on the conformation of the chain in a thin film was investigated through the direct observation by the excitation polarization modulation microscopy and SNOM. The orientation at the monomeric scale was changed by the rubbing. On the other hand, the conformation at the whole chain scale was hardly

changed by the rubbing near the room temperature. The increase in the chain dimension along the rubbing direction was observed in the film rubbed at the higher temperature, which showed a surface morphology with the fine ordered groove. This conformational change at the whole chain scale below the bulk glass transition temperature is expected to be caused by the reduced number of entanglements and the stress-enhanced chain mobility. The extension ratio of the whole chain in rubbed film was much smaller than that in the uniaxially stretched film. This indicates that rubbing process mainly induces the conformational change at the length scale of the monomer unit rather than the whole chain.

List of Publications

Chapter 2

"Conformation of single PMMA chain in uniaxially stretched film studied by scanning near-field optical microscopy"

Toru Ube, Hiroyuki Aoki, Shinzaburo Ito, Jun-ichi Horinaka, Toshikazu Takigawa

Polymer **2007**, *48*, 6221–6225.

Chapter 3

"Affine deformation of single polymer chain in poly(methyl methacrylate) films under uniaxial extension observed by scanning near-field optical microscopy"

Toru Ube, Hiroyuki Aoki, Shinzaburo Ito, Jun-ichi Horinaka, Toshikazu Takigawa, Toshiro Masuda

Polymer **2009**, *50*, 3016–3021.

Chapter 4

"Relaxation of single polymer chain in poly(methyl methacrylate) films under uniaxial extension observed by scanning near-field optical microscopy"

Toru Ube, Hiroyuki Aoki, Shinzaburo Ito, Jun-ichi Horinaka, Toshikazu Takigawa, Toshiro Masuda

Macromolecules, submitted.

Chapter 5

"Relaxation of single polymer chain in binary molecular weight blends observed by scanning near-field optical microscopy"

Toru Ube, Hiroyuki Aoki, Shinzaburo Ito, Jun-ichi Horinaka, Toshikazu Takigawa, Toshiro Masuda

To be submitted.

Chapter 6

"Conformation of single polymer chain in rubbed thin film observed by scanning near-field optical microscopy"

Toru Ube, Akihiko Shin, Hiroyuki Aoki, Shinzaburo Ito

To be submitted.

Acknowledgement